Characterisation of Reactive Ion Etch Processes for Ternary III-V Semiconductors

Thesis by
Andrew Stuart Bunting

Submitted for the degree of Doctor of Philosophy to the
Department of Electronics and Electrical Engineering of the University of Glasgow

September 1996

ProQuest LLC.
789 East Eisenhower Parkway
P.O. Box 1346
Ann Arbor, MI 48106 – 1346

For Nicola

Abstract

The work presented within this thesis concerns the development and characterisation of reactive ion etch processes for the compound III-V semi-conductors $Al_{0.3}Ga_{0.7}As$, $In_{0.53}Ga_{0.47}As$ and $In_{0.52}Al_{0.48}As$. Two different etch chemistries, one based on the mixture of methane and hydrogen and the other formed from halogenated gases were studied.

The halogenated gases $SiCl_4$ and BBr_3 were assessed for suitablity as etch gases for etching $In_{0.53}Ga_{0.47}As$. Only $SiCl_4$ has proved to be a practical etch chemistry, giving smooth, vertical wall profiles and a high selectivity for $In_{0.53}Ga_{0.47}As$ over $In_{0.52}Al_{0.48}As$ at a temperature of 180^0C. At all temperatures BBr_3 produced a rough etch surface and undercutting of the mask.

The major part of this work is however based on the gas mixture of methane and hydrogen. With all three semiconducting materials etch rates are observed to rise as the methane content is increased until a point is reached, the polymer point, where the gas mixture becomes too rich in methane and results in deposition of a polymeric layer onto the semiconductor surface. The precise conditions for the onset of polymer deposition are determined by the material being etched, gas flow rates and pressures, rf power and the cleanliness of the chamber. Generally the higher the applied rf power the more rich the gas mixture can be in methane before the polymer point is reached. The trend of etch rates between the different materials was found to be $Al_{0.3}Ga_{0.7}As > In_{0.53}Ga_{0.47}As > In_{0.52}Al_{0.48}As$, which follows the trend in volatility of the group III etch product. Increasing the applied rf power increases etch rates as more reactive species are created within the plasma and ion energies increased. Polymer deposition will however, still occur but with even higher methane content gas mixtures.

Analytical studies of the etched $In_{0.53}Ga_{0.47}As$ surface have shown that within a 6 nm deep surface layer, arsenic is depleted relative to the total amount of indium and gallium. The ratio of indium to gallium also increases on etching, the change in surface composition being due to the difference in vapour pressures of the etch products under ion bombardment. The modification of surface stoichiometry has been observed by the increase in ratio of the InAs-like to GaAs-like LO phonons when using Raman spectroscopy and by the appearence of an InAs-like surface quantum well feature in the photoluminescence spectra.

The electrical behaviour of the surface of n-doped $Al_{0.3}Ga_{0.7}As$ has been characterised by the formation of Schottky contacts. During etching the surface depletion layer increases as hydrogen ions penetrating into the semiconductor, passivate donor silicon atoms. Annealing the sample prior to contact formation supplies energy to break the Si-H bond, allowing hydrogen to out-diffuse from the semiconductor, partially restoring donor activity. The semiconductor is not totally restored to the pre-etch state as the etch introduces physical damage which alters surface state density. The rf power used to etch $Al_{0.3}Ga_{0.7}As$ determines the energy with which the ions will impact on, and penetrate the surface. High rf powers show greater depletion depth enhancement, but it is the use of low powers that leads to the greatest degradation of ideality factor. At high powers the high etch rate removes a higher proportion of the already damaged material at the surface, resulting in less overall damage to the surface (as determined by ideality factor). Hydrogen penetration increases more rapidly with power than does the etch rate resulting in an observed increase of depletion layer thickness with power.

The low Schottky barrier height of $In_{0.53}Ga_{0.47}As$, approximately 0.2 eV, makes estimating etch induced damge difficult with this material by Schottky contact characterisation. To gain an indication of induced damage comparisons with bulk GaAs and GaAs/AlGaAs based MESFET and HEMT structures were made. With a

dc self bias of -1000 V the depletion depth of GaAs of 54.6 nm was determined by Raman spectroscopy, but this is reduced to 25.2 nm when a dc self bias of -65 V is used. If methane is added to the hydrogen plasma so that etching is initiated, damaged material is removed at the same time that donor passivation occurs. At -1000 V dc self bias the observed depletion width is reduced to 41.6 nm, lower than with hydrogen alone.

After removing the GaAs capping layer from the δ-doped HEMT layer A777, hydrogenation of the material at a DC self bias of -65V resulted in only a slight degradation to the carrier concentration in the channel. This suggested that careful design of the device layer structure, the use of δ-doping and a low DC self bias would enable gate recessing to be performed using the metahne/hydrogen gas chemistry. This is particularly important if InGaAs caps are to be used where etching with halogenated gases, those normally used for GaAs/AlGaAs gate recessing at low temperatures is impossible.

During an etch, the sidewalls of a feature formed will experience hydrogenation by scattered ions. Fabrication of a set of narrow conducting InGaAs wires reveals that even after annealing a small amount of residual depletion width enhancement is observed.

The etching of $In_{0.53}Ga_{0.47}As$ with high methane content (> 8% CH_4) gas mixtures leads to undercutting of the etch mask for all rf powers. The addition of a small amount of oxygen or chlorine to the CH_4/H_2 gas mixture improves wall verticality by reducing polymer formation upon the mask. Etch rate are increased as the flux of inhibitors to the etch surface is reduced and their sputter rate when on the surface is enhanced. The undercut of the sidewalls is further reduced by the formation of a protective, passivating layer which prevents lateral etching.

Acknowledgements

The work presented within this thesis would not have been possible without the support of many people. Firstly I must thank my supervisor Professor Wilkinson for his boundless patience and unswerving support of the Dry Etch facility. My thanks go to Oxford Plasma Technology for financial support and for allowing me to spend time in their labs playing with their new etch machines. Also to Adrian Murrell my supervisor at OPT, Rob Grimwood and Andy Chambers who made me so welcome.

The support of Professor Laybourn, Head of department and his predecessor the late John Lamb cannot be underestimated. One small research group cannot function in isolation and without a coherent plan for the department, the assistance of workers and equipment based within other groups, little work would have been possible. Of these people may I thank, from the second floor cleanroom Louis Hobbs and Joan Carson and from USSL, Douglas McIntyre, Dave Gourlay, Susan Ferguson, Helen McLelland, Steve Thoms, Nigel Cameron, Iain Thayne and Mike Taylor. From the nanospectroscopy group Pei Dong Wang, Clivia Sottomayor-Torres and Alex Ross and from MBE, Mark McElhinney, Francois Pottier, Colin Stanley and John Cochrane. A long distance thank you to John Sullivan and Sayah Saied of the Surface Science Group, Department of Electronic Engineering and Applied Physics at Aston University for carrying out the XPS measurements and for help with their interpretation. Also to Andy Abbot for technical assistance.

The people who perhaps deserved the most praise and thanks are Ray Darkin, Dave Clifton and Gillian Hopkins the technicians within the Dry Etch group. I can't begin to describe how much hassle and running around they've had to put up with.

Thanks Folks! Also within the dry etch group my thanks go out to Simon Hicks, Saad Murad, Bill Parkes, Yi Ping Song and Majeed Foad, fellow students and research assistants. Over the years we've shared lots of beer and many enjoyable, stimulating and sometimes heated conversations.

Finally many thanks to my wife, Nicola and other members of my family for the support over the three years I spent in Glasgow and previously whilst I was an undergraduate, in St. Andrews.

Contents

Abstract i

Acknowledgements iv

1 **Introduction to Semiconductor Device Fabrication Techniques** 1

1.1 Semiconductor devicess 2
1.2 Dry etching 5
1.2.1 Introduction 5
1.2.2 Reactive Ion Etching 6
1.2.3 Ion Beam Etching 12
1.3 Lithography 16
1.3.1 Optical Lithography 16
1.3.2 Electron -Beam Lithography 19

References 22

2 ***In-situ* Diagnostic Techniques** 23

2.1 Introduction 24
2.2 Temperature Measurements 24
2.3 Optical Emission Spectroscopy 30
2.3.1 Introduction 30
2.3.2 Chamber Leak Integrity 35
2.4 Laser Reflectometry of Multi-layer Structures 37
2.4.1 Introduction to Reflectometry 37
2.4.2 Maskled Reflectometry 37
2.4.3 Maskless Reflectometry 39
2.5 Chapter Summary 50
References 51

3 **Reactive Ion Etching of III-V Semiconductors with CH_4/H_2 Gas Mixtures** 53

3.1 Introduction to CH_4/H_2 RIE 54
3.2 The CH_4/H_2 Plasma 55

3.2.1 Plasma Phase and Surface Reactions 55
3.2.2 DC Bias with Plasma Composition 61
3.2.3 Chamber Cleanliness 63
3.2.4 Surface Temperature 67
3.3 CH_4/H_2 RIE of AlGaAs 70
3.3.1 Etch Rates and Profiles 70
3.3.2 Induction Time 75
3.4 CH_4/H_2 RIE of InGaAs and InAlAs 78
3.4.1 Etch Rates of InGaAs and InAlAs 78
3.4.2 The Effect of Pressure and Total Flow Rate 80
3.4.3 Selectivity of InGaAs over InAlAs 81
3.4.4 Etch Profiles 84
3.4.5 CH_4/H_2 RIE for Fabrication of an S-SEED Array 90
3.5 Chapter Summary 98
References 101

4 The Addition of O_2 or Cl_2 to the CH_4/H_2 Plasma 104

4.1 The Addition of O_2 105
4.1.1 Introduction 105
4.1.2 Etch Characteristics of InGaAs 106
4.1.2.1 Etch Rates and Profiles with O_2 Content 106
4.1.2.2 Etch Rates with Pressure 109
4.1.2.3 Mask Considerations 110
4.1.3 Etch Characteristics of InAlAs 112
4.1.4 Optical Emission Spectroscopy of the $CH_4/H_2/O_2$ Plasma 113
4.2 The Addition of Cl_2 115
4.2.1 Introduction 115
4.2.2 Etch Characteristics of InGaAs 116
4.3 Chapter Summary 119
References 120

5 RIE of InGaAs with Halogenated Gases 121

5.1 Introduction 122
5.2 RIE of InGaAs with SiCl4 at Elevated temperatures 125
5.3 RIE of InGaAs with HBr and BBr_3 129
5.4 Chapter Summary 133
References 135

6 Damage Assessment Techniques 137

6.1 What is Damage? 138
6.2 Schottky Contact Damage Assessment of AlGaAs 139
6.2.1 The Theory of the Schottky Contact 139
6.2.2 Schottky Covntacts on Etched AlGaAs 142
6.3 Raman Spectroscopy 148
6.3.1 Background Theory 148
6.3.1.1 General 148
6.3.1.2 Binary Semiconductors 148
6.3.1.3 Ternary Semiconductors 151
6.3.2 H_2 and CH_4/H_2 Plasma Treatment of GaAs 153
6.3.3 CH_4/H_2 RIE of InGaAs 157
6.4 Low Temperature Photoluminescence 159
6.4.1 Photoluminescence Theory 159
6.4.2 Photoluminescence of CH_4/H_2 Etched InGaAs 161
6.5 X-ray Photoelectron Spectroscopy 163
6.5.1 Introduction 163
6.5.2 XPS of CH_4/H_2 etched InGaAs 164
6.6 The Transmission Line Model 172
6.6.1 The Transmission Line Model Method 172
6.6.2 TLM Studies of Hydrogenated HEMT Structures 173
6.6.3 Band Structure Modelling 177
6.7 Van der Pauw Measurements 179
6.7.1 The Hall Effect and Van der Pauw's Method 179
6.7.2 Van der Pauw Measurements on δ-doped HEMT Structures 180
6.8 Sidewall Damage to n^+-InGaAs 183
6.8.1 Conduction of Narrow Wires 183
6.8.2 Wire Design 185
6.8.3 Ohmic Contacts 187
6.8.4 Wire Exposure Tests 188
6.8.5 Wire Mask Materials 189
6.8.6 Conductance Measurements of Etched Wires 191
6.9 Chapter Summary 194
References 197

7 Conclusions and Future Work 202

7.1 Instrumentation and Process Monitoring. 203
7.2 RIE with Methane and Hydrogen. 205
7.3 Fabrication of S-SEEDs. 208
7.4 Addition of O_2 or Cl_2 to the CH_4/H_2 plasma. 209

7.5 RIE Induced Damage. 210
7.6 RIE with Halogens at Elevated Temperatures. 214
7.7 Chapter Summary. 214

Chapter 1

Introduction to Semiconductor Device Fabrication Techniques

Chapter Outline

This chapter introduces the reader to the basic concepts of semiconductor device fabrication techniques. Lithography, both optical and electron-beam are discussed, showing how patterns may be transferred into the material underlying the resist by dry etching. Of the many types of dry etching, reactive ion etching is the most relevant to this thesis and described in detail along with the various etch machines used in this study.

1.1 Semiconductor Devices

Today the vast majority of semiconductor integrated circuits are still fabricated on substrates of the group IV element, silicon (Si). The plentiful supply of raw materials, mechanical strength and the ability to closely control the growth of the native oxide make silicon the first choice for mass manufacture of semiconductor devices.

Material	E_g (eV)	μ_n (cm^2/Vs)	μ_h (cm^2/Vs)	m^*/m_0 (electron)	m^*/m_0 (hole)	n_i (cm^{-3})
Si	1.12_i	1,500	450	$0.98_l\ 0.19_t$	$0.16_l\ 0.49_t$	$1.45x10^{10}$
GaAs	1.42_d	8,500	400	0.067	0.082	$1.79x10^6$
InAs	0.36_d	33,000	460	0.023	0.4	-
InP	1.35_d	4,600	150	0.077	0.64	-

Table 1.1
Some properties of important semiconducting materials. i=indirect, d=direct, l=longitudinal, t=transverse (Reference 1.1).

The high effective electron mass in silicon and low mobility make the material unsuitable for fabrication of high speed devices operating at clock speeds of a few GHz and above. The III-V compound semiconducting materials such as GaAs with its high electron mobility are therefore used. For optoelectronic device fabrication GaAs has the benefit of a high radiative recombination efficiency arising from the material's direct band gap, allowing electrons and holes to recombine readily at the zone centre. Optoelectronic devices such as optical modulators, LEDs and lasers may therefore made from III-V materials.

The band gap of the semiconductor can be engineered by alloying two III-V semiconductors e.g. GaAs and AlAs with the band-gap determined by alloy

composition. Alloying AlAs with GaAs to form $Al_XGa_{1-X}As$ will increase the band gap above that of GaAs alone (for x>0.4 the alloy becomes an indirect gap material). Electrons can therefore be confined to materials of narrow band-gap (e.g. GaAs) by barriers formed from wide band-gap materials (e.g. $Al_xGa_{1-x}As$). If the layer of narrow band-gap is thin, comparable with the electron wavelength and is sandwiched between layers of wider band gap, a quantum well (QW) can be formed.

The alloys of InAs and GaAs are particularly important. $In_{0.53}Ga_{0.47}As$ possesses the same lattice parameter as InP and so can be grown upon an InP substrate without the introduction of strain. This material has a low electron effective mass and high mobility (higher than GaAs) and so is favoured for the fabrication of high speed electronic devices. The deliberate introduction of strain into the InGaAs layer by growing a composition with $x \neq 0.53$ may be advantageous. Strain, either compressive or tensile alters the band gap slightly, allowing for fine tuning absorption or emmision bands of the material.

$In_{0.53}Ga_{0.47}As$ is also a direct gap material and emits light in the region of 1.6 μm, within the third optical fibre transmission window. Telecommunications lasers therefore contain layers of $In_{0.53}Ga_{0.47}As$. Analogous with the GaAs/AlGaAs system, barrier materials for InGaAs are formed form the alloy of InAs and AlAs. $In_{0.52}Al_{0.48}As$ is lattice matched to InP with band-gap greater than $In_{0.53}Ga_{0.47}As$. The difference in band gap between $In_{0.52}Al_{0.48}As$ and $In_{0.53}Ga_{0.47}As$ is greater than that of $Al_{0.3}Ga_{0.7}As$ and GaAs resulting in higher carrier concentrations being formed in the now higher confinement of the 2-dimensional electron gas (2DEG) at the hetrojunctions of InGaAs/InAlAs electronic devices. The lack of DX centres in $In_{0.52}Al_{0.48}As$, unlike $Al_xGa_{1-x}As$, reduce effects such as persistent photoconductivity.

It should be noted that at the time of writing $In_XGa_{1-X}As_YP_{1-Y}$ is a far more important optoelectronic material for fabrication on InP substates. $In_XGa_{1-X}As$ is only lattice matched ti InP at one compostition, x=0.53. Only one band gap can therfore be formed at this lattice constant. $In_XGa_{1-X}As_YP_{1-Y}$ can be looked on as the alloy of $In_{0.53}Ga_{10.47}As$ and InP thus over all the possible compositions and band gaps the material will always lattice mateched to InP. $In_XGa_{1-X}As_YP_{1-Y}$ is often to be found in optoelectronic devices, such as when sandwhiched between the lower refractive index InP to form waveguides.

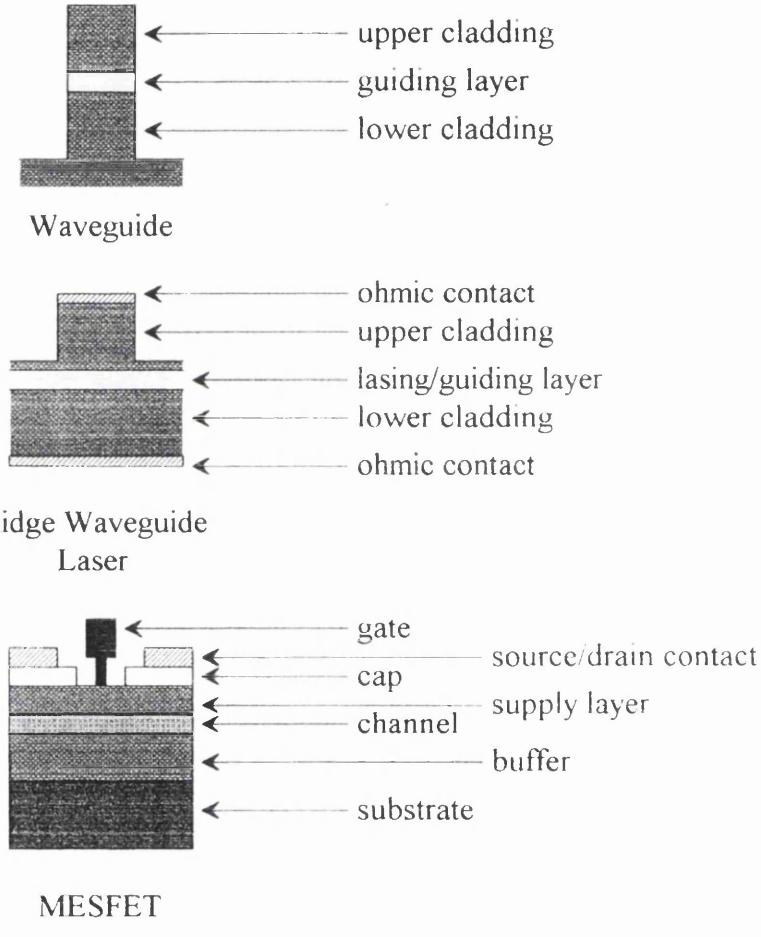

Figure 1.1
Schematic of three semiconductor devices that require at least one stage of etching during fabrication. (a) ridge wave-guide, (b) ridge wave-guide laser and (c) gate recess of a metal-semiconductor field effect transistor.

Fabrication of semiconductor devices may require one or more stages in which material is to be removed by etching in a specified area. Etching may be required in the formation of passive devices such as waveguides (Figure 1.1a), active devices such as lasers and field effect transistors (FET) (Figure 1.1b, c), or to remove material between devices so as to electrically isolate them. To prevent etching of areas where material is to remain a protective coating (a mask patterned by lithography) is laid down upon the semiconductor surface.

1.2 Dry Etching

1.2.1 Introduction

In the infancy of the semiconductor industry all etching was performed by using liquid chemical solutions. Wet etches as a whole tend to etch isotropically, that is to say etch rates are equal in all directions with the result that the etch surface undercuts the mask and produces a rounded profile. This type of etch makes it difficult to precisely control feature widths and does not allow for the extreme close packing of devices onto the surface of the wafer. Anisotropic etches may be formed using a wet chemical solution. If the chemical does not attack one particular crystal plane, or etches it only slowly compared to other planes then anisotropic wall profiles are formed. Beacuse of the general high etch rates achieved with wet chemical processing and poor control of reactant concentration, uniformity of etch depth across the wafer is poor.

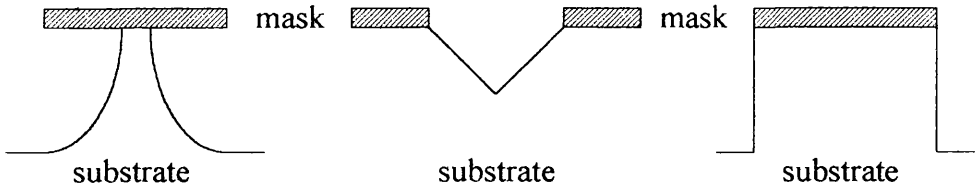

Figure 1.2
Schematic of (left) isotropic wet etch showing undercutting of the mask and a rounded etch surface, (centre) an anisotopic etch due to crystalographic effects and (right) anisotropic dry etch with vertical walls and no undercutting.

The development of dry etching processes over the past few years has allowed for a greater versatility to be introduced into the etch process. Dry etching techniques will be described at greater length in subsequent sections but the point of interest at this stage is that these processes may generally produce anisotropic etching (etch rates are unequal in the vertical and horizontal directions).

1.2.2 Reactive Ion Etching

Dry etching is so termed because the etch is performed without a liquid chemical. The reactant species are in the gas phase with etching typically performed in a low pressure vessel in the range 1-100 millitorr. Gas is introduced into the chamber and a plasma struck between the two electrodes. Reactive positive ions are created within the plasma by electron impact and chemical reaction and are electrostatically extracted and directed to the surface of the semiconductor where the etch reaction takes place. Volatile product species are formed on the surface which can then pumped away. In reactive ion etching machines one electrode is earthed, termed the anode and the other driven by an rf power supply operating at 13.56 MHz and is termed the cathode. The polarity of the cathode follows that of the rf signal,

resulting in electron and than ions being alternately attracted to or repelled from the cathode. The less massive electrons are more mobile than the massive ions, resulting in a greater flux of electrons than ions to the cathode during the appropriate half-cycle of the applied voltage. The presence of a blocking capacitor allows negative charge to build up on the cathode until the flux of electrons and ions to the cathode is balanced by attractive/repulsive forces. The DC potential of the cathode is termed the DC self bias.

A simplistic approach [1.2] using gas-phase thermodynamic principles, shows that the dc potential of the cathode is related to the areas of the anode and cathode through the relationship;

$$V_C \propto \left(\frac{A_A}{A_C}\right)^n \qquad \text{(eqn. 1.1)}$$

where V_C is the cathode dc potential, A_A and A_C the areas of the anode and cathode respectively and n=4. In realistic systems $n \neq 4$ but is in the range $1<n<2$.

An alternative approach to the problem of the relationship between the physical areas of the electrodes equates to the dc bias formed at the cathode has been proposed by Song *et al* [1.3]. It has been shown that the dc bias V_{DC} is related to the ac voltage, V_0, applied at the cathode and the area of cathode and anode, A_C and A_A respectively.

$$V_{DC}=V_0\sin[(\pi/2)(A_A-A_C)/(A_A+A_C)] \qquad \text{(eqn 1.2)}$$

which gives the well known relationship that $V_{DC}=0$ for $A_A=A_C$.

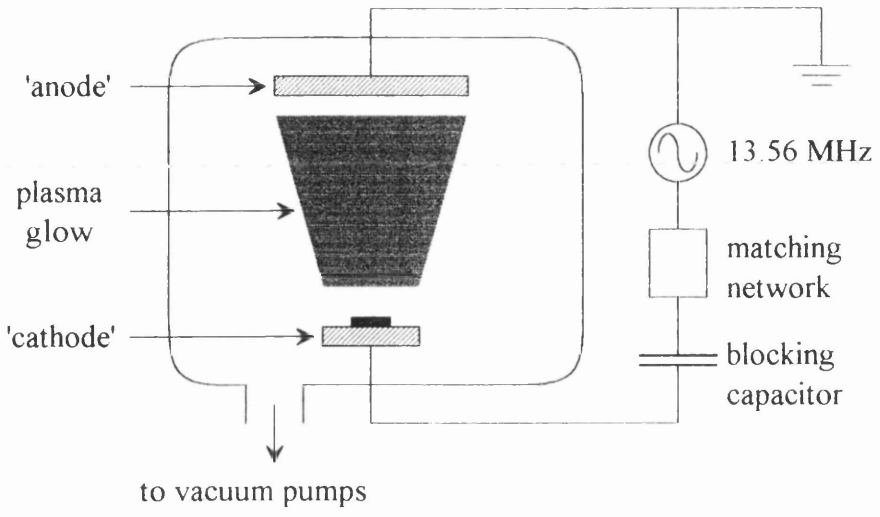

Figure 1.3
Schematic Diagram of a Reactive Ion Etcher.

Within the etch chamber the region immediately above the cathode is termed the dark space in which no plasma exists but an electric field is present due to the difference in potential of the plasma (slight positive potential) and the cathode (-ve DC self bias). The dark space is a result of the difference in mobilities of ions and the electrons. The reactive ions being formed in the plasma at the edge of the dark space or being transported to the edge of the dark space can be accelerated across the dark space impacting on the surface of the test sample or cathode. The magnitude of the DC self bias can be used as a guide to the energy the ions gain whilst crossing the dark space. If the ion leaves the plasma with thermal energy and crosses the dark space without undergoing any scattering processes the energy gained by the ion will be the difference in potential between the plasma and the potential of the sample being etched. Scattering processes within the dark space results in ions at lower energies and lead to the formation of energetic neutral species. Fuller account of topics relating to dry etching can be found in references 1.2 and 1.4.

The design of the etch chamber can influence the properties and composition of the plasma and the DC self bias created for a given rf power. For this reason the etch characteristics of materials will vary form one reactor design to another. In this thesis several different design of reactor were used as illustrated in Figure 1.4. The Oxford Plasma Technology (OPT) system comprises of the upper anode (diameter 27 cm) and the lower cathode (diameter 17 cm) separated by a gap of 5 cm. The sidewalls of the chamber are made from quartz. An earthed shield around the cathode prevents parasitic discharges concentrating the plasma above the cathode. All metal surfaces exposed to the plasma are anodised in order to minimise etching of the metal.

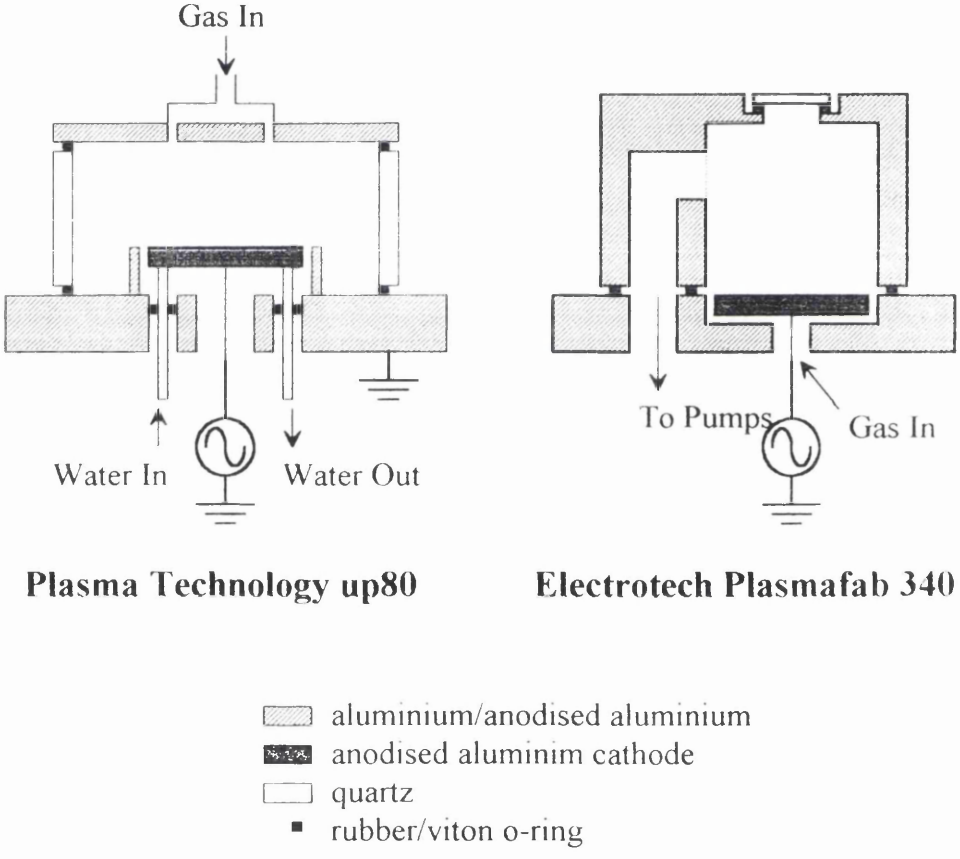

Figure 1.4
Schematic of Oxford Plasma Technology μp80 and Electrotech Plasmafab 340 reactive ion etch machines.

The Electrotech (ET) system is constructed with all aluminium reactor walls and a cathode diameter of 14 cm. All the walls act as the anode with the result that for a given rf power the DC self bias of the ET system will be much greater than with the OPT system. Both machines are driven by 300 W rf generators operating at 13.56 MHz and pumped with a Roots/Rotary pump combination.

Under ideal conditions the extracted ions would travel across the dark space in a direction normal to the surface of the sample to be etched. On reaching the surface the chemical reaction and desorbtion of products would occur instantly. The mask would not etch and no deposition from the plasma would occur resulting in the perfect anisotropic etch profile (Figure 1.5a). In practise scattering of ions by neutral species within the dark space or from the etch surface result in ions impinging upon the sidewalls creating a lateral etch rate (Figure 1.5b) which causes undercutting of the mask. Deposition of material onto the mask (Figure 1.5c) causes the mask to grow in dimension. The increased size of the mask will cause areas that were originally unmasked to become masked halting etching at that point and forming an overcut profile. Overcut profiles can be created by the deposition of material onto the sidewall (Figure 1.5d) again causing the masked region to grow in dimensions. The mask material may itself be etched by the reactive ions (Figure 1.5e). As time progresses the mask is reduced in all dimensions exposing new material at the uppermost surface of the sample to ion bombardment. This material can now be etched in the same way as material in originally unmasked regions.

During the etch one or more of the processes outlined above may take place. The resultant etch profile can therefore be very complex. Figure 1.6 shows such a complex etch profile in CdTe after etching with CH_4/H_2 through a holographically defined mask. Scattering of reactant species within the confines of the trench, either by collision with other gas phase species or with the walls and etch surface lead to the formation of a near circular profile.

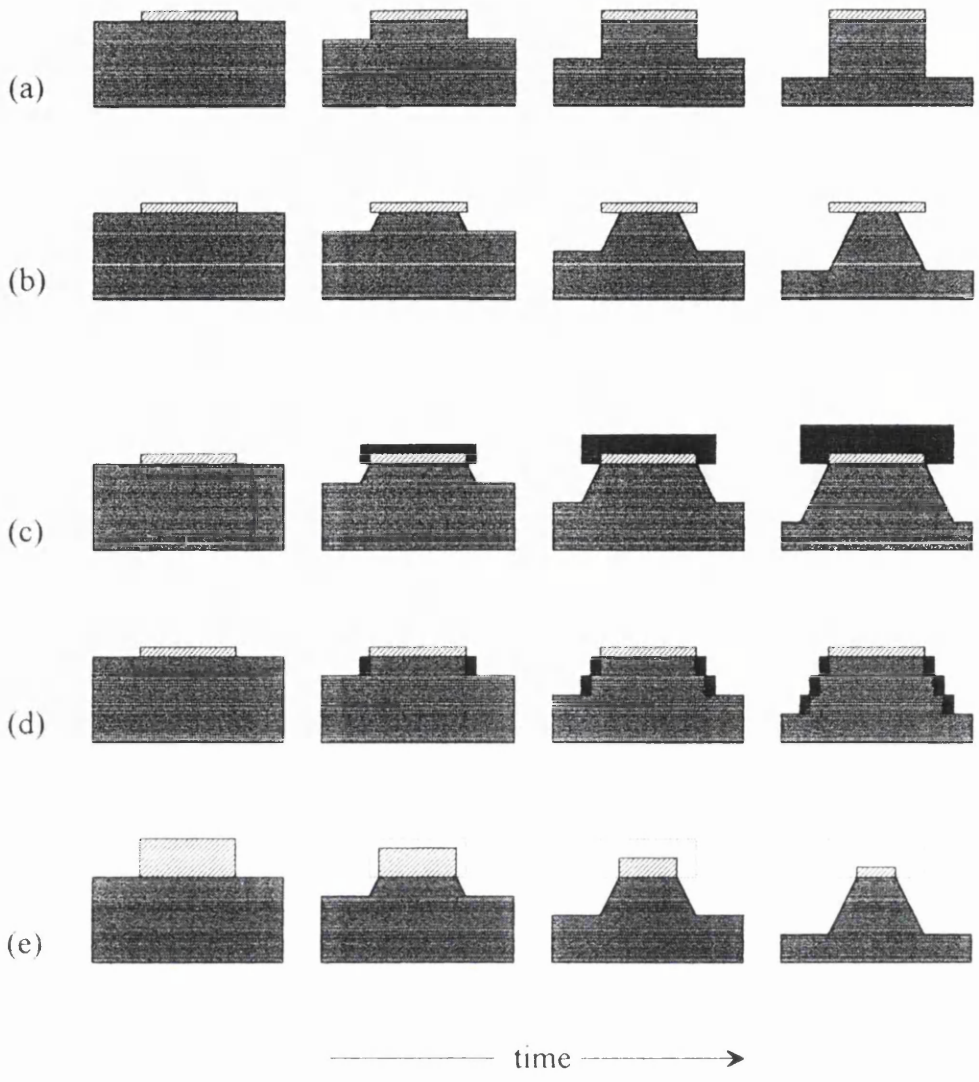

Figure 1.5
Formation of wall profiles during RIE. (a) truly anisotropic, (b) with lateral etching causing undercutting of the mask, (c) shadowing of the etch surface by the growth of polymer upon the mask, (d) deposition upon the sidewall and (e) etching of the mask.

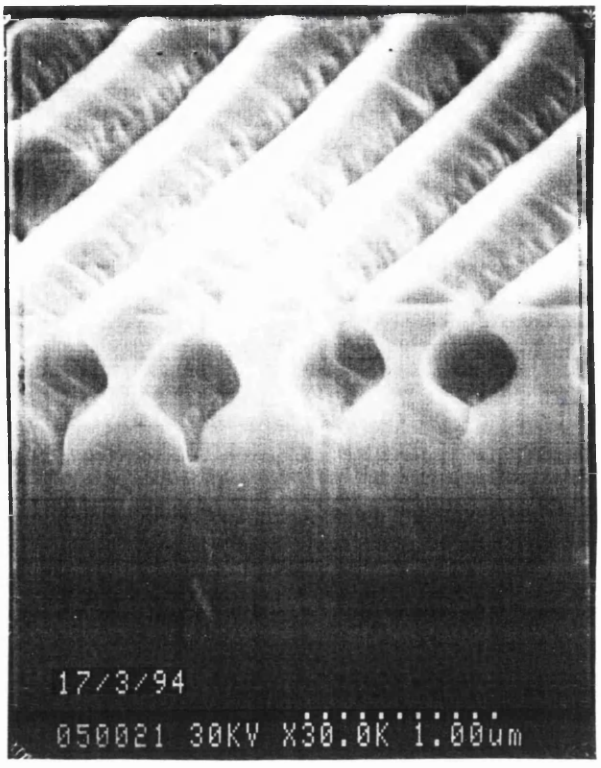

Figure 1.6
CdTe etched with CH_4H_2 showing the effect of the width of the open area on etch profile and rate.

1.2.3 Ion Beam Etching

So far etching has only been described in terms of reactive ions removing material by ion assisted chemical reactions at the surface of the semiconductor. Etching can also be implemented by sputtering, a process where material is removed by physical bombardment alone. Consideration of the loss of energy as the ion penetrates the crystal lattice by Stewart and Thompson [1.5] shows that sputter rate can be linked to the angle the incident ion beam makes with the normal to the surface of the material.

The sputter rate is assumed to depend upon the amount of energy the ion deposits within the surface layer of thickness R, where R is of the order of 10 Angstrom. The surface layer is introduced because although the ion may have enough energy to release an atom from deep within the lattice that atom will then be blocked from leaving the crystal by the large layer overlying it.

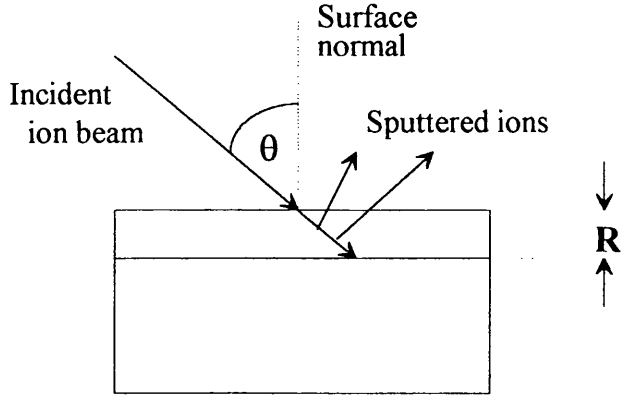

Figure 1.7
Schematic diagram of ion beam sputtering geometry.

Elementary analysis thus shows that the energy lost in this surface layer is;

$$\int_0^{R\sec\theta} \frac{dE}{dx} \qquad \text{(eqn. 1.3)}$$

where is the angle to the surface normal, E the ion energy in the beam and x the depth into the surface. Assuming that the surface potential energy is of the inverse square form then;

$$\frac{dE}{dx} = \left(\frac{\pi a}{2}\right)^2 nE_a \qquad \text{(eqn. 1.4)}$$

Here a is the Bohr radius, n the density of atoms per unit volume and E_a the value of E that allows the ion to approach to a distance of $a=a_0/(Z_1Z_2)^{1/6}$. Z_1 and Z_2 are the atomic numbers of ion and atom in the crystal.

Thus S the yield per ion at any angle is;

$$S(\theta) = \left(\frac{\pi a}{2}\right)^2 nE_a R\sec(\theta) \qquad \text{(eqn. 1.5)}$$

where s is the yield per ion. The sputter yield follows this relationship well for small angles but a maximum is encountered in the sputter yield with the yield falling as the angle of incidence becomes more acute and it becomes harder for the ion to penetrate the lattice. The sputter rate falls to zero at near to 90^0 at which angle the ions are completely reflected from the surface potential.

Lindhard [1.6] shows that the angle of the maximum sputter yield is given by;

$$\left(\frac{\pi}{2-\theta_m}\right)^2 = \left(\frac{5\pi.a_0^2.n^{2/3}Z_1.Z_2.E_R}{E.Z_1^{2/3}Z_2^{2/3}}\right) \qquad \text{(eqn. 1.6)}$$

Silicon samples were etched with an Ar beam with a total operating pressure of $9x10^{-4}$ millibar, a beam current of 0.8 mA and at a beam voltage of 500V.

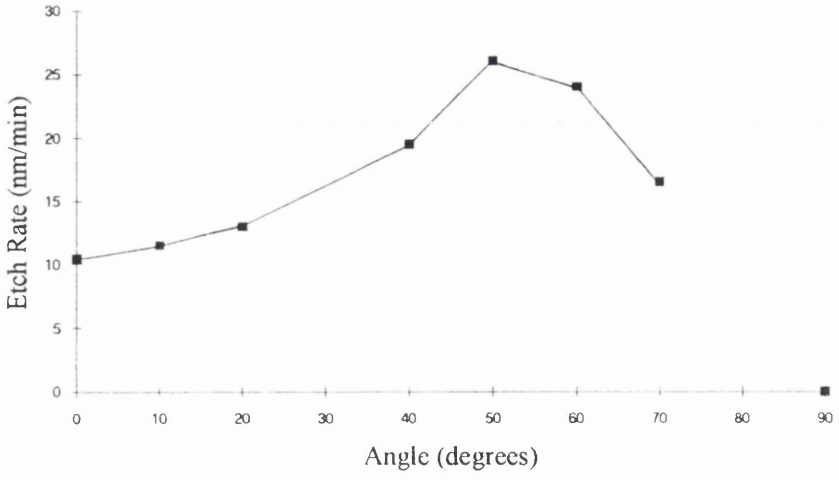

Figure 1.8
Sputter rate for silicon in 500 V Ar^+ IBE.

Using the theory of Lindhard the maximum sputter rate should occur at an angle of 57.5^0. The experimental data presented in Figure 1.8 shows sputter rate with incident angle, the maximum rate being in good agreement with theory.

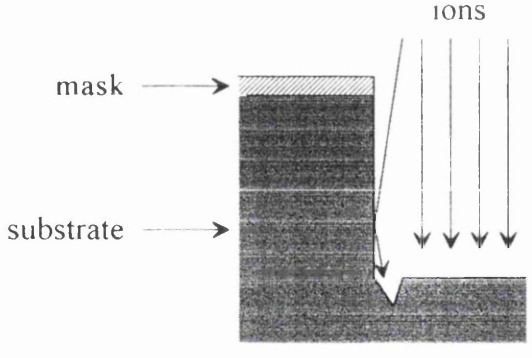

Figure 1.9
Formation of a trench at foot of sidewall.

The relationship between incident angle and sputter yield suggests that at angles approaching 90^0 the majority of ions are reflected from the surface. This has important implications when etching produces features with near vertical walls. Ions

can be reflected from the walls with the result that at the foot of the wall the flux of ions is higher than in open areas. The extra flux enhances etching so a trench is formed. The presence of trenches is discussed in chapter four when chlorine is added to the methane/hydrogen gas mixture.

1.3 Lithography

1.3.1 Optical Lithography

Lithography is the means by which etch masks, ohmic contacts and dielectric layers patterns are transferred or patterned. The pattern to be transferred is formed on a transparent plate with areas that are opaque to the illuminating radiation. The regions that do not transmit radiation can be either chromium (reflective) or ferrous oxide (absorptive). To transfer the pattern with a scale of 1:1 the mask plate is brought into hard contact with a layer of resist that has previously been spun onto the sample and baked. The viscosity of the liquid resist and the spin speed combine to determine the thickness of the resist. Baking the resist removes the solvents.

The resist is exposed to the radiation (usually in the UV region where the shorter wavelength allows for smaller, closer packed features to be formed) and developed in the appropriate wet chemical developer. A resist that is removed on developing where the illumination has taken place is termed a positive resist. A negative resist remains where illumination occurred.

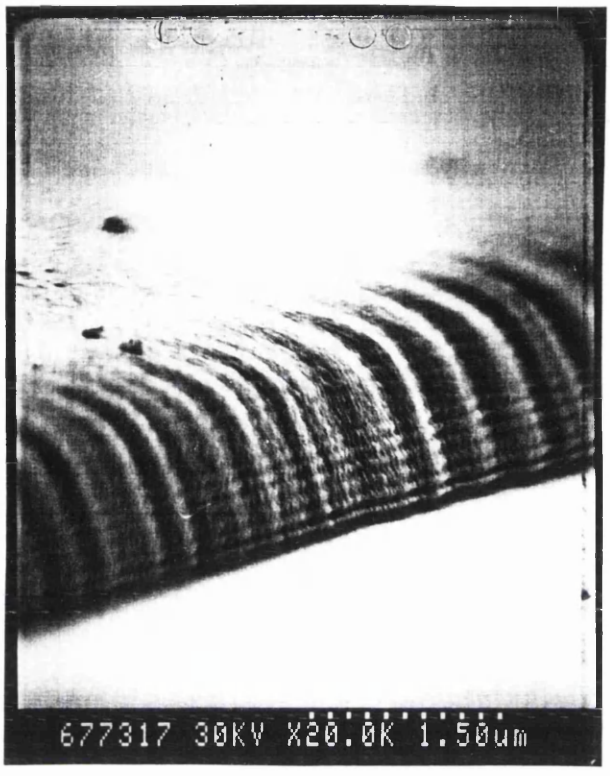

Figure 1.10
Micrograph of patterned Shipley S1400-31 photoresist showing standing waves caused by reflections at the resist substrate boundary.

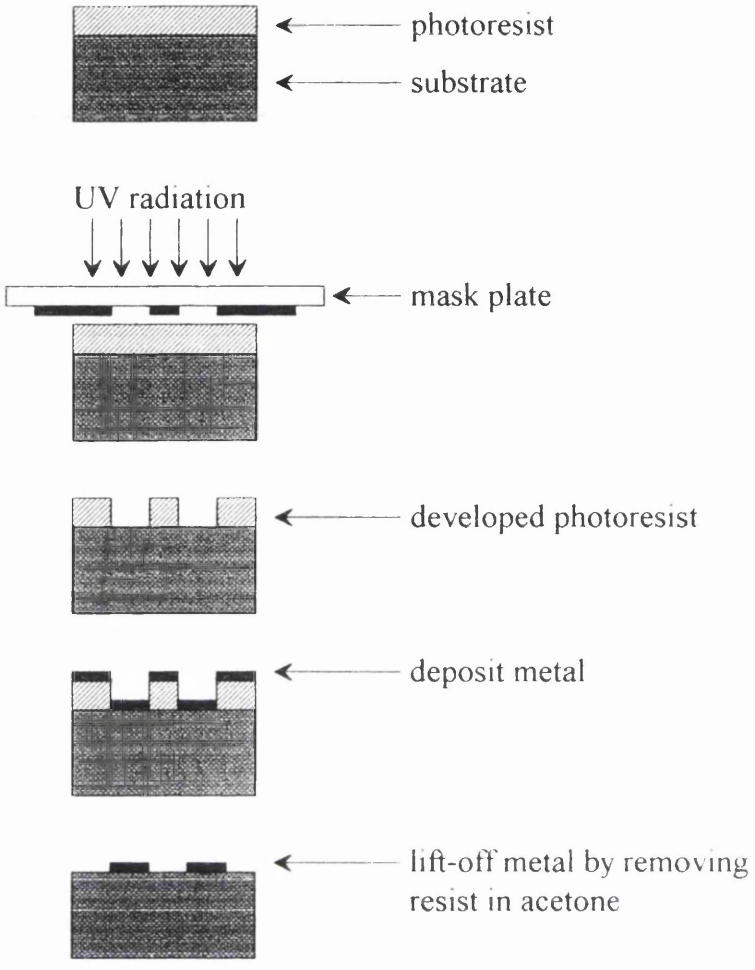

Figure 1.11
Schematic of metal mask formation by lift-off using a photoresist mask.

Depositing a layer of metal onto the patterned resist and dissolving the resist in acetone will allow the metal that was on top of the resist to float free leaving the metal deposited straight onto the sample to remain in place. This is the technique referred to as lift-off. For the procedure the resist must be at least 3 time the thickness of the metal layer and ideally a great deal more. The walls of the resist need to be as vertical as possible to ensure as little metal is deposited upon them and that the edges of the metal pattern are clean and true. As the dimensions of patterned

features decreases it becomes increasingly more difficult to maintain these requirements for good lift-off. Electron-beam lithography with the ability to write features down to sub 10 nm sizes and the use of bi-level resists overcomes many of the problems associated with optical lithography for small feature sizes.

1.3.2 Electron-beam Lithography

Electron-beam (e-beam) lithography is similar in many ways to optical lithography except that a well collimated beam of mono-energetic electrons are used as the irradiating source. The electrons of energy for example, 50 KeV have a much shorter wavelength than UV light suffering less diffraction and are able to be focused more tightly into a spot. E-beam lithography can therefore produce smaller feature sizes than possible with optical lithography.

Where the e-beam strikes the poly-methyl methacrylate (PMMA) resist the polymer chains are broken down which may then be dissolved away in a solution of methyl iso-butyl ketone (MIBK) diluted with iso-propyl alcohol (IPA). Two molecular weights of PMMA are available. A low molecular weight (LMW) PMMA supplied by BDH and hence referred to as BDH and a high molecular weight (HMW) version named Elvesite. To break the same type of bond in the PMMA molecule will require the same energy for both BDH and Elvesite. BDH because of its LMW will require however a lower electron dose than Elvesite to break the molecule down to a size where the developer can remove the exposed material. For a given amount of charge deposited into the resist by the e-beam, the Gaussian profile of electron density in the beam will result in narrower line widths in Elvesite than those formed in BDH. By spinning a thin layer of Elevsite onto an already prepared layer of BDH the resulting resist profile upon writing and development shows the HMW resist

over-hanging the underlying LMW resist. The subsequent lift-off of a metal mask produces a more precise pattern transfer.

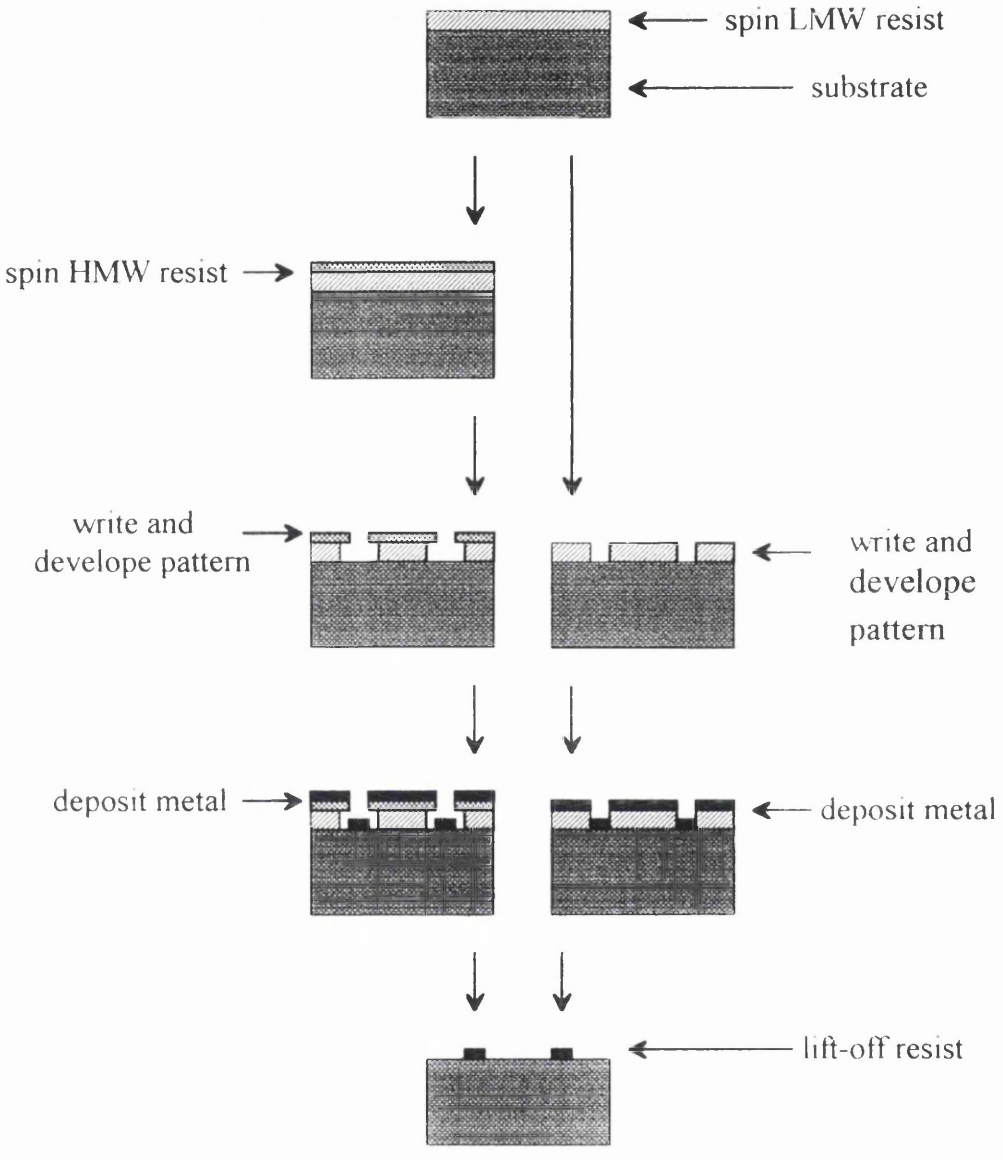

Figure 1.12

Schematic of mask patterning using lift-off with a single low molecular weight (LMW) and bi-level low and high molecular weight (HMW) electron beam resists.

The majority of electrons in the beam pass through the resist with only slight scattering then pass into the substrate. The high density of the substrate material

compared to the organic resist causes many primary electrons to be scattered and secondary electrons to be created. These electrons are scattered over a large distance in all directions and can pass through the resist exposing it further. These electrons can effect resist up to several microns from their first point of entry into the substrate. A pattern written close to another will therefore be effected by scattered electrons from the first pattern. These proximity effects are observed on developing the resist with resulting changes to the desired pattern.

References

[1.1] "Physics of Semiconductor Devices" Second Edition
S.M. Sze. John Wiley and Sons (1981)

[1.2] "Glow discharge Processes"
B.N. Chapman. John Wiley and Sons (1980)

[1.3] Y.P. Song, D. Field and D.F. Klemperer, "Electrical potentials in RF discharges", *J. Phys. D.*, 1990, **23**, pp.673-681.

[1.4] "Dry etching for VLSI"
A.J. van Roosmalen, J.A.G. Baggerman and S.J.H. Brader. Plenum (1991)

[1.5] A.D.G. Stewart and M.W. Thompson, "Microtopography of surfaces eroded by ion-bombardment", *J. Mater. Sci.*, 1969, **4**, pp.56-60

[1.6] J. Lindhard, *Matt. Fys. Medd.*, 1965, **34 (14)**

Chapter 2

In-situ Diagnostic Techniques

Chapter Outline

Three diagnostic techniques for monitoring conditions during the etch process are introduced in this chapter. The surface temperature of the samples are made using a Fluoroptic Thermometer. Measurements have been made during the etch and can provide information upon mask suitability. Optical emission spectroscopy has found a role in monitoring the leak integrity and cleanliness of the etch chamber whilst laser reflectometry has been demonstrated to be a powerful tool for determining the precise position of the etch surface within a multi-layer wafer.

2.1 Introduction

Analysis of the environment in which reactive ion etching leads to an insight into the precise conditions within the plasma and at the etch surface during etching. Such analysis and the need to accurately determine the etch end-point requires the use of specialised techniques. In-situ techniques provide the ability to monitor plasma and gas-phase species present within the etch chamber allowing for optimisation of the plasma to obtain the desired conditions in which to perform the etch. Such techniques can also provide for a fast and highly sensitive method of monitoring the integrity of the etch chamber allowing for the early diagnosis of problems.

A technique that uses metal probes with either electric or magnetic fields would alter the condition of the plasma and hence change the system under investigation. The physical presence of an object in the chamber may also shadow the surface of the sample under investigation from the plasma. This object would then be acting as a mask. For these reasons non-contact methods external to the etch chamber have been used as far as possible to investigate etching mechanisms and enviroments. Although the temperature measurement technique was indeed a contact method, it was only used to gain general information about surface temperatures and not used whilst etching devices.

2.2 Temperature Measurements

A chemical reaction in which the rate of reaction is related to the concentration of a reactant species in a linear fashion, can be described in terms of a rate equation.

Rate of reaction = k [A] (eqn. 2.1)

where k = k(T) the temperature dependent rate constant and [A] the concentration of reactant A (moles per unit volume). This is termed a reaction of the first order. Under the correct conditions reactive ion etching can occur in the flow rate limited regime where etch rates are limited by the supply of reactant species to the etch surface. For examples of etching in the flow rate limited regime see section 3.4.2. The rate of reaction is dependant on the flux (equivalent to concentration for liquid solutions) of reactant species and can thus be classified as a first order reaction. In 1889 Arrhenius recognised that the rate constant typically behaved in an exponential manner with increasing temperature. Empirically this can be expressed as

$$k=C\exp\left(\frac{-E_a}{RT}\right) \quad \text{(eqn. 2.2)}$$

where C is the pre-exponential factor, E_a the activation energy of the reaction and R the ideal gas constant ($R = k.N_A$ with k Boltzman's constant and N_A Avogadro's number) and T the absolute temperature.

$$\text{Rate of reaction} = [A].C.\exp\left(\frac{-E_a}{RT}\right) \quad \text{(eqn. 2.3)}$$

The term [A]C can be alternatively expressed using a new rate constant for the reaction, R_0. A fuller description of chemical reactions and their rates of reaction can be found in reference 6.1 or any of the wide range of physical chemistry text books.

Reactive ion etching as the name implies involves chemical reactions at the surface that is exposed to the plasma, and thus to aid in understanding the surface reactions it is useful to gain an insight into the temperature of the etch surface. In a simple system an alteration to the surface temperature can bring about the regime

where one chemical reaction may be favoured over another, changing the product species with the result that there is a change to the etch behaviour. Such a change in reaction chemistry can be clearly seen when the logarithm of the etch rate is plotted against the inverse of the absolute temperature using an Arrhenius plot. The transition from one reaction type to the other will be observed by a discontinuity in the slope of the plot, with the chemical activation energy of the reaction being proportional to the slope.

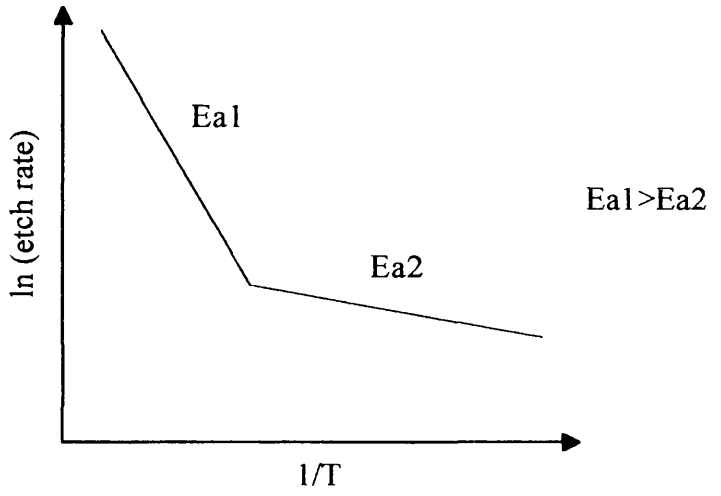

Figure 2.1
An Arrhenius plot showing a change in reaction rate with temperature

It is important to have knowledge of surface temperatures when etching with a photoresist or other organic material as the etch mask. These masks may become soft and even flow if excessively heated leading to poor pattern transfer, wall profile and etch surface morphology. A knowledge of the surface temperature allows for best use of the available masking materials to be made.

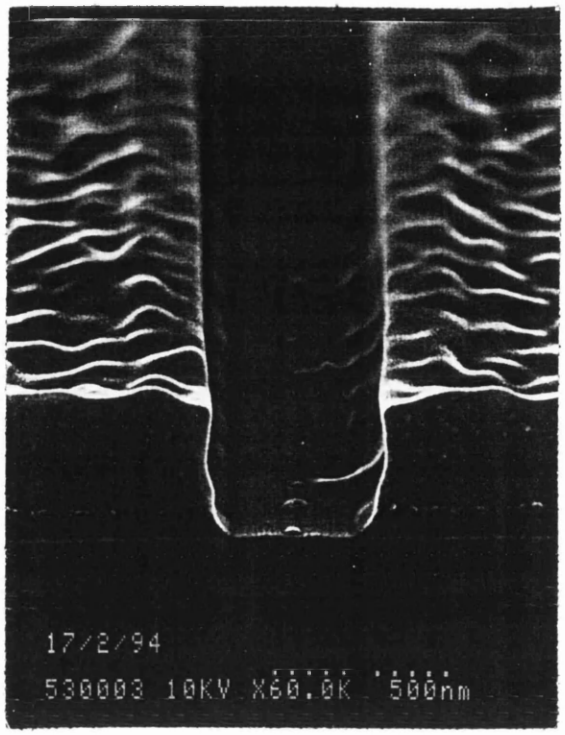

Figure 2.2
Self-aligned gate recess and T-gate mask in PMMA etched in $SiCl_4$ at 150 ^{0}C showing etching of the resist mask due to too high an etch temperature

Surface temperature measurements were made possible using a Luxtron Model 755 fluoroptic thermometer system. An absolute measure of the temperature is obtained by placing a phosphor in intimate contact with the surface under investigation. The fluorescence decay time of the manganese-activated magnesium fluorogermanate phosphor changes with temperature. Bonding the phosphor to the end of a quartz optical fibre allows for excitation of the phosphor by a pulse of blue-violet light generated by a filtered xenon flashlamp. The decay time of the deep red fluorescence is measured within the instrument and the temperature of the phosphor calculated.

A MIW-X wide range probe operational over the temperature range -195 ^{0}C to +300 ^{0}C was used. The fibre is coated with PFA Teflon which provides an inert

outer surface and is strengthened with Kevlar cabling. The probe tip has a maximum outside diameter of 1.0 mm and hence a small thermal mass ensuring little disturbance of the surface temperature and a fast response to a change in surface temperature.

The fibres are circular in cross-section so easily passed into the chamber using a Swagelok® feed-through with the vacuum seal being made with a rubber o-ring. The tip of the probe is placed in contact with the sample surface under a small amount of pressure ensuring the best thermal contact possible.

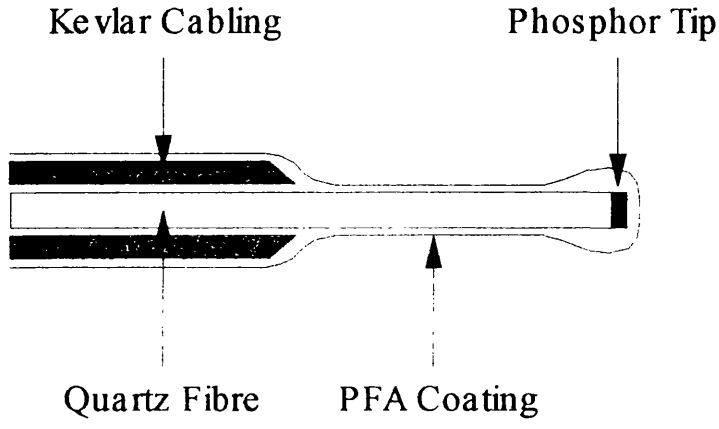

Figure 2.3
Schematic diagram of the MIW-X wide range probe.

The probe is however primarily designed to assist in the measurement of bulk materials where the tip is fully immersed in the medium under investigation. The manufactures claim that the true temperature may be in the region of 5-7 ^{0}C higher than the measured temperature for surface applications at 100 ^{0}C and 10-15 ^{0}C at 200 ^{0}C. The offsets approximately double when working under vacuum.

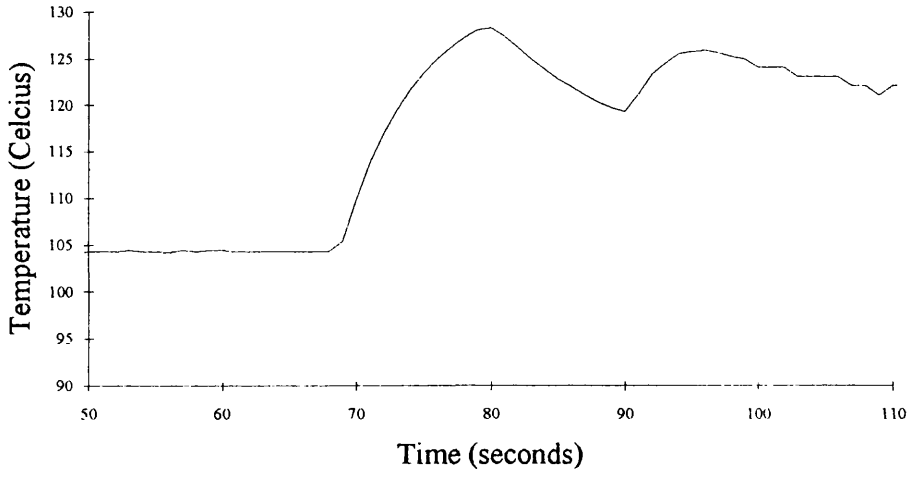

Figure 2.4
Cathode temperature during a chamber vent cycle using an oil bath temperature of 180 ^0C .

The effect of the relationship between measured temperature and the actual temperature of a sample as the environment in which measurements are being made can be clearly demonstrated if the cathode temperature is monitored whilst the chamber is vented from base pressure to atmospheric pressure with dry nitrogen gas. Under vacuum the probe registers a cathode temperature of 105 ^{0}C for an oil bath temperature of 180 ^{0}C. As soon as the vent gas is introduced into the chamber the temperature is seen to rise by 22 ^{0}C over a few seconds. This rise can be attributed to the increased thermal contact between the probe tip and the cathode caused by the improved heat transfer by conduction in a higher pressure gas.

2.3 Optical Emission Spectroscopy

2.3.1 Introduction

Excited atomic, ionic and molecular species are produced within the glow discharge by collisions with energetic electrons. The collision process can have one of several outcomes;

atomic or molecular excitation:

$$X+e^- \longrightarrow X^*+e^- \qquad \text{(eqn. 2.4)}$$

molecular excitation and dissociation:

$$X+e^- \longrightarrow Y^*+Z+e^- \qquad \text{(eqn. 2.5)}$$

The excited atom, molecule or ion may then lose energy by the emission of a characteristic photon.

Other processes can occur within the glow discharge that result in the formation of species that are not in an excited state.

Atomic or molecular ionisation:

$$X+e^- \longrightarrow X^++2e^- \qquad \text{(eqn. 2.6)}$$

Molecular dissociation:

$$X+e^- \longrightarrow Y+Z+e^- \qquad \text{(eqn. 2.7)}$$

Molecular dissociative ionisation:

$$X+e^- \longrightarrow Y^++Z+2e^- \qquad \text{(eqn. 2.8)}$$

Excitation of the species within the glow discharge may also be accomplished by stimulated absorption of a photon. Under typical conditions found in the reactor chamber the electric field strength is however too weak due to the low photon density to allow stimulated absorption (or stimulated emission) to become significant.

Under steady state conditions the excitation rate of a species is in direct proportion to the electron collision rate. If the lifetime of the excited state is short in comparison to the time between electron collisions then the intensity of a transition will be proportional to the density of species within the glow discharge.

Transitions from atomic species are characterised by narrow lines as the electron changes from one well defined electronic state to another i.e. a change from an initial principle quantum number to another of lower energy. Such transitions produce spectral lines characterised by very narrow line widths e.g. the Hβ and Hγ lines of atomic hydrogen which can be seen in the plasma spectra of Figure 2.5. Molecular species are characterised by more complex transitions and hence emission spectra. Molecules possess a greater number of degrees of freedom than atoms due to rotation of the whole molecule or vibrations between nuclei along the directions of chemical bonding. Molecular transitions give rise to three distinct emission types. Emission continua such as that associated with hydrogen which peaks at 360 nm but stretches for 100 nm each side of the maxima. Molecular bands which are composed of many closely spaced emission lines that merge over a small wavelength region to give an emission band e.g. the many CO_2 bands of Figure 2.6 extending from 330 nm to beyond 500 nm. Finally molecular transitions can result in singlet, doublet and

triplet spectral lines. The two lines associated with CO_2^+ at 288.3 and 289.6 nm are in fact two closely spaced doublets i.e. four emission lines in total.

A Sofie Instruments MultiSEM 340 OES system was used. Light from the glow discharge is collected by a quartz optical fibre, the light passing out of the chamber through a quartz window. A quartz window is used because of the low absorption of quartz over the range of wavelengths (200-680 nm) detectable by the monochromator. The light is then passed to the 0.35 m long monochromator containing a grating with 2400 grooves mm^{-1}. The monochromator has a variable slit-width of between 50 and 500 μm giving an ultimate resolution of 0.01 nm with the narrowest slit. The grating rotated under computer control allowing light of the appropriate wavelength to be detected by a Hamamatsu R928 photomultiplier. For a lower dark count and thus better signal to noise ratio the temperature of the photomultiplier can be lowered using a Peltier effect cooler which itself is reduced in temperature by chilled water.

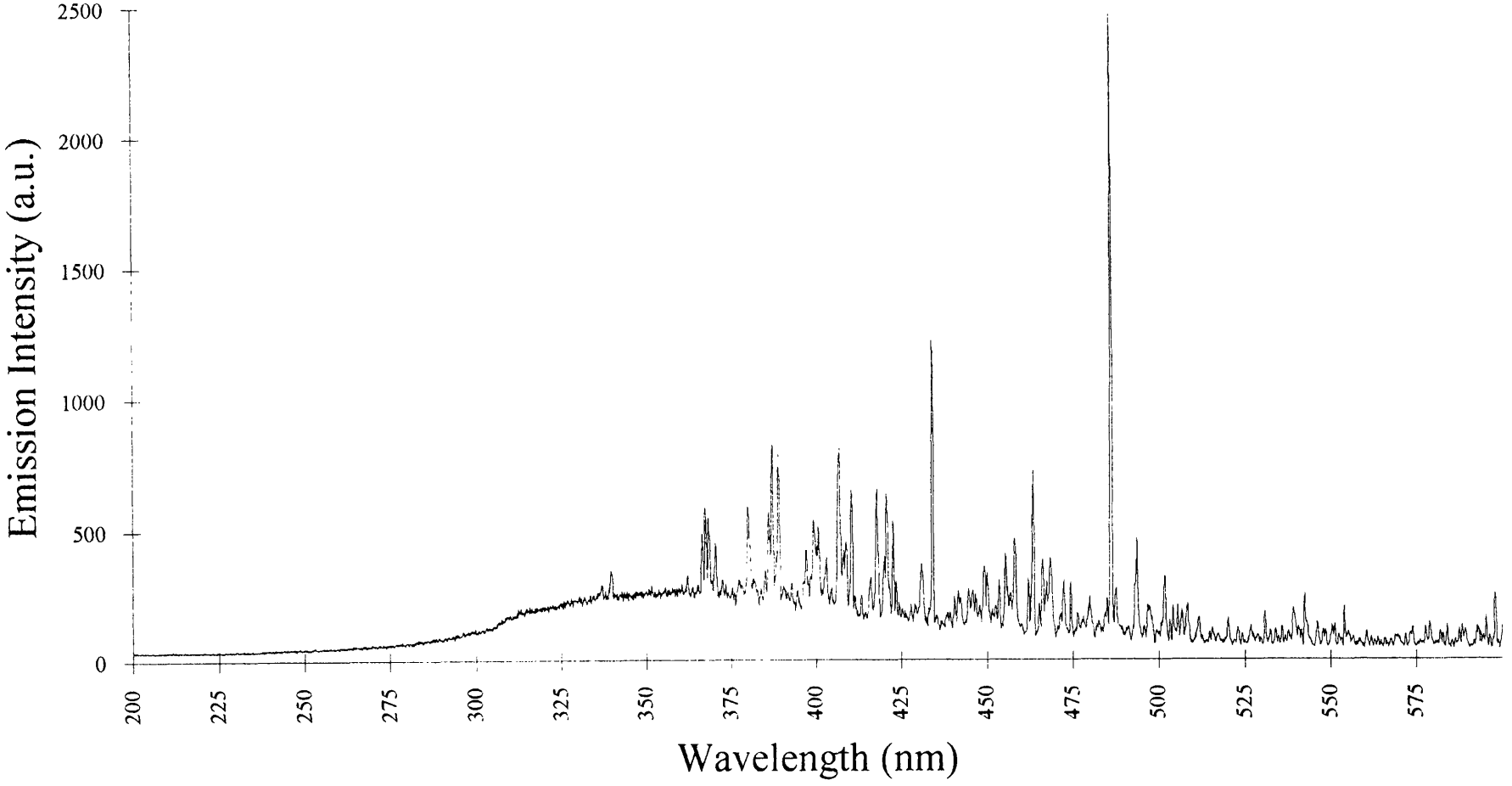

Figure 2.5 Optical emission spectra of hydrogen

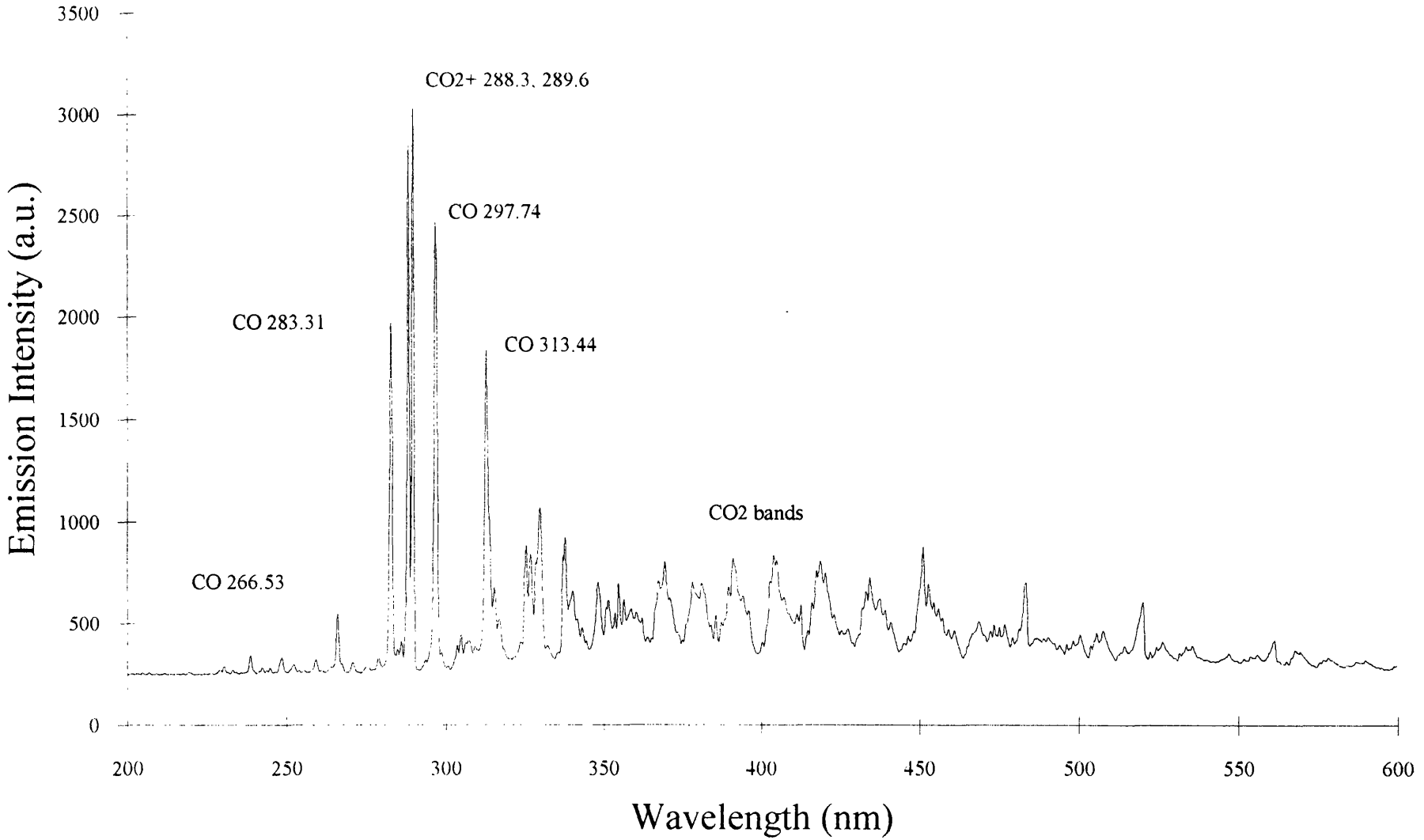

Figure 2.6 Emission Spectra of 25 sccm CO2 at 20 mT and 50 W in ET340

2.3.2 Chamber Leak Integrity

A common problem with non-loadlocked etching machines is damage that can be caused to the rubber o-rings that form the vacuum seal between the moving parts of the chamber. Damage caused to the o-ring such as a scratch or through fatigue or a bad vacuum seal due to dirt becoming trapped by the o-ring can result in a leak of air into the chamber.

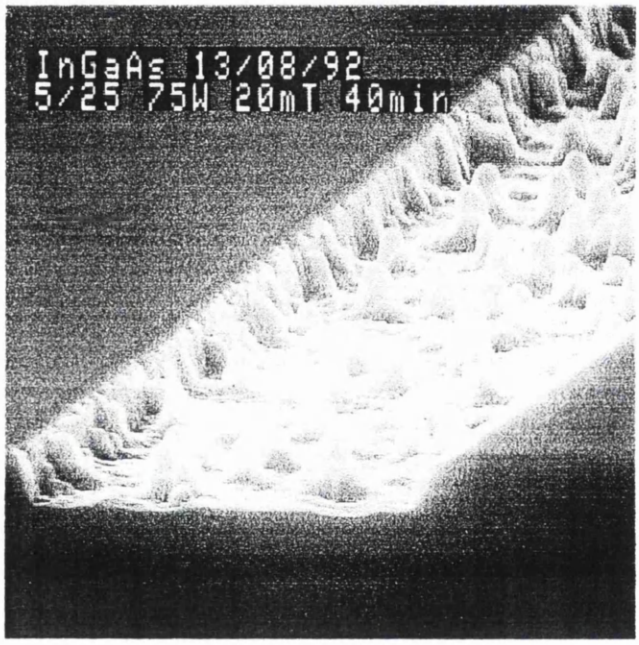

Figure 2.7
Micrograph of InGaAs etched with an air leak.

Figure 2.8 demonstrates how air inadvertently added to the methane/ hydrogen plasma due to a leaking o-ring seal can produce an exceedingly poor etch. Nitrogen ions are very efficient at sputtering causing much erosion to the masking material. Nitrogen or oxygen may also chemically react with the etch surface creating

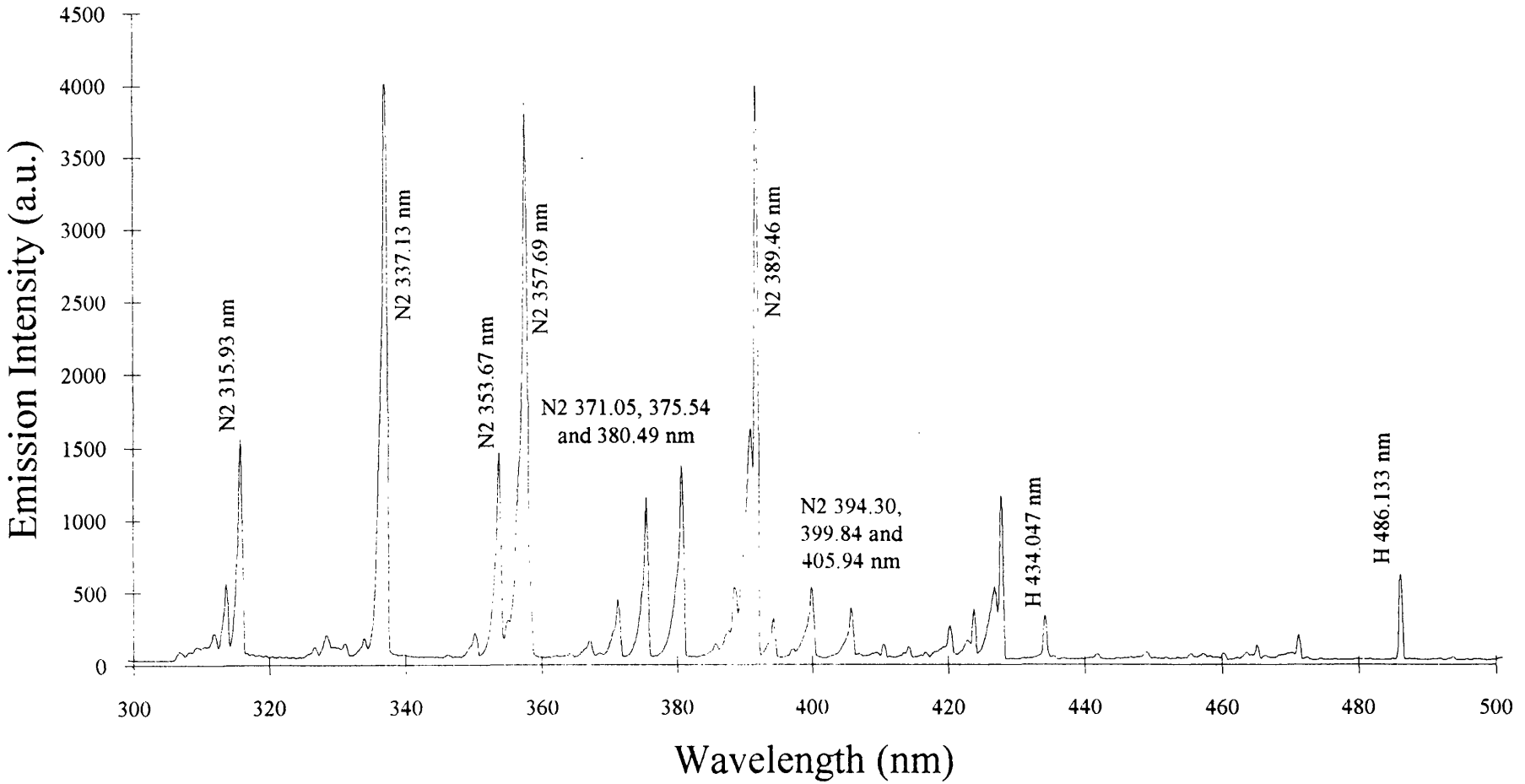

Figure 2.8 Optical emission spectra of hydrogen plasma with an air leak

low volatility compounds on the surface that are difficult to remove during the etch and can themselves act as micromasks resulting in the poor quality of the etch surface as demonstrated in Figure 2.7. Even a small air leak can have a dramatic and damaging effect on the etch. The leak integrity of the system is ascertained by monitoring the leak-up rate, the rate at which the pressure of the system rises when the gate valve is closed isolating the chamber from the vacuum pumps. Normal leak-up rates are of the order of 1 millitorr per minute with rates as low as 0.4 millitorr per minute possible. The leak-up rate is never allowed to deteriorate above 2 millitorr per minute.

2.4 Laser Reflectometry of Multi-layer Structures

2.4.1 Introduction to Reflectometry

Laser reflectometry is a powerful in-situ tool that has been used to investigate both growth rates and refractive indices during III-V semiconductor growth by methods such as MOCVD [2.2, 2.3]. In this work reflectometry has also used to monitor dry etch processes. When used for following the progress of an etch it is convenient to differentiate between two methods of using laser reflectometry, those that use a mask as a reference level [2.4, 2.5] and those without a mask that use the differences in refractive indices of a multilayer structure [2.5-2.8].

2.4.2 Masked Reflectometry

In this method light is reflected from both a hard etch mask and from the unmasked region and allowed to interfere. The mask and etch surface are illuminated

by a collimated beam of light whose coherence length is much greater than the depths involved in etching. Provided the mask is not completely etched away it is possible to use this method when etching a material of uniform composition. The intensity of light reflected from unmasked areas will be constant if the etch surface remains smooth and if the wafer is composed of one material only. However relative phase of the reflected light from the mask and that from the etch surface changes as the etch surface recedes. The relative phase change between the two signals produces an interference pattern from which information about the progress of the etch front can be gained.

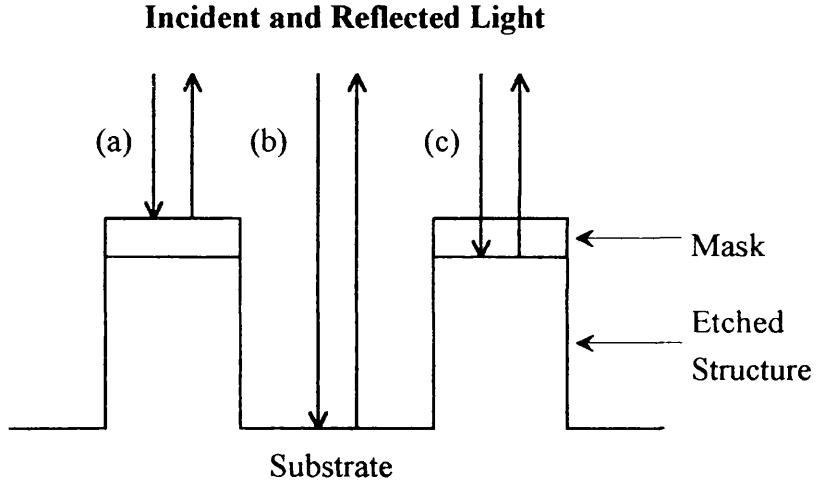

Figure 2.9
Masked reflectometry. Interference may occur between the top of the mask and the etched surface (a, b), between the top and bottom surfaces of the mask (a, c), and between the bottom surface of the mask and the etched surface (b, c).

The intensity of the interference signal will complete one cycle when the etched surface recedes by a depth that equals one half wavelength of the illuminating light. Accuracy in etch depth control will therefore increase as the wavelength of the illuminating light is decreased. Consideration must however be made for the

possibility of changes in mask thickness and reflectance which can and have been allowed for [2.4].

2.4.3 Maskless Reflectometry

When the sample to be monitored consists of several layers of differing semiconductor materials reflectometry can be used without a mask. The multilayer structure behaves in an analogous manner to the reflection and anti-reflection coatings used in conventional optics. Light penetrating below the top surface of the sample will undergo reflections at each interface encountered. The strength of the reflection will be determined by the refractive indices of the two layers forming the interface. The total surface reflectance will be a function of all reflections at all interfaces. During etching the thickness of the topmost layer is reduced and from time to time as the layer is etched completely through the material of the top layer will change. The reflectance will thus follow the position of the etch surface and can be used as an indicator for the progression of the etch.

The theoretical reflectance from the top surface has been calculated using the transmission line theory [2.5]. A detailed description of the transmission line theory can be found in reference [2.9]. The transmission line is thought of as a cascaded network of resistance (R), impedance (L), conductance (G) and capacitance (C).

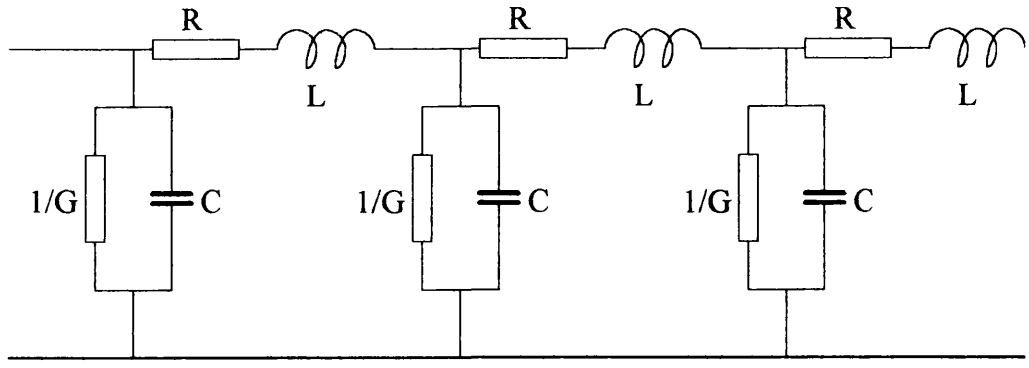

Figure 2.10
Cascaded network representation of the transmission line.

Consideration of the voltage and current flow through an R, L ,G, C element shows that the characteristic impedance Z_0 is given by;

$$Z_0 = \left[\frac{(R+j\omega L)}{(G+j\omega C)}\right]^{\frac{1}{2}} \qquad \text{(eqn. 2.9)}$$

and the propagation constant of the electromagnetic wave travelling along the transmission line is given by;

$$\gamma^2 = \frac{(R+j\omega L)}{(G+j\omega C)} \qquad \text{(eqn. 2.10)}$$

or can be expressed further as

$$\gamma = \alpha + j\beta \qquad \text{(eqn. 2.11)}$$

where α is the attenuation coefficient and β the phase factor.

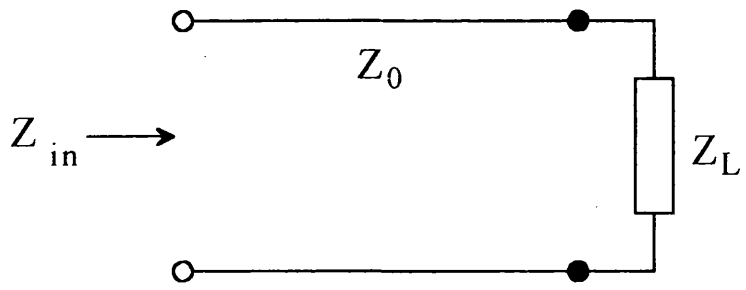

Figure 2.11
Transmission line, Z_0 terminated by load impedance, Z_L.

If a transmission line of characteristic impedance Z_0 is terminated by a load of impedance Z_L, the wave will be reflected at the junction of the transmission line and the load due to the impedance mismatch. The relative magnitude of the reflected wave in relation to the incident wave is given by the voltage reflection coefficient ρ;

$$\rho = \frac{Z_L - Z_0}{Z_L + Z_0} \qquad \text{(eqn. 2.12)}$$

which can be compared with the reflection at a boundary for light where

$$\rho = \frac{N_0 - N_L}{N_L + N_0} \qquad \text{(eqn. 2.13)}$$

where N_0 is the refractive index of the medium the light is passing and N_1 the index of the medium into which the light is trying to pass. The impedance of a length of transmission terminated by the load is called the sending end impedance and is given by;

$$Z_{in} = Z_0\left[\frac{Z_L + Z_0 \tanh \gamma l}{Z_0 + Z_L \tanh \gamma l}\right] \qquad \text{(eqn. 2.14)}$$

where γ is the propagation constant already established and l the length of the transmission line of characteristic impedance Z_0. If the transmission line is made from many lengths of differing characteristic impedance and terminated by a load impedance the total sending end impedance can be found by breaking the whole line down into smaller elements of a single characteristic impedance. Z_{in} is calculated for the load and the length of line directly connected to it. This calculated impedance can then be thought of as a new load terminating the remaining transmission line. The impedance of the new load and it nearest length of line is calculated and taking successive loads and lengths of transmission line the sending end impedance of the whole line can be found.

If instead of a load and lengths of transmission line we have a substrate and semiconductor epi-layers the impedance of the whole structure can be found, the sending end impedance and hence the reflection coefficient calculated.

$$\rho = \frac{Z_{in} - Z_{vac}}{Z_{in} + Z_{vac}} \qquad \text{(eqn. 2.15)}$$

Where Z_{vac} is the impedance of free space which approximates the optical impedance of the plasma in the etch chamber. The reflectance, R is thus given by

$$R = \rho.\rho^* \qquad \text{(eqn. 2.16)}$$

where ρ^* is the complex conjugate of ρ.

In converting the theory of high frequency transmission lines to that of optical waves travelling through dielectrics, minor adjustments have to be made. The impedance of a semiconductor layer to the illuminating light is give as

$$Z = \frac{Z_{vac}}{N_\lambda} \qquad \text{(eqn. 2.17)}$$

Where N_λ is the refractive index of the semiconductor at the illuminating wavelength. In calculating the 'sending line impedance' the propagation constant it is useful to modify γ so as to be consistent with electromagnetic theory for optical waves.

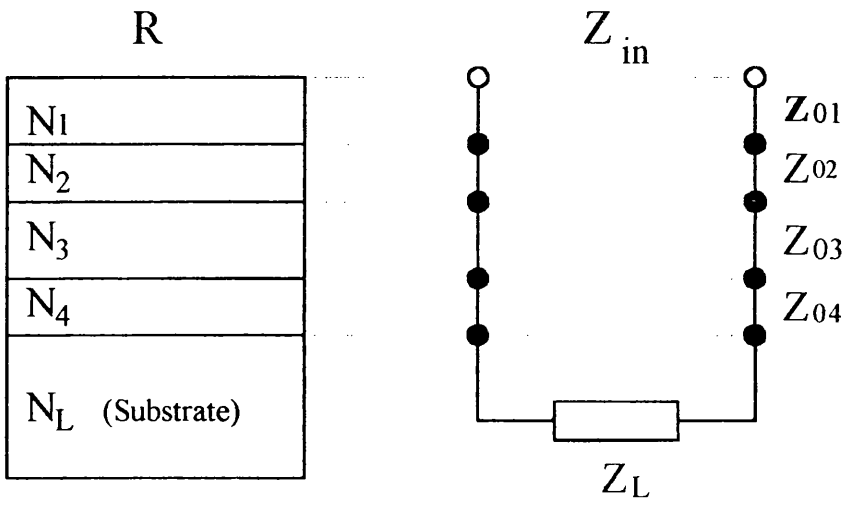

Figure 2.12
A multiple layer wafer structure shown on the left compared to on the right a composite transmission line.

Given Maxwell's wave equation for an electromagnetic wave propagating through an isotropic medium,

$$\nabla^2 \tilde{\mathbf{E}} - \varepsilon\mu \frac{\delta^2}{\delta t^2} \tilde{\mathbf{E}} = 0 \qquad \text{(eqn. 2.18)}$$

we can assume the solution for the electric field vector, $\tilde{\mathbf{E}}$ of a plane wave travelling in the x-direction, (this is also the description used for voltage and current waves in the high frequency transmission line).

$$\tilde{\mathbf{E}} = E_0 \exp[j\omega t \pm \gamma x]\hat{\mathbf{x}} \qquad \text{(eqn. 2.19)}$$

where ω is the angular frequency, t the time, γ the propagation constant, x the distance along the direction of propagation defined by the unit vector $\hat{\mathbf{x}}$. Substituting back into the wave equation we have;

$$\gamma^2 \tilde{\mathbf{E}} + \varepsilon\mu\omega^2 \tilde{\mathbf{E}} = 0 \qquad \text{(eqn. 2.20)}$$

and hence;

$$\gamma 2 = -\varepsilon\mu\omega^2 \qquad \text{(eqn. 2.21)}$$

Assuming that the propagation constant γ can be written in the form

$$\gamma = \alpha + j\beta = j\sqrt{\varepsilon\mu}\,\omega = j\sqrt{\varepsilon_r\mu_r}\,\frac{\omega}{c} \qquad \text{(eqn. 2.22)}$$

as the speed of light c is

$$c = \frac{1}{\sqrt{\varepsilon_0\mu_0}} \qquad \text{(eqn. 2.23)}$$

and that the complex refractive index, N of the material in which the wave is propagating can be written as

$$N = n - jk = \sqrt{\varepsilon_r\mu_r} \qquad \text{(eqn. 2.24)}$$

so

$$\gamma = \alpha + j\beta = j(n - jk)\frac{\omega}{c} = k\frac{\omega}{c} + jn\frac{\omega}{c} \qquad \text{(eqn. 2.25)}$$

then the real and imaginary parts of the propagation constant are

$$\alpha = \frac{2\pi}{\lambda}k, \beta = \frac{2\pi}{\lambda}n \qquad \text{(eqn. 2.26)}$$

The theoretical reflectance from the surface of a multi-layer semiconductor can thus be calculated.

Theoretical calculations of surface reflectance as a function of etch depth were performed using Mathworks Matlab for Windows V4.2b. An example of the type of calculation is shown below.

```
ZL=Zsub
count=0

For material_count = material_bottom to material_top

        Z0=Zvac/N(material_count)
        alpha=2.pi.imaginary(N(material_count))/illuminating_wavelength
        beta=2.pi.real(N(material_count))/illuminating_wavelength
        gamma=alpha+j.beta

        For step_count = step_size to layer_thickness

                count=count+1

Zin=Z0((ZL+Z0.tanh(gamma.step_size))/(Z0+ZL.tanh(gamma.step_size)))
                R(count)=(Zin-Zvac)/(Zin+Zvac)
                ZL=Zin
        end

end
```

Firstly the load impedance Z_L is assigned the impedance of the substrate. Because the substrate is 'infinitely thick' compared to the epi-layers and the absorption coefficient of the illuminating radiation is sufficient to ensure no radiation can reach the back surface of the substrate the back substrate/air interface can be ignored. The Reflectance is a function of depth so results are stored in a matrix R and a counter (count) is kept to identify the unique position within the layer structure. Two nested loops are then initiated, the first stepping through the material types from the substrate towards the surface. The impedance of the layer and its propagation constant are calculated. The nested loop steps through each material layer in small steps defined by step_size until the layer thickness is reached at which point the main loop changes the material type. At each step within a single layer the 'sending end' impedance is calculated and the reflectance found and stored in the matrix (R(count)). Since the calculation is iterative Z_{in} is then assigned to Z_L and then calculation repeated.

As the etch surface progresses from one type of material to another the etch rate may also change. These changes in material will be revealed in the reflectance from the surface as has already been demonstrated. Changes in the etch rates will also be revealed. The peak-to-peak separation of the reflectance signal will become stretched relative to the theoretical signal if the etch rate is low and the separation compressed for high etch rates. The number of peaks and their relative peak intensities will however remain unchanged.

A Sofie instruments laser interferometer operating at a wavelength of 679 nm was used to take experimental reflectance values whilst etching. The interferometer head is mounted upon an xy-table to allow for accurate alignment of the 50 μm diameter laser spot. A CCD camera allows the user to see the laser spot on the surface of the material and focusing is achieved with the aid of a telescope system. The reflected light is passed through a 10 nm bandpass filter to a photomultiplier.

As an example, using published data for the complex refractive indices of MBE grown InP, InAs [2.10], AlAs [2.11], and InGaAs [2.12] lattice matched to InP the theoretical reflectance curves could be calculated. No available data for the refractive index of InAlAs could be obtained at the illuminating wavelength. The real part was assumed to be approximately half way between that for InAs and AlAs, a value of 3.2 and an initial value of k = 0.1 was chosen. For the InGaAs/InAlAs multilayer structure the first theoretical calculation of reflectance verses depth was found to disagree with the experimental result. By investigating the theoretical curves with changing k-values for InAlAs a figure of 3.2-j0.4 was found to be in agreement with experiment. This change in k could most clearly be seen in the way the reflected signal changes when etching through the 500 nm InAlAs buffer layer immediately above the substrate.

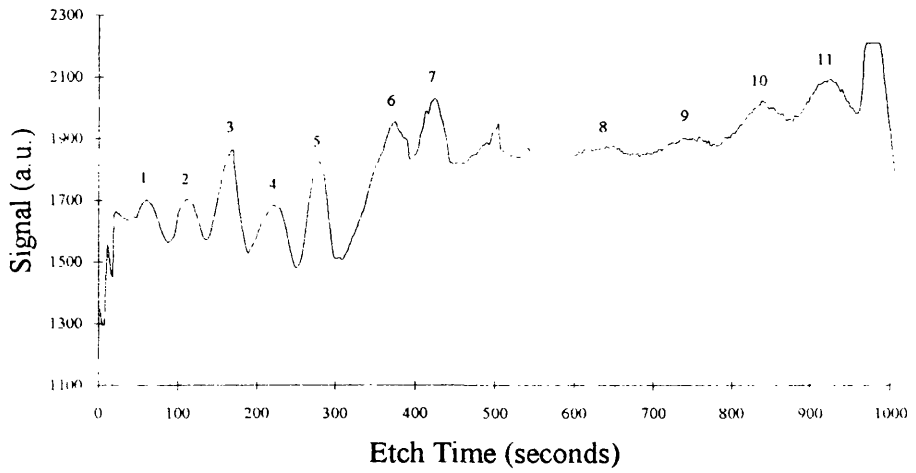

Figure 2.13
Experimental curve for InGaAs/InAlAs multilayer structure.

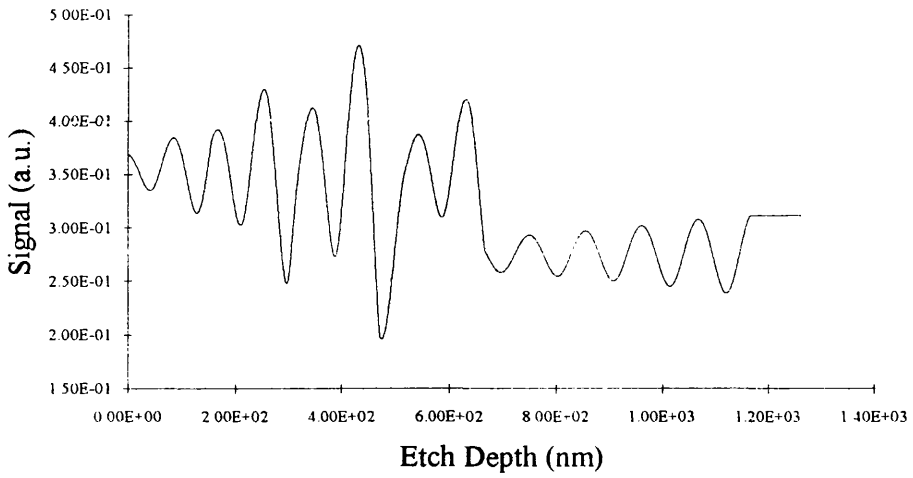

Figure 2.14
Theoretical reflectance with k=0.1.

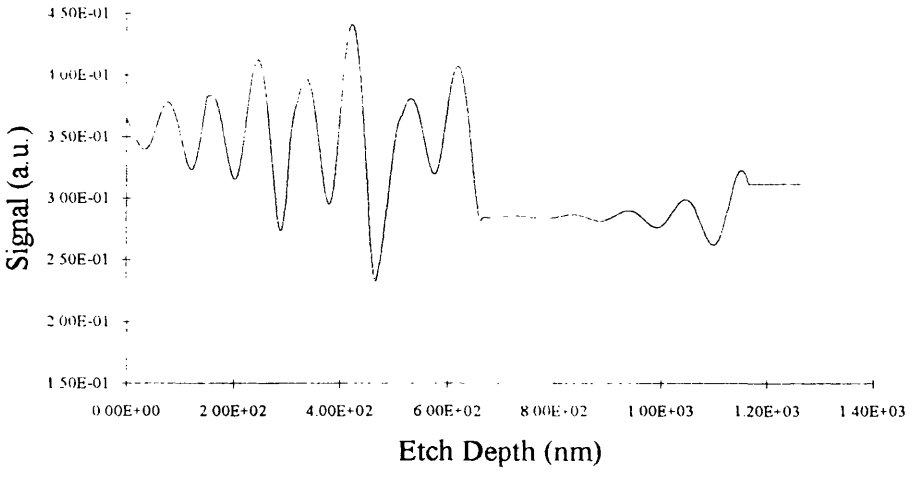

Figure 2.15
Theoretical reflectance calculated using k=0.5. The numbered peaks correspond with those of Figure 2.13.

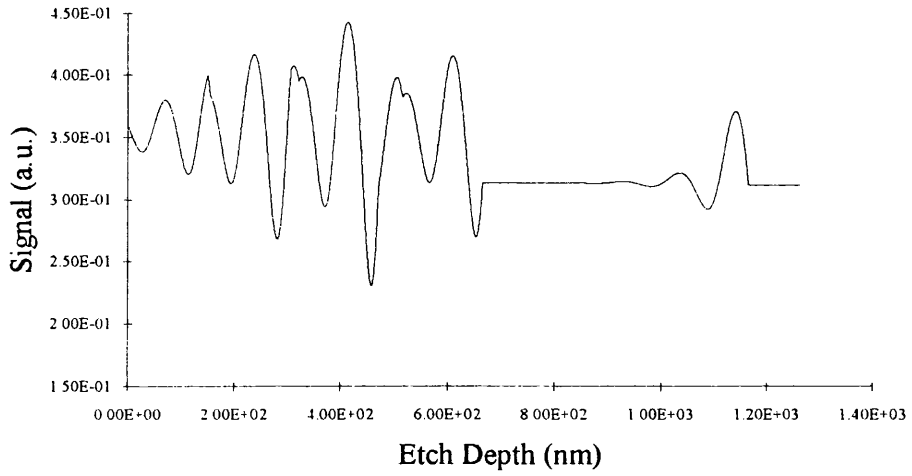

Figure 2.16
Theoretical reflectance with k=1.0.

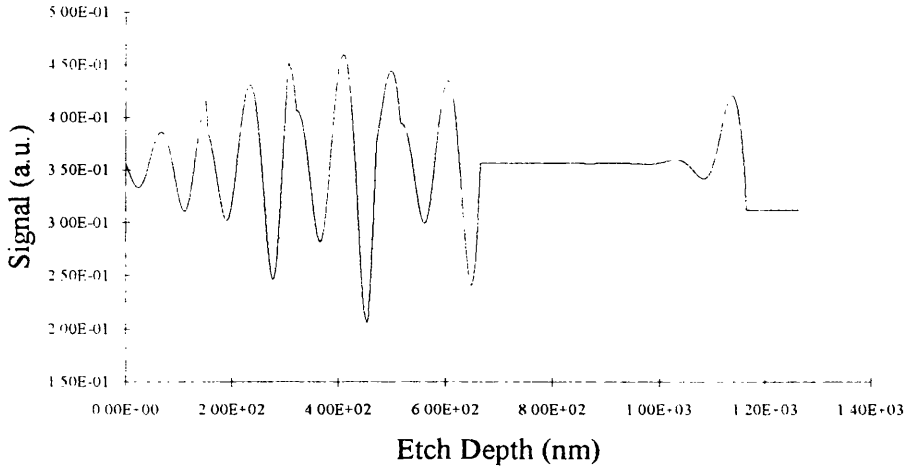

Figure 2.17
Theoretical reflectance with k=2.0.

2.5 Chapter Summary

Three *in-situ* techniques have been introduced that allow the user to monitor the plasma state and the position of the etched surface during an etch. The surface of the semiconductor has been shown to rise quickly in temperature once the methane/hydrogen plasma has been struck. The energy required for heating of the surface is supplied by the bombardment of the surface by energetic ions the total energy and flux of which determine the final surface temperature. Increasing the rf power supplied to the plasma increases the ion energy and flux resulting in the observed rise in temperature.

The background of optical emission spectroscopy has been discussed and various elements of characteristic emission features demonstrated. OES has been used as a tool to monitor the leak integrity of the etch chamber and pumping system.

Maskless laser reflectometry has been shown to be a powerful method of detecting the position of the etch surface within multi-layer structures in real time. Modelling the theoretical reflectance has been discussed and used in determining the complex refractive index of InAlAs.

References

[2.1] "Physical Chemistry" Second Edition
G.M. Barrow Chp.18 McGraw-Hill (1988)

[2.2] H. Kawai, S. Imanaga, K. Kaneko and N. Watanabe,
"Complex refractive indices of AlGaAs at high temperatures measured by in situ reflectometry during growth by metalorganic chemical vapor deposition",
J. Appl. Phys. **61** pp. 328-332 (1986)

[2.3] T. Makimoto, Y. Yamauchi, N. Kobayashi and Y. Horikoshi,
"In-situ optical monitoring of the GaAs growth process in MOCVD",
Jap. J. Appl. Phys. **29** pp. L210-L209 (1990)

[2.4] S. Yin, F.T.S. Yu and S. Wu,
"Optical monitoring for plasma-etching depth process",
IEEE Photon. Technol. Lett. **4** pp. 894-896 (1992)

[2.5] S.E. Hicks, W. Parkes, J.A.H. Wilkinson and C.D.W. Wilkinson,
"Reflectance modelling for in-situ dry etch monitoring of bulk SiO_2 and III-V multilayer structures",
J. Vac. Sci. Technol. **B12** pp. 3306-3310 (1994)

[2.6] S.M. Ojha, R. Turner, J.P. Stagg, D. Boyle and G.H.B. Thompson,
"Monitoring and control of fabrication processes for integrated optics devices",
Proc. 6th Int. Conf. InP and related materials (1994)

[2.7] P. Collot, T. Diallo and J. Canteloup,
"Dry-etch monitoring of III-V hetrostructures using laser reflectometry and optical emission spectroscopy",
J. Vac. Sci. Technol. **B9** pp. 2497-2502 (1991)

[2.8] M.J. Mondry, D.I. Babic, J.E. Bowers and L.A. Coldren,
"Refractive indexes of (Al, Ga, In)As epilayers on InP for optoelectronic applications",
IEEE Photon. Technol. Lett. **4** pp. 627-629 (1992)

[2.9] "Telecommunications Engineering" Second Edition
J. Dunlop and D.G. Smith Chapman and Hall (1989) Chp. 6

[2.10] "Properties of indium phosphide"
INSPEC (1991)

[2.11] "Properties of gallium arsenide" Second Edition
INSPEC (1990)

[2.12] "Properties of lattice-matched and strained indium gallium arsenide"
Edited by P. Bhattacharya. INSPEC (1993)

[2.13] S. Nojima and H. Asahi,
"Refractive index of InGaAs/InAlAs multiplequantum-well layers grown by molecular-beam epitaxy",
J. Appl. Phys. **63** pp. 479-483 (1988)

Chapter 3

Reactive Ion Etching of III-V Semiconductors with CH_4/H_2 Gas Mixtures

Chapter Outline

This chapter introduces the methane/hydrogen plasma and demonstrates how the character of the plasma may be changed by altering the relative concentrations of the gases and the applied rf power. The state of the plasma can be observed by optical emission spectroscopy. Changes to the state of the plasma have direct implications for the etching characteristics of the compound semiconductors (AlGaAs, InGaAs and InAlAs) studied. Etch rates, induction times and profiles of features fabricated in these materials have been investigated for a range of plasma conditions. The effect of total flow rate and etch pressure are briefly investigated to understand the role they play in the etch process. The cleanliness of the etch chamber can also have an important role to play in determining these etch rates. A rigorous cleaning procedure has been implemented to overcome such problems.

3.1 Introduction to CH_4/H_2 RIE

Reactive ion etching of the III-V semiconducting material InP using the gas mixture of methane (CH_4) and hydrogen (H_2) was first reported by Niggebrugge *et al.* [3.1] in 1985. The technique was extended by Cheung *et al.* [3.2] to cover etching of GaAs and since numerous workers have reported etching of a wide variety of III-V materials and their alloys using this gas mixture [3.3-3.10]. It has been demonstrated that the methane in the gas mixture can be replaced by the related hydrocarbon gas ethane (C_2H_6) [3.11]. Recently methane/hydrogen RIE has been extended to the II-VI material system etching such materials as ZnSe and CdTe [3.12]. The addition of argon (Ar) to the methane/hydrogen gas mixture is a widely used technique [3.13-3.15] with the reported benefits of improved etch surface morphology and lower polymer deposition rates onto the mask. In the work presented here the need for Ar addition was not evident since surface morphologies were excellent using methane/hydrogen mixtures alone.

In all the material systems reported, the etching characteristics due to methane/hydrogen RIE are broadly similar. Etch rates are seen to increase as the methane content of the gas mixture is increased (with all other parameters held constant), then will cease to rise and eventually etching is halted by the deposition of a polymeric layer onto the etch surface. It is also found that etching can only be initiated provided the rf power supplied and hence DC self bias is over a threshold value, the precise value of which will vary according to the type of etching machine used and the type of material to be etched. As the rf power is increased further, etch rates also rise as they do when the total flow rate or pressure in the chamber are raised. Little variation of etch rate with cathode temperature has been reported for InP, GaAs and InAs [3.10].

3.2 The CH_4/H_2 Plasma

3.2.1 Plasma Phase and Surface Reactions

It has been postulated but only recently observed by secondary ion mass spectrometry (SIMS) that the etching mechanism could be likened to the reverse of the metalorganic chemical vapour deposition (MOCVD) process [3.16,]. In MOCVD the group III elements are contained within a trimethyl or triethyl complex, e.g. $Ga(CH_3)_3$ or $Ga(C_2H_6)_3$,. The group V elements being supplied as a suitable hydride, e.g. AsH_3. Heating of the substrate breaks up the molecules liberating the desired elements which remain on the growth surface with the remaining material pumped away in the form of hydrocarbons.

During reactive ion etching with methane and hydrogen the gas molecules are fragmented by collisions with energetic electrons to form unsaturated hydrocarbons,

$$CH_4+e^- \rightarrow CH_3+H+e^- \qquad \text{(eqn. 3.1)}$$

$$CH_4+e^- \rightarrow CH+3H+e^- \text{ etc.} \qquad \text{(eqn. 3.2)}$$

together with atomic carbon and hydrogen all of which may be found in a number of states be they ionised, excited neutrals or radicals. It must however be restated that the majority of species in the typical RIE glow discharge are the etch gas itself and other neutral species, not ions. The positive ions cross the dark space above the cathode to the surface where reactions can occur that form the volatile group III trimethyl compounds or the group V hydrides. Evidence of the etch products $In(CH_3)3$ and PH_3 have been observed by mass spectroscopy whilst etching InP [3.17]. These species were subsequently used for end-point detection whilst etching through InP/InGaAs multilayer structures.

Under normal configurations the etching machines used in this study are operated in the flow rate limited regime. This is to say that the ultimate factor effecting the etch rate (when operating away from extremes of power and methane flow where polymer can become a problem) is the supply of reactant species to the surface where the etch process takes place. In this regime we are making the most efficient use of these species, and if we were to in a simplistic approach to double the total flow then the etch rate should double. In practice events can be complicated by the change in residence time of the gas species in the chamber or by a change in pressure but generally the flow rate argument holds true.

Not only do collisions between species in the plasma produce cracking of large molecules but collisions between two species may promote polymerisation. These polymers may also be transported to the etch surface but may not be chemically active and actually inhibit etching. For example the reaction two methyl molecules could lead to the formation of the ethyl species;

$$CH_3+CH_3 \rightarrow C_2H_6 \qquad \text{(eqn. 3.3)}$$

The ethyl molecule could then react with another methyl to form a propyl molecule;

$$CH_3+C_2H_6 \rightarrow C_3H_9 \qquad \text{(eqn. 3.4)}$$

or any number of permissible combinations of reactions between the species present in the chamber could occur producing ever more massive hydrocarbons. At the same time as the polymeric species are being formed collisions with energetic electrons will cause large polymer chains to brake-up. An equilibrium condition is formed between polymer formation and destruction.

The polymer species are responsible for the build up of polymeric layers upon etch masks during methane/hydrogen RIE. Hayes et al. [3.8] have studied these deposits. Combustion analysis showed that the ratio of carbon to hydrogen was 1.2:1 indicating a highly cross-linked structure. It was also found that the polymer was not soluble in standard organic solvents such as trichloromethane. Neutral species from within the plasma be they the original constituent gas species, simple fragments of the etch gas or more complex species formed by polymerisation will diffuse to the walls of the reactor chamber where they may adhere.

Studying the emission lines present in the glow of the plasma may assist in establishing the composition of the plasma. The spectra will change as the gas mixture, flow rates and applied power are changed altering the nature of the plasma. Due to the low etch rates of the material systems under investigation in this study there are usually insufficient etch product species present within the plasma to produce a strong enough emission to allow for the product species to be identified. The strong and complex emission bands of molecular hydrogen however tend to further obscure any potentially useful spectral lines from the product species. OES does allow the observation of the species created by the breakdown of methane and hydrogen. Figures 3.1 and 3.2 show the spectra obtained from various gas mixtures over the emission wavelength range of 200-600 nm. Within the spectra are strong lines from atomic hydrogen at 434.1(Hγ) and 486.1 nm (Hβ). A strong emission line from the CH molecule is observed at 431.4 nm.

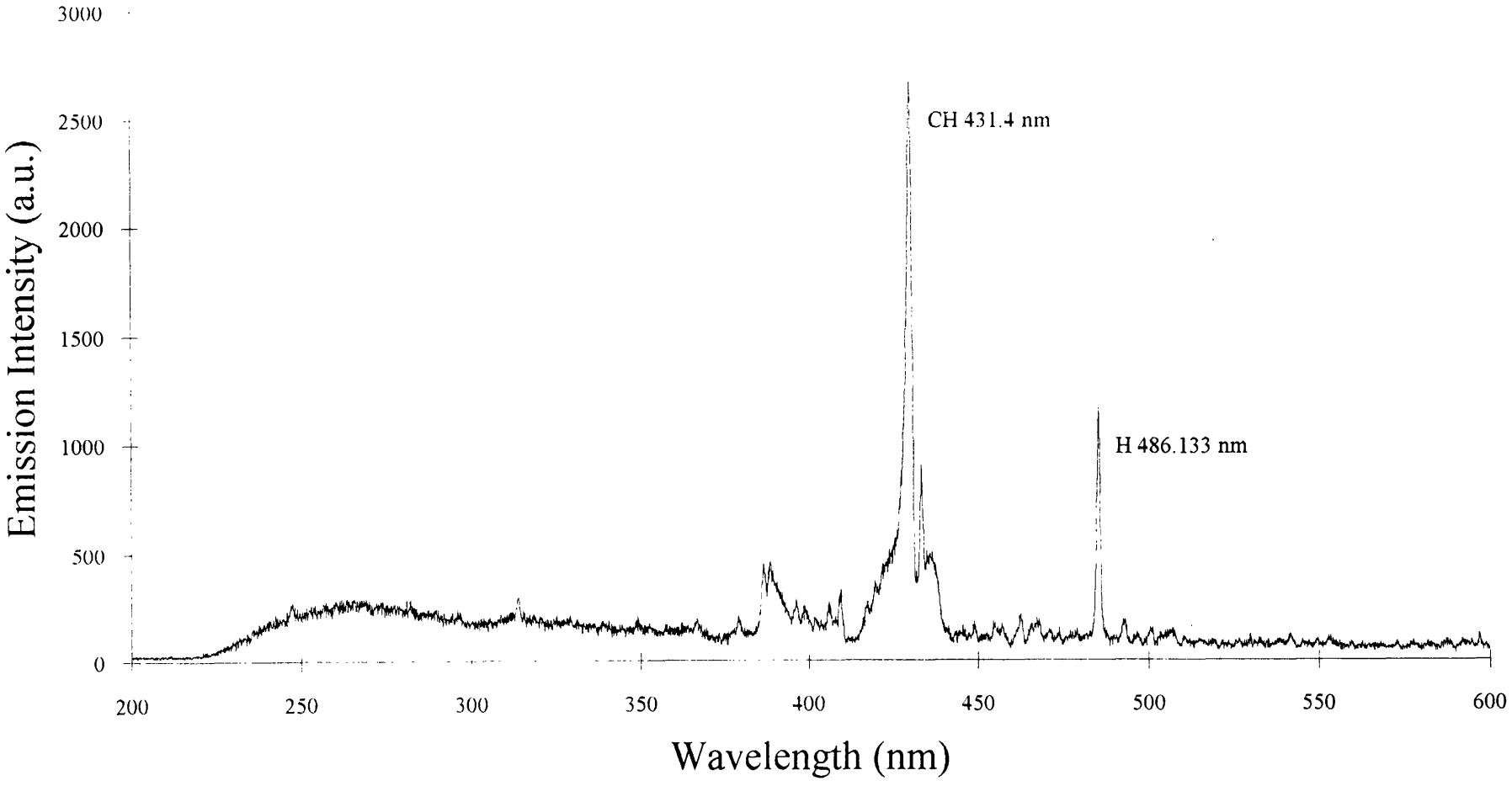

Figure 3.1 Emission spectra of 10 sccm CH4 at 20 millitorr and 75 W rf power

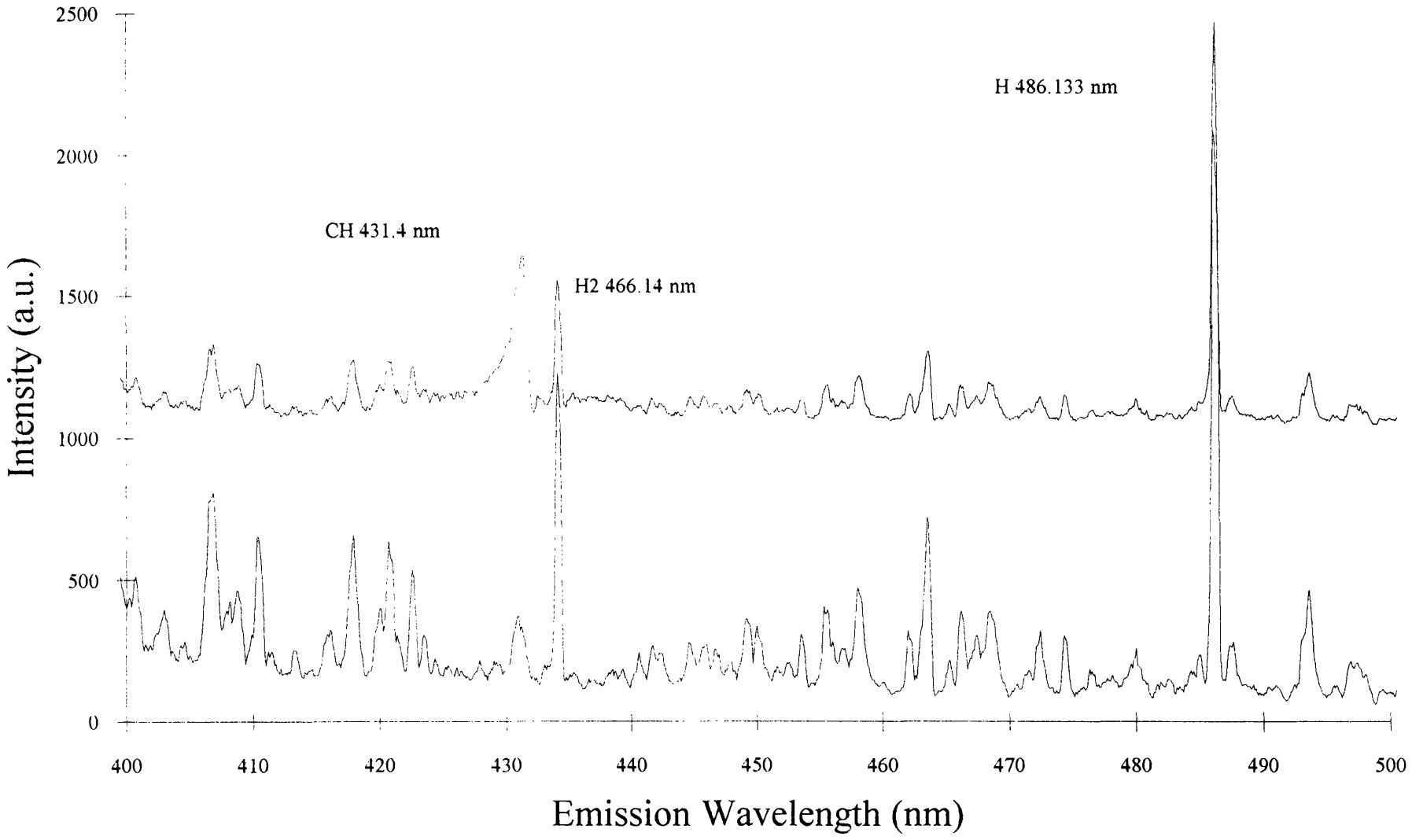

Figure 3.2 Optical emission spectra of CH4/H2 (upper spectra) and H2 (lower spectra).

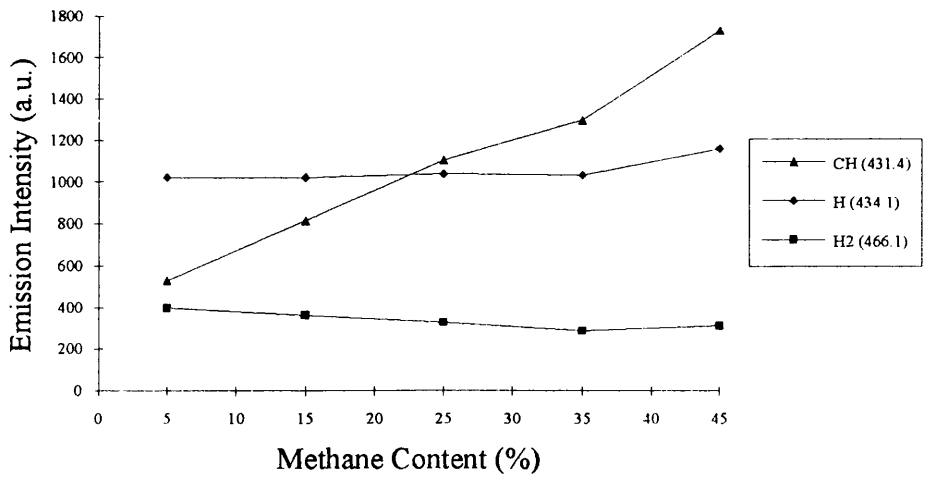

Figure 3.3
Peak intensities with methane content for a total gas flow of 25 sccm at 175 W.

A change in the ratio of the etch gases will lead to a change in the number density of each species and hence to a change in the intensity of their associated emission lines. On increasing the proportion of methane in the gas mixture we see that the intensity of the CH 434.1 nm line increases linearly. More methane in the gas mixture leads to a greater number of the CH breakdown products and thus to a higher emission. The emission lines from molecular hydrogen at 466.1 nm is seen to decrease as more methane is introduced and the proportion of hydrogen in the total gas mixture is correspondingly decreased.

The emission intensity from the atomic hydrogen peak at 434.1 nm is however seen to be constant for all methane content plasmas. This is reasonable if we take into account the atomic hydrogen formed by the breakdown of methane in the plasma, which will also contribute to the overall emission intensity. The emission from atomic hydrogen is thus not only from the breakdown of molecular hydrogen but from the dissociation of methane.

With a constant methane content in the gas mixture all peak intensities are observed to increase with the applied power, a situation that is consistent with an increased electronic excitation rate. The ratios of the intensities however do not remain constant indicating a change in the plasma chemistry due to an increase of one species relative to another. Here atomic hydrogen as indicated by the emission at 434.1 nm is seen to increase the most rapidly. Again this can be explained by an increased rate of formation of atomic hydrogen from the breakdown of methane, and increased dissociation of molecular hydrogen at a greater rate than excitation of molecular hydrogen.

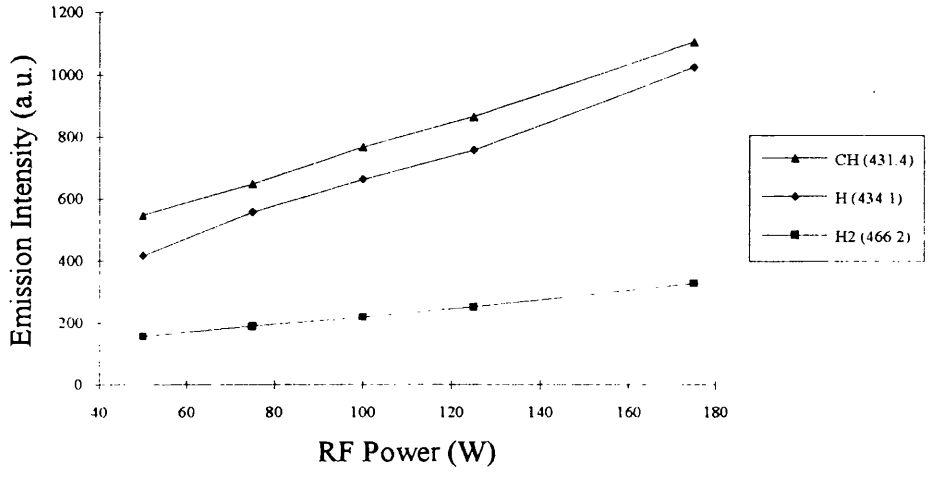

Figure 3.4
Peak intensities with rf power for 5 sccm CH_4 20 sccm H_2 at 20 millitorr.

3.2.2 DC Bias with Plasma Composition

Because etch rates during methane/hydrogen RIE are low and therefore lead to long etch times the amount of polymer formed upon the chamber walls may be considerable and effect the quality of the etch. It is noticeable when starting from the condition of a clean etch chamber that as polymer forms and increases in thickness (altering the impedance of the chamber) a fall in the DC self bias of the cathode is

observed. Many minutes may elapse until a steady state is achieved and the bias voltage becomes constant.

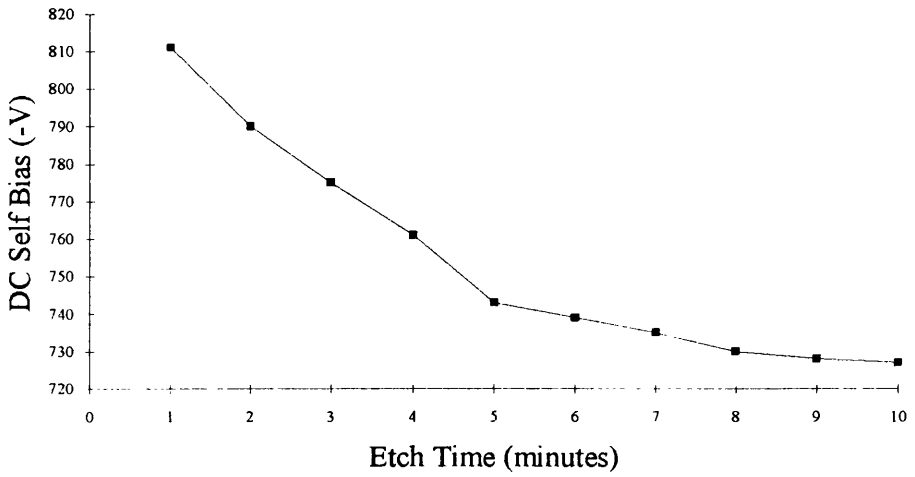

Figure 3.5
Fall of DC self bias with time for 1 sccm CH_4 24 sccm H_2 at 75 W.

The steady-state DC bias for a range of gas mixtures and rf powers are shown in figure 3.6. Most noticeable is the rise of DC bias for all gas compositions with rf power as greater ionisation is achieved.

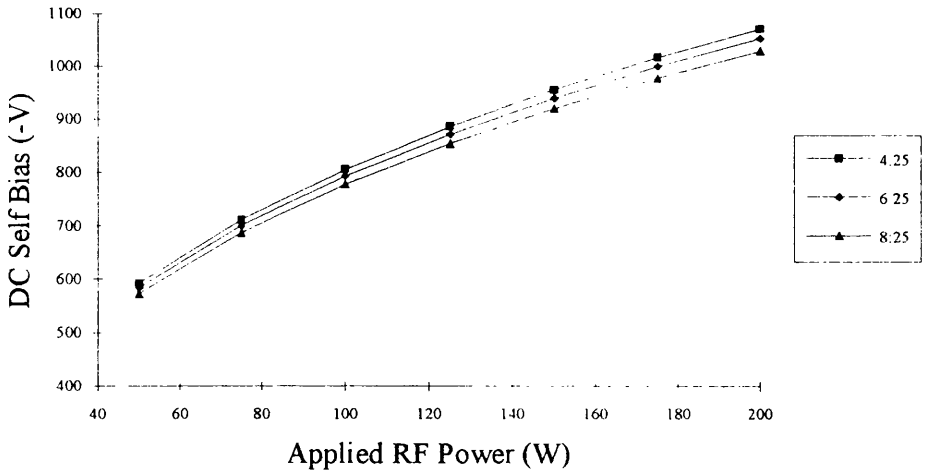

Figure 3.6
DC self bias with gas composition and rf power.

These two results when taken together suggest two separate chamber conditions under which a set of experiments should be performed. The first is to allow the chamber to become coated in a thick layer of polymer, and remain so during the experiment. This method may work well under some circumstances but there is the risk that material may be liberated from the walls of the chamber with the consequence that the quality of the etch may be degraded. A modification of this mode of operation is to clean the chamber before the etch removing all polymer. The chamber is then preconditioned so that a consistent amount of polymer is deposited prior to etching. The wall chemistry will then be the same throughout the etch.

The second method and the one used throughout the experiments presented in this thesis, is to clean the chamber before attempting the etch but not to precondition the chamber. As the etch progresses the chamber walls become coated with polymer and the DC self bias falls. Because there was no polymer in the chamber at the start of the etch it is unlikely that a coating will become thick enough to start to breakdown and re-enter the plasma. It is important to note that again the etch is performed with a known chamber condition.

3.2.3 Chamber Cleanliness

As demonstrated in section 3.2.2 the DC self bias is seen to fall as the chamber is coated with polymer. The condition of the etch chamber may therefore be an important factor in the etch process. When the chamber is dirty the etch can be slowed or even brought to a halt by the presence of excessive polymer upon the chamber walls which can re-enter the gas phase and be transported to the etch surface. After each methane/hydrogen or methane/hydrogen/oxygen etch the chamber is cleaned of polymer deposits by the application of an oxygen plasma. Typically during the oxygen clean an oxygen flow of 40 sccm at a pressure of 50 mT

with 50 W of power is used producing a DC self bias of -500 V. The design of the etch chamber is such that visual inspection whilst still under vacuum is difficult and a true assessment of the state of the chamber can only be made by venting the chamber to atmosphere and then inspection, a wasteful procedure in terms of time and vent gas. There is the added disadvantage of exposing the chamber to the atmosphere more times than is desirable. Optical emission spectroscopy of the oxygen plasma clean has been found to be a valuable aid in establishing when the chamber is clean. Because the plasma emission lines are monitored during the oxygen cleaning stage the need to vent the chamber to atmosphere is negated easily establishing the point of optimum cleanliness, making more efficient use of the etching machine.

The backbone of the polymer formed in a methane/hydrogen plasma is the carbon atom, which having a valence IV can form up to four covalent bonds with other atoms. The carbon can form single, double or even triple bonds with other carbon atoms to form the backbone of the chain. An example of a hydrocarbon chain is

CH3-CH=CH-CH2-CH3 (eqn. 3.5)

containing five carbon atoms with single and double carbon-carbon bonds. In this example the full compliment of bonds of the carbon atoms is achieved by bonding to hydrogen. It is possible in the etch chamber for bonding to occur with trace elements such as oxygen or nitrogen. Energy supplied from the oxygen plasma creates reactive oxygen radicals which can then react with and remove the polymer.

Two major products responsible for the removal of carbon during an oxygen clean are carbon monoxide (CO) and carbon dioxide (CO_2). Optical emission spectroscopy allows for monitoring of the emission lines at 283.31 and 288.3 nm associated with CO and CO_2^+ respectively. The point at which the intensity of the

lines falls to a background noise level is taken to correspond to the complete removal of carbon, and hence polymer from the chamber.

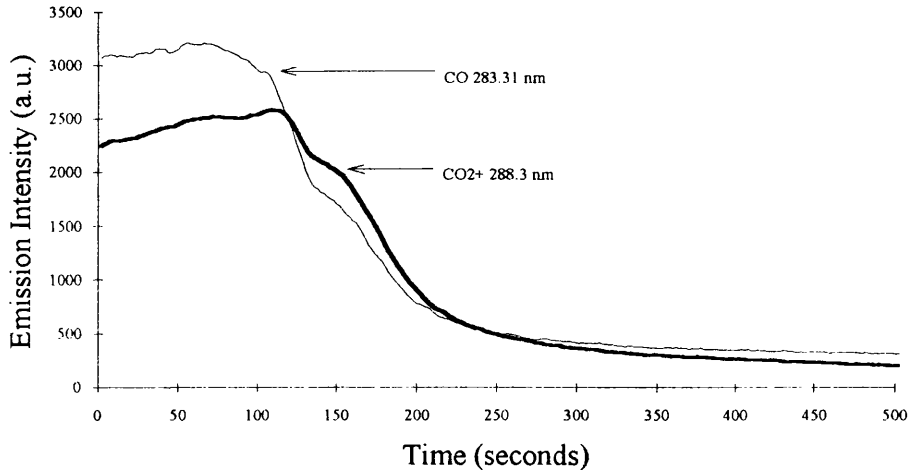

Figure 3.7
Intensity of CO and CO_2^+ emission lines with time during an oxygen plasma clean.

The emission intensities of CO and CO_2^+ when plotted against time are seen to contain two distinct regions. At the start of the clean the emission intensity is high indicating a high removal rate of polymer from the etch chamber. The intensity is firstly flat or may rise slightly. The rise of intensity may real but it is more likely that as the quartz window through which light is collected is cleaned of any deposited polymer the transmission of the window will increase giving the effect of an increased concentration of CO and CO_2^+ in the chamber. There is then a sharp fall in intensity which correlates with the total removal of polymer from the cathode.

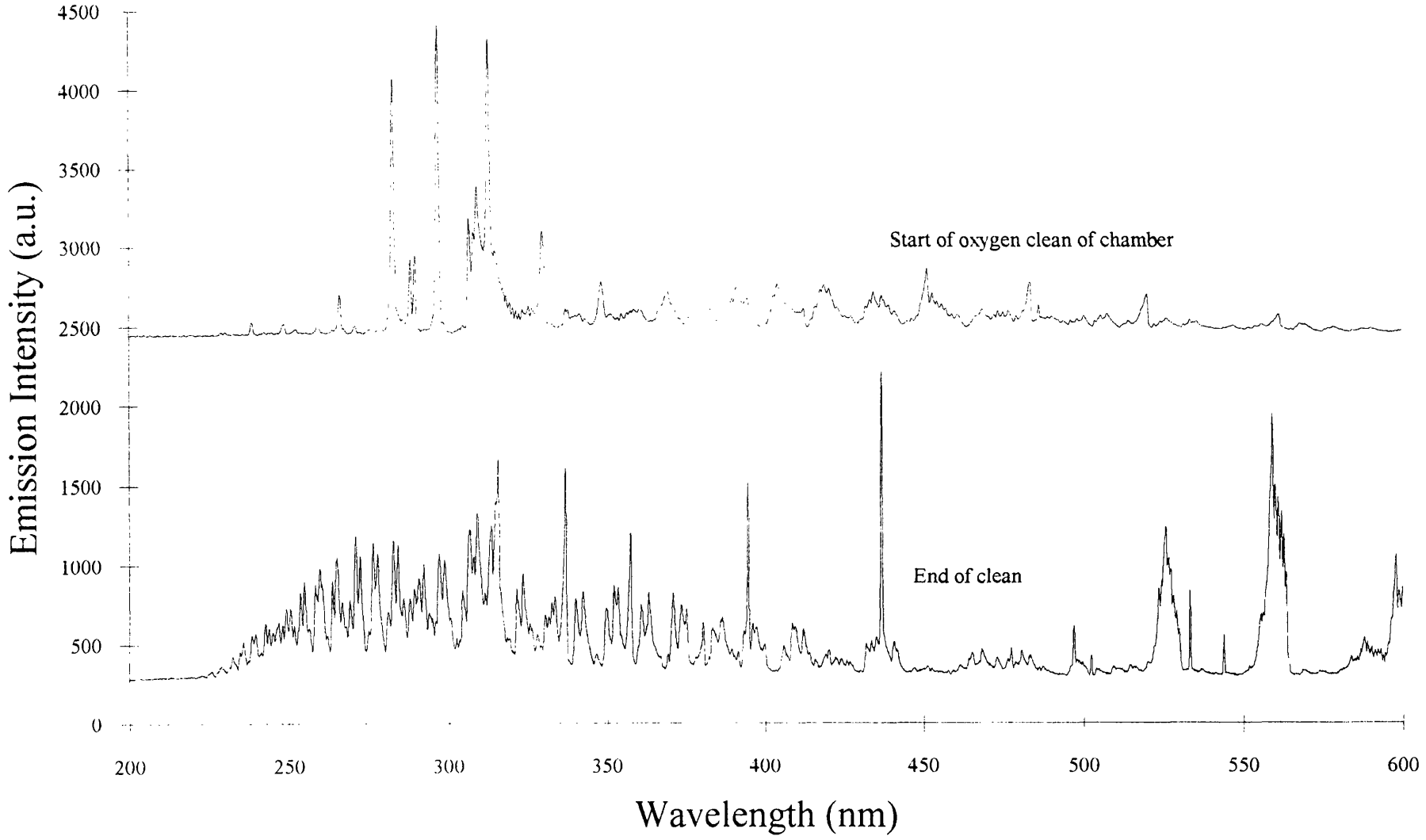

Figure 3.8 OES of O2 clean of polymer coated chamber. Upper spectra shows start of clean, with prominent CO and CO2 peaks. The lower spectra is taken near the end of clean and is dominated by oxygen.

If the clean is halted at this point and the chamber opened, inspection reveals that the cathode has been cleaned of all polymer deposits whilst the walls of the chamber remain coated. The cathode is cleaned faster than the chamber walls due to the direct ion bombardment to which it is subjected and hence a high ion flux and energy supply rate. The walls of the chamber do not benefit from this direct bombardment but only receive neutrals or ions and scattered by collisions within the plasma. The polymer removal rate at the walls will therefore be lower than at the cathode. Complete cleaning of the chamber will require longer oxygen plasma times and product species may be observed in the emission spectra for a greater length of time.

After an oxygen plasma clean a hydrogen plasma using similar flow rates pressures and rf powers is used to remove residual oxygen from the chamber. The hydrogen plasma clean is typically of the order of 50 % longer in time than the oxygen clean in order to ensure that all oxygen has been removed from the system and replaced by hydrogen, a gas which is compatible with the following methane/hydrogen etch.

3.2.4 Surface Temperature

Energy transferred from ions that cross the dark space to the surface of the semiconductor will lead to heating of that surface as well as helping to drive the surface chemical reactions. It was noted in section 3.1 that the final etch rate has been demonstrated to be independent of the temperature of the substrate during etching. It is however interesting to gain an insight into the temperature of the surface of the sample as it is etched. Valuable information may be gained as to the suitability of the masking material under ion bombardment and the temperatures to which the substrate rises during the etch. Photoresists are known to become soft and

even flow if heated excessively. This would have a degrading effect upon etch quality if allowed to happen.

Figure 3.9 demonstrates the temperatures of the surface of an InGaAs test sample during a 15 minute etch with a constant gas chemistry and at three different rf powers. Most noticeable is the sudden rise in temperature as the plasma is struck with the surface rising to within a few degrees of the final temperature in a matter of 2 minutes. At the start of each etch the sample surface is at 28 ^{0}C rising to 112, 154 and 178 ^{0}C with 75, 125 and 175 W of rf power.

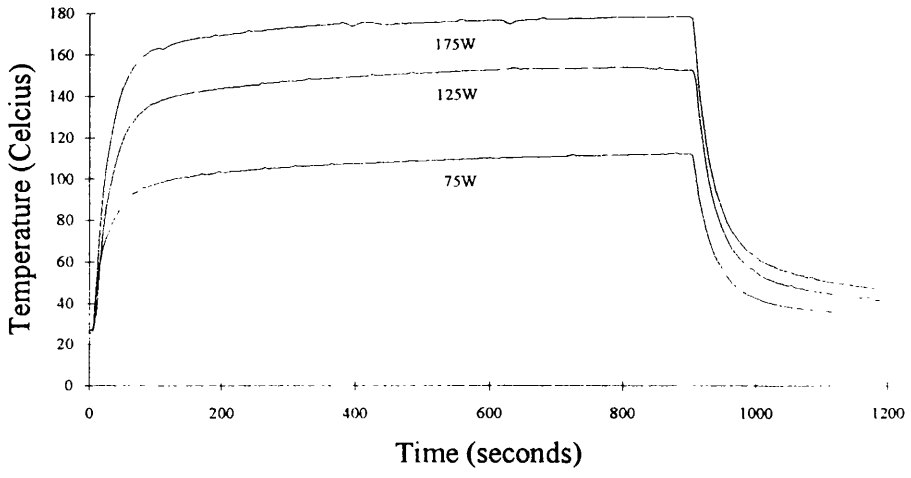

Figure 3.9
Temperature rise during a 15 minute etch for
1 sccm CH_4, 24 sccm H_2 at 20 millitorr. Heater chiller set to 30 ^{0}C.

Rapid cooling is observed on extinguishing the plasma. As may be expected the higher the rf power applied (higher DC bias) the higher will be the final temperature obtained. An increased rf power increases both the energy and flux of the ions to the surface and thus temperatures are seen to increase with applied power.

It has already been shown that the DC bias is affected only slightly by the change in composition of the gas mixture. Figure 3.10 represents the surface temperature rise for two differing gas compositions but with the same applied power. There is little difference in the surface temperature when etching with 1 sccm methane and 5 sccm methane in a total flow of 25 sccm with the same rf power and chamber pressure. Such a result may be expected if we consider the DC self bias generated for each etch condition. It was shown in section 3.2.2 that the DC bias changes only slightly with gas composition for a fixed rf power.

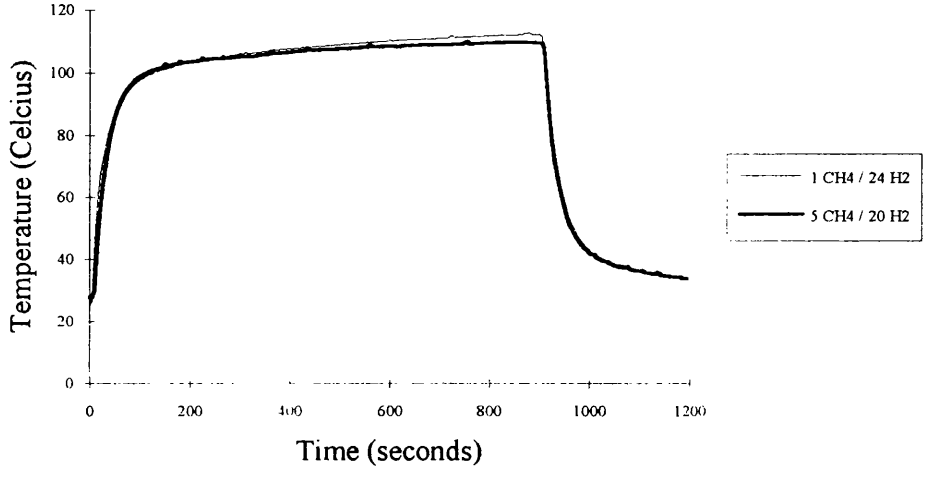

Figure 3.10
Near identical temperature rise during a 15 minute etch with 1 and 5 sccm of CH_4 in a total of 25 sccm at 20 millitorr and 75 W.

Since the DC bias reflects the flux of ions and hence energy to the cathode it is not surprising that the surface temperatures are similar for different gas compositions. The slightly higher DC bias obtained with the lower methane content gas mixture may be responsible for the higher surface temperature obtained in this experiment.

3.3 CH_4/H_2 RIE of AlGaAs

3.3.1 Etch Rates and Profiles

1μm of $3x10^{17}$ silicon doped $Al_{0.3}Ga_{0.7}As$ grown by molecular beam epitaxy upon a n^+ GaAs substrate with a 10 nm GaAs capping layer to prevent oxidation of aluminium was used. The etch mask was 400 nm of PECVD Si_3N_4. At the time of the experiments on AlGaAs the RIE machine was not fitted with an automatic pressure controller (APC), a device that would be present for the etching of InGaAs and InAlAs. In this situation the flow rate will determine the etch pressure.

In the work of Cheung *et al.* [3.2] a standard process had been formulated for the reactive ion etching of GaAs. Using 6.9 sccm methane, 34.5 sccm hydrogen at 150 W and 14 millitorr an etch rate of 20 nm/min was obtainable. Etching however was not possible at powers of 40 W and below. At these low powers the formation of a polymeric layer covering both the mask and etch the surface was observed. At low rf power there is sufficient energy supplied to crack gas molecules and initiate chemical reactions leading to the formation of sites suitable for the formation of polymer. The DC bias is too low to supply the ions with enough kinetic energy to become efficient at sputtering of the polymer, hence polymer layers build up on all surfaces exposed to the plasma.

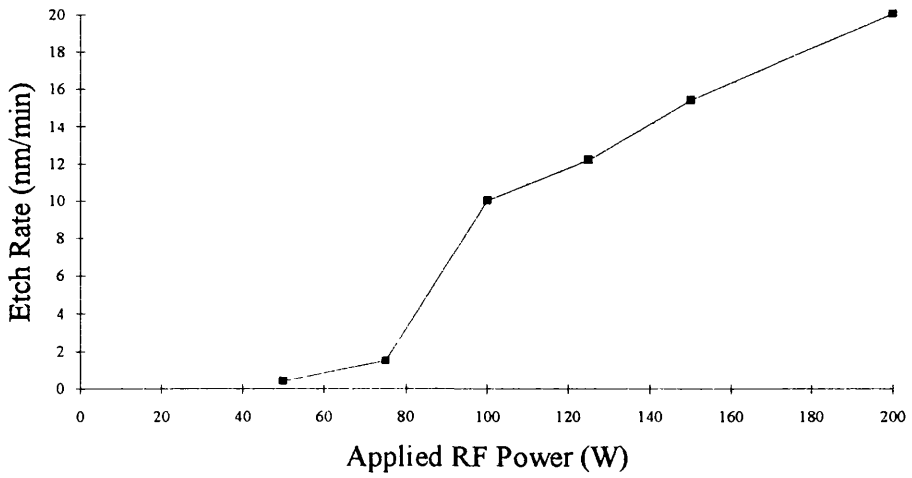

Figure 3.11
Etch rate for AlGaAs with rf power for 5 sccm CH_4 and 25 sccm H_2.

Etching of AlGaAs using 5 sccm methane, 25 sccm hydrogen (the same ratio of methane to hydrogen as that used for the etching of GaAs) at 150 W and 16 millitorr resulted in an etch rate of 15.5 nm/min. Etching however was not possible until powers of greater than 50 W were used, at 50 W or below polymer was deposited upon the surface of the sample. A possible selective etch process has therefore been identified that will only permit GaAs to be etched at low rf powers, stopping upon an underlying layer of AlGaAs by the formation of a polymeric layer upon the AlGaAs surface that prevents etching of the AlGaAs layer itself. Such a selective etch process would require a post etch treatment of the surface to remove the deposited polymer from the AlGaAs layer prior to any further fabrication stages on that layer. A low dc bias oxygen etch could be used to remove both polymer and photoresist etch mask.

Better selective methods are however available using gases such as the chlorofluorocarbon (CCl_2F_2) [3.18] commercially known as Freon 12. This has been the mainstay of selective etching of GaAs/AlGaAs structures in the commercial

sector, but since the world-wide ban on the production of these ozone depleting chemicals alternative etch chemistries have been sought. Silicon tetrachloride ($SiCl_4$) [3.19] may be used to selectively etch GaAs/AlGaAs where the selectivity may be of the order of several thousand to one. SiF_4 can be added to the $SiCl_4$ plasma to form a chemical environment that mimics that of CCl_2F_2 where there is a mixture of Cl and F within the plasma.

When etching with CCl_2F_2 or $SiCl_4/SiF_4$, Cl and F will react with Ga or As forming volatile products. GaAs can therfore be etched using both chemistries. If the removal of a layer of GaAs exposes an underlying layer of AlGaAs, etching will be halted by the formation of an involatile, unreactive product covering the etch surface. The involatile etch product AlF_3 is formed when using CCl_2F_2. The etch product believed to give high selectivites with $SiCl_4$ is Al_2O_3 formed by reaction with residual oxygen or water vapour within the vacuum chamber

The etch rate can also be dependant upon the methane content of the gas mixture. With an increase in methane content it follows that there would be an increase in the number of methyl species available for reaction on the etch surface thus an increase in etch rate.

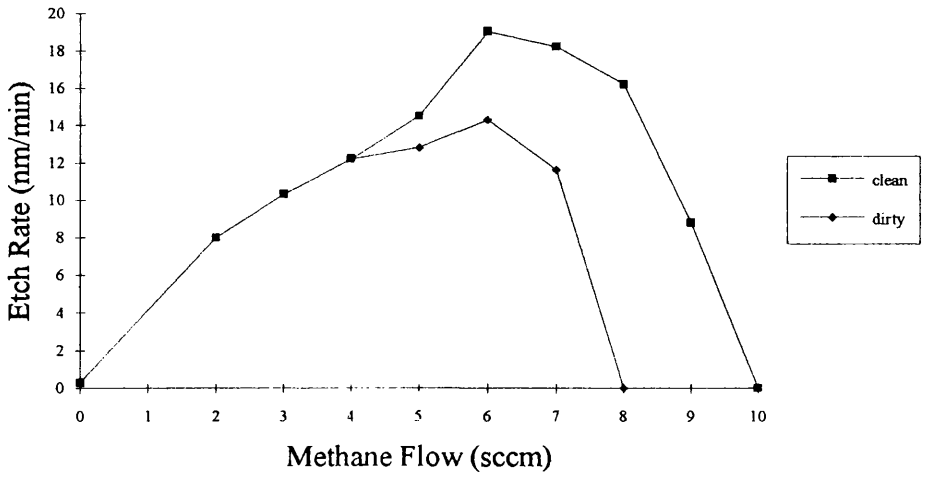

Figure 3.12
Etch rate for AlGaAs with methane content at 150 W and 25 sccm H_2.

Such behaviour is indeed seen with the etch rate increasing monotonically with methane content until etching is halted by the presence of non-reactive species from the plasma or non-volatile products upon the surface which can clearly be seen as a coating film over both sample and mask upon removal of the sample from the etch chamber. The etch profile was seen to become most vertical (9^0 of overcut) at a methane content of 6 sccm, corresponding to the point of maximum etch rate. If the chamber is allowed to become severly contaminated with polymer then the etch rate is seen to fall off and the polymer point seen to move to mixtures containing a lower methane content. It is believed that polymer from the chamber wall is re-entering the gas phase increasing the relative abundance of high carbon species and eventually finding its way to the etch surface where it inhibits etching.

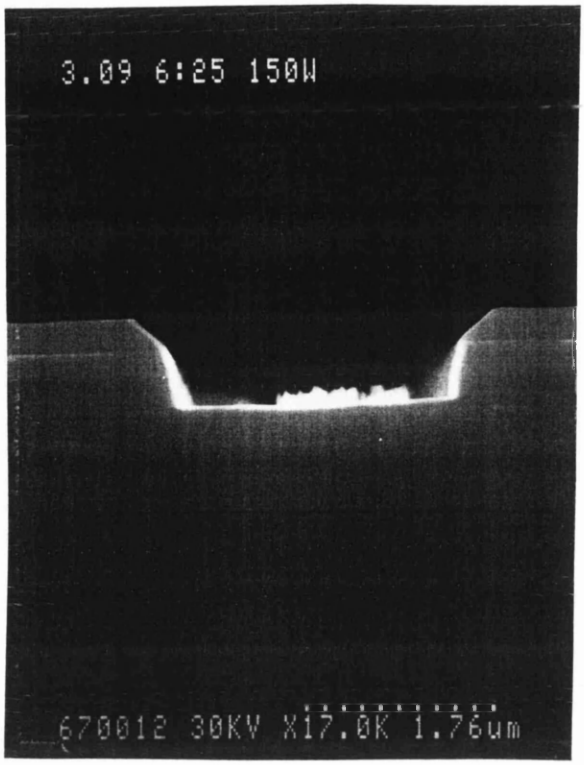

Figure 3.13
AlGaAs trench etched using methane hydrogen with a Si_3N_4 mask. The mask shows signs of sputtering

The mechanism responsible for the overcut profile and lower etch rate than GaAs is believed to be a combination of residual oxygen in the chamber forming the very involatile aluminium oxide (Al_2O_3), and the lower volatility of the etch product trimethylaluminium ($Al(CH_3)_3$) than the product trimethylgallium ($Ga(CH_3)_3$) the only group III product formed whilst etching GaAs. The presence of either of the aluminium oxide or the trimethy- aluminium species upon the surface will on average slow down the rate of reaction reducing the etch rate, higher powers (higher DC self bias) are therefore needed to supply enough energy to remove these species by sputtering and begin etching.

3.3.2 Induction Time

When it is desired to etch features to a particular depth not only is it important to know how gas flows, rf power and pressure effect the etch rate but the linearity of the etch process with time is of great importance. If the rate was non-linear with time to etch a feature three times as deep as the test sample would not take three times as long but may vary in a complex way. To investigate the linearity of the etch process with time the gas mixture, 6 sccm of methane in 25 sccm hydrogen at 150 W was used to etch 5 μm wide trenches in $Al_{0.3}Ga_{0.7}As$ capped with 10 nm of GaAs. By etching over a range of etch times the linearity of the etch rate could be established

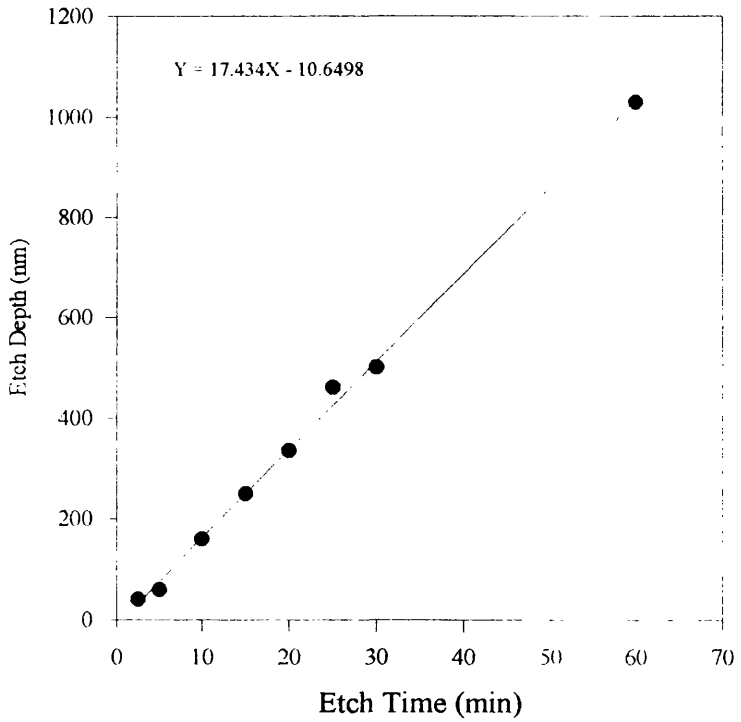

Figure 3.14
Etch rate of $Al_{0.3}Ga_{0.7}As$ with time.

Figure 3.14 demonstrates that to within measurable accuracy at high power the etch rate is indeed constant with time and an induction time (the time taken before etching commences) of less than one minute was observed. Using the least squares fit method the linear relationship has been found for the etch depth as a function of the etch time.

Etch Depth = 17.434.t -10.6498 (eqn. 3.6)

Where the etch depth is measured at time t.

Extrapolating back to the point at which the etch depth becomes zero yields a value for the etch time of 37 seconds. The induction time has two contributing factors; the time taken to etch through the tough native oxide and the time to etch the GaAs capping layer. The longer it takes to remove the thin oxide the longer it appears that it takes for etching of the semiconductor to be initiated and the greater the induction time. With this material system the GaAs etches slightly faster than AlGaAs under the same conditions. The presence of the 10 nm GaAs cap will therefore slightly decrease the observed induction time, however since the difference in etch rates between GaAs and AlGaAs is only slight this effect will be minimal. Taking into account these two contributions it is possible to conclude that the true oxide layer etching time is only slightly greater than 37 seconds. The linearity of this result indicates that the fall of DC bias with time as polymer is deposited within the chamber has little overall effect on the etch over a long period of time.

Reflectometry may also be used to demonstrate the induction time. Reflectance measurements made upon a GaAs/AlGaAs multiple quantum well sample show a large induction time (Figure 3.15). The extremely long induction time that was observed was caused by the formation of a thick layer of aluminium oxide when the uncapped $Al_{0.4}Ga_{0.6}As$ surface was exposed to the atmosphere for a considerable

length of time. Oxides of gallium and arsenic will of course be formed but it is believed to be the formation of oxides of aluminium with their extremely high melting/boiling points that are responsible for the resilience of the native oxide.

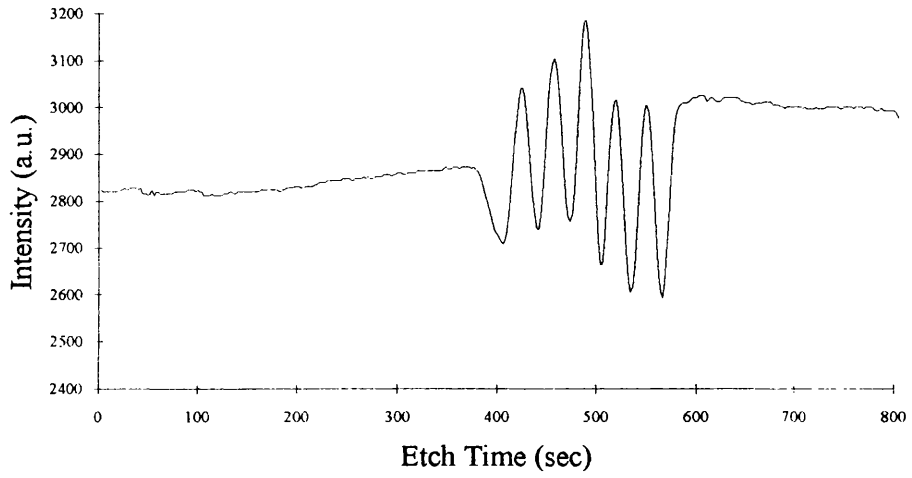

Figure 3.15
Experimental reflectance curve for GaAs/AlGaAs MQW.

It would have been nearly impossible to judge the induction time by experience alone and hence difficult to achieve an accurate etch depth. The etch was terminated after etching to a depth of about 600 nm corresponding to the top of the of another $Al_{0.4}Ga_{0.6}As$ layer on which the growth had been interrupted and an oxide layer allowed to form. Again a great deal of time is needed for the surface oxide layer to be removed. The temporary suspension of the etch is seen in the second horizontal portion of the reflectance trace.

3.4 CH_4/H_2 RIE of InGaAs and InAlAs

3.4.1 Etch Rates of InGaAs and InAlAs

The etching of AlGaAs was achieved without the ability to control independently the flow rate and pressure of the etch gas mixture. A pressure controller was available for the etching of the indium containing semiconductor alloys thus increasing the process parameters available and hence the possible complexity of establishing optimum conditions. For this set of experiments the pressure was in most cases held at 20 millitorr and optimisation of the etch process achieved at this pressure.

The materials used were 5 μm of undoped $In_{0.52}Ga_{0.48}As$, 3 μm of undoped $In_{0.53}Al_{0.47}As$ with 10 nm of InGaAs as a capping layer to prevent surface oxidation, an InGaAs/InAlAs multilayer structure and an InP/InAlAs multilayer structure (both of which are to be fully described later). All materials were designed to be lattice matched to the InP substrates and were grown by molecular beam epitaxy by Glasgow University MBE Research Group or by MOCVD by British Telecom Research Labs.

The etch rates were investigated for InGaAs and InAlAs over a range of rf powers maintaining the total flow rate at 25 sccm but varying the ratio of methane to hydrogen flows within the gas mixture. The heater-chiller unit connected to the cathode was set throughout the experiments to 30°C.

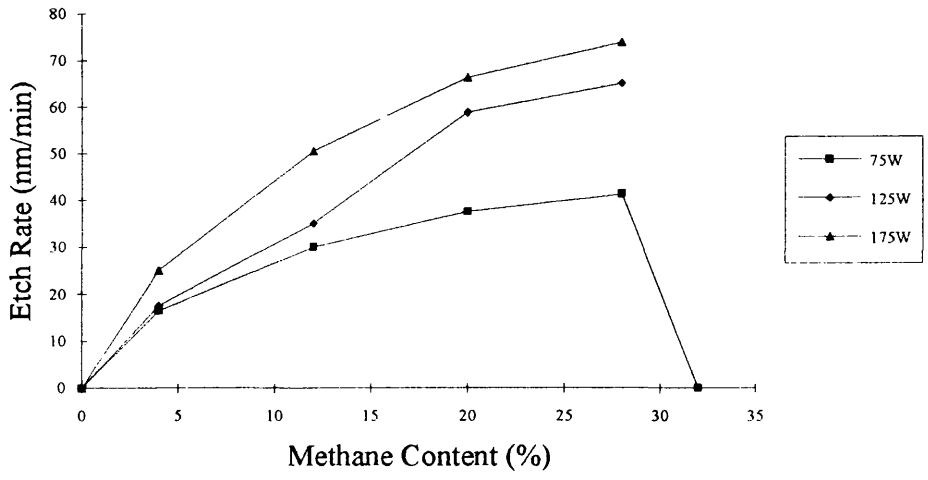

Figure 3.16
Etch rate of InGaAs with methane flow and rf power.

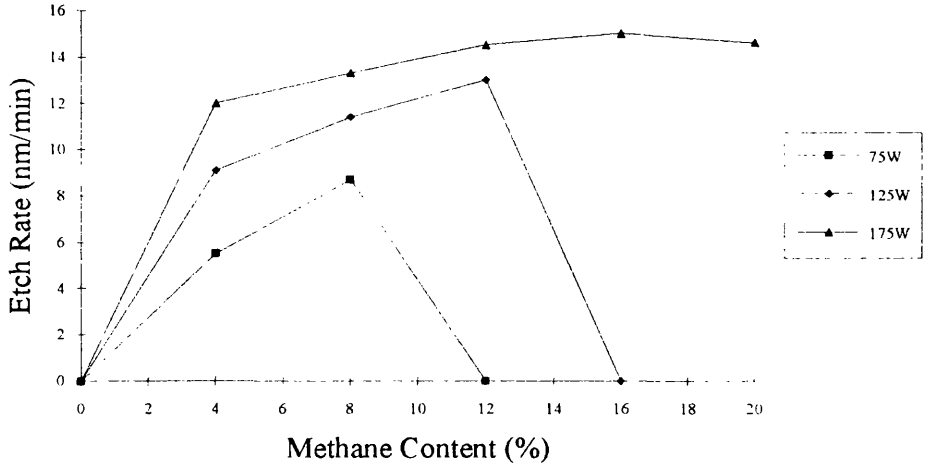

Figure 3.17
Etch rate of InAlAs with methane flow and rf power.

An increase in the applied rf power results in an increase in the etch rate of InGaAs and InAlAs in a similar manner to that observed with AlGaAs. At the higher powers more methane molecules can be broken down to form the methyl ions needed for etching. Higher etch powers will lead to the formation of a higher DC self bias and thus more energy will be gained by the ions as they cross the dark space. The

combined effect of a greater flux of reactive species to the surface and the higher energies of the ions will increase the probability of a reaction taking place and at the same time ensure efficient sputtering of any polymer that may have formed upon the etch surface and be inhibiting the etch process.

3.4.2 The Effect of Pressure and Total Flow Rate

With AlGaAs, InGaAs and InAlAs it was found that the etch rates increased as the supply of reactive species available for etching increased. Etch rates were seen to increase with an increase in the rf power which cracks more of the methane parent molecules or by increasing the concentration of methane in the gas mixture.

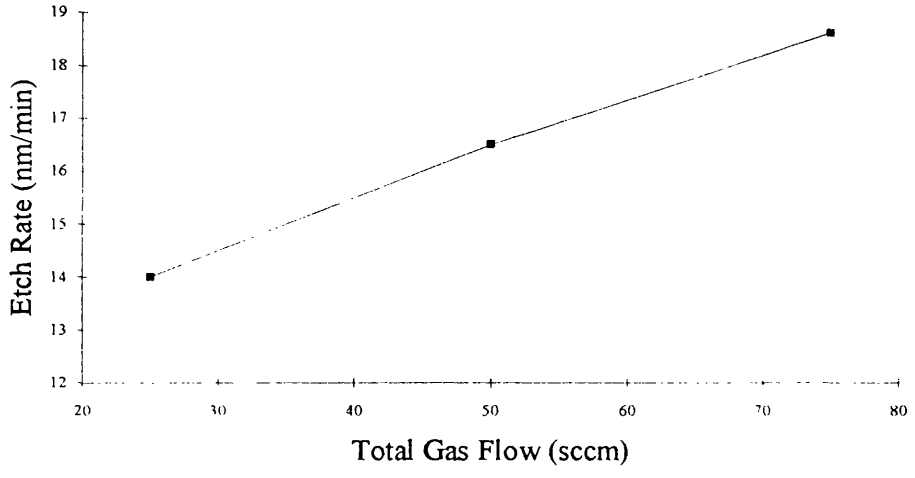

Figure 3.18
The effect of total gas flow upon the etch rate of InGaAs using a 1 sccm CH_4, 24 sccm H_2 at 20 millitorr and 75 W.

Increasing the total gas flow increases or the chamber pressure increases the potential for the formation of reactive species. Such an increase will inevitably lead to an enhancement in etch rate. The rise in etch rate with total flow rate indicates that

reactant species are being utilised efficiently and the process can be said to be operating in the flow rate limited regime.

The gas mixture and power used for this brief study were those used to form vertical wall profiles in InGaAs (1 sccm CH_4, 24 sccm H_2 at 20 millitorr and 75 W). The low methane content ensures that the etch is performed far from the polymer point and as a result changes made to the etch conditions are not sufficient to bring about polymer formation instead of etching.

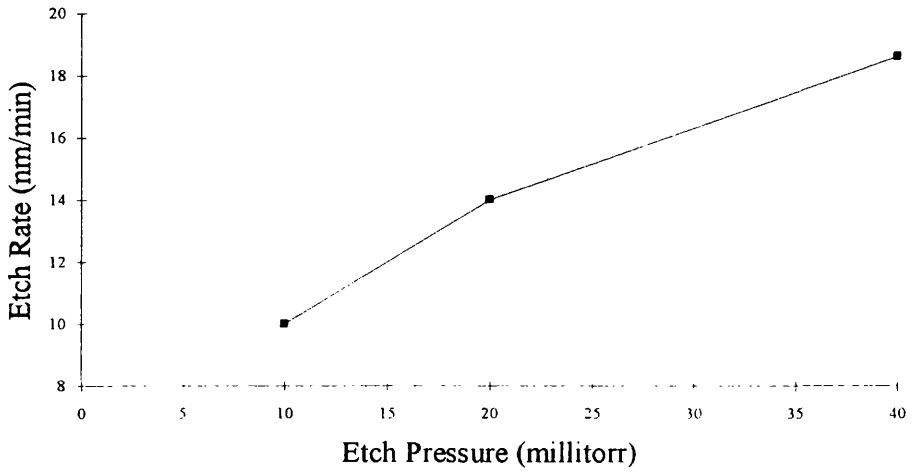

Figure 3.19
Change of etch rate of InGaAs with etch pressure using 1 sccm CH_4, 24 sccm H_2 with 75 W rf power.

3.4.3 Selectivity of InGaAs over InAlAs

Of particular interest for device fabrication purposes is the selectivity of one material with respect to another. For example when it is desired to etch a gate recess for a MESFET or HEMT device, an etch-stop layer is often introduced into the material structure. The uppermost material, the cap will be removed but surface

reactions with the material of the etch-stop layer when it is exposed to the plasma will prevent further etching.

Devices such as rib-waveguide lasers can again also contain several layers of different materials but in this instance it may be desired to etch through all of these layers and so similar etch rates in each material are desirable. The selectivity of material A over material B is defined as the etch rate in material A divided by the etch rate in material B and is only valid if the etch conditions at which the etch rates were measured were the same.

When etching InGaAs and InAlAs with methane and hydrogen mixtures the point at which there is infinite selectivity of InGaAs over InAlAs has already been demonstrated under the conditions for which InGaAs will etch but InAlAs will be coated in polymer. Under conditions at which both materials normally are etched it can be seen in figure 3.20 that the selectivity rises for all rf powers as the methane content of the gas mixture is increased. Conversely we can regard the etch selectivity as falling as the methane content is reduced.

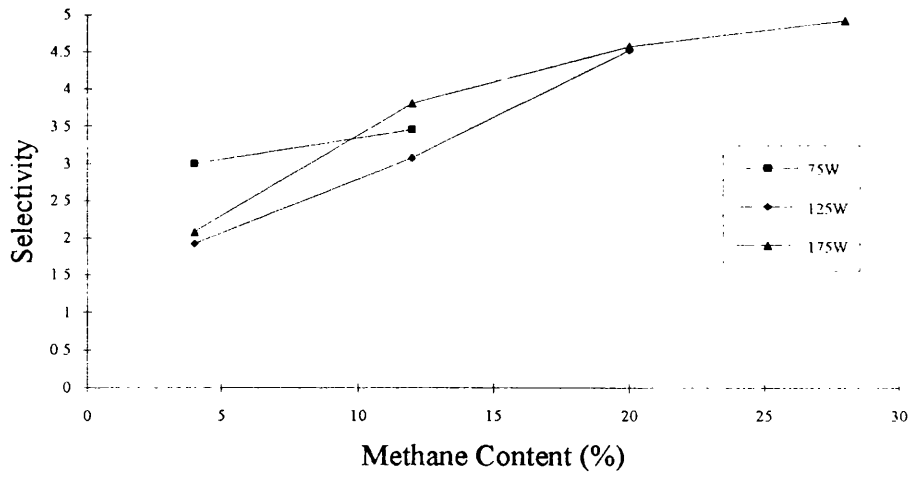

Figure 3.20
Selectivity of InGaAs over InAlAs during CH_4/H_2 RIE.

In moving away from the polymer point, there are insufficient hydrocarbon inhibitors present to prevent some etching of the InAlAs. Lowering the methane content further reduces the concentration of inhibitors, etch mechanism are less encumbered by the inhibitors and etching improves with respect to InGaAs.

The selectivity of one material relative to another can also be investigated by observing the change in etch depth with time for a multi-layer structure. Figure 3.21 shows the etching of a multi-layer of 150 nm InP / 5 nm InAlAs / 150 nm InP / 20 nm InAlAs / 150 nm InP / 50 nm InAlAs / 150 nm InP / 100 nm InAlAs upon an InP substrate.

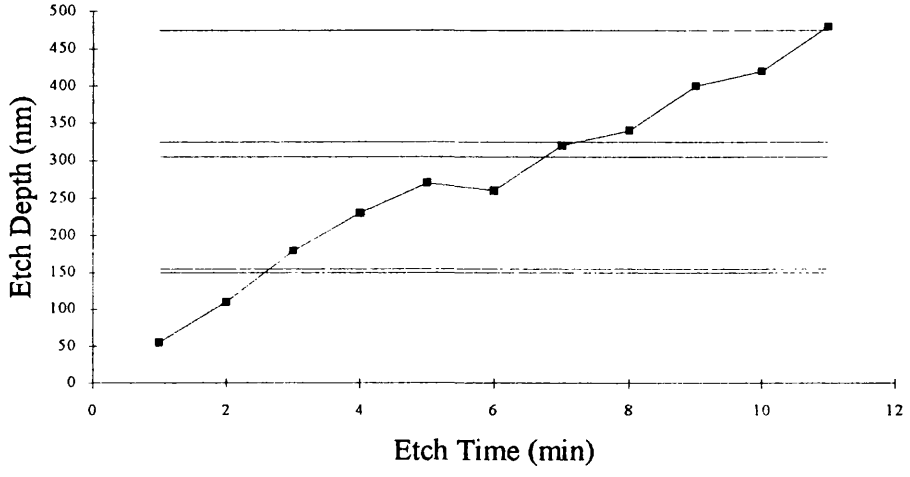

Figure 3.21
Etch depth in InP/InAlAs multi-layer with time demonstrating the difference in etch rates between the two material systems.

A discontinuity in etch depth can be clearly seen close to the position of the 20 nm InAlAs layer. If the material being etched were only InP a straight line would be produced for etch depth with time, so the time interval for which the etch depth in InP line has been shifted and the thickness of the InAlAs layer give the etch rate of the InAlAs layer. Little induction time has been observed for InP. Etching was performed with 3 sccm methane, 22 sccm hydrogen at 125 W and 11 millitorr. The

InP etch rate was found to be 56.7 nm/min. The time to etch the InAlAs was 1.75 minutes giving an etch rate of 11 nm/min and a selectivity of InP to InAlAs of 5:1. Under similar conditions the selectivity of InGaAs to InAlAs is approximately 3:1. All selectivities will of course change with a change to the plasma conditions.

3.4.4 Etch Profiles

The cross-sectional profile of the features etched was investigated at the same time as the etch rates of InGaAs and InAlAs. The two most striking features of etch profiles formed in InGaAs is the non-linear nature of the profile and the polymer deposited upon the mask. The deposition of the polymer upon the mask can effect the shape of the sidewall. If a high methane content gas mixture is used the build up of polymer can be so great that the edge of the mask itself will also become coated as the deposition rate is higher than the rate at which the polymer can be removed by sputtering. The polymer has the effect of increasing the width of the mask and hence a foot is created where the surface that we require to be etched is shadowed from the plasma by the polymer. The base of the feature etched is now wider than the original mask.

The deposited polymer also shows signs of sputtering. The polymer coating in not uniformly thick across the mask but shows distinct angled facets towards the edge of the mask. The faceting is due to ion bombardment which can more readily remove material that is at the edge where polymer particles are less tightly bound into the bulk.

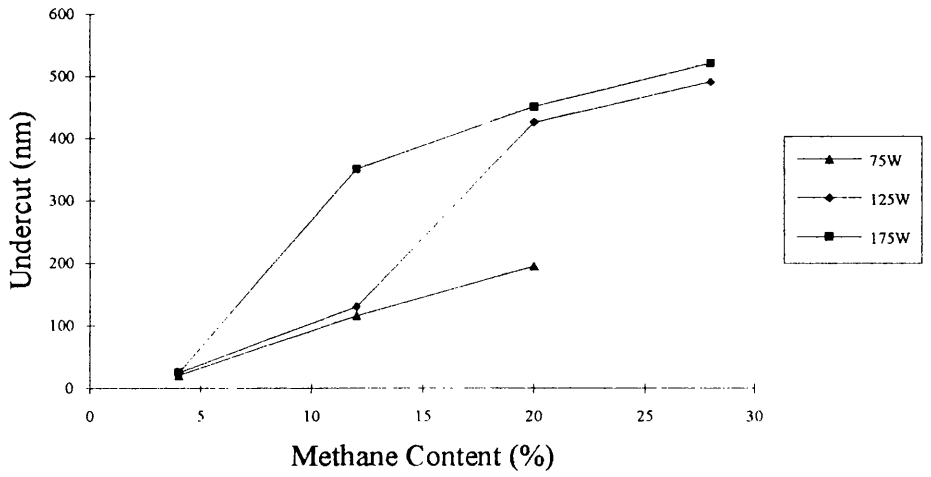

Figure 3.22
Undercut with methane content and power for InGaAs during a 40 minute etch.

Reactive ions that cross the dark space may not interact with the etch surface but be reflected from etch surface. These reflected ions or ions that may be scattered within the dark space by collisions with neutral species or from features such as the mask may then impinge upon the sidewall where they are free to react. Such reactions are responsible for the undercutting of the mask that is seen and as the supply to the sidewall is increased by having higher rf powers and higher methane concentrations the amount of undercut is seen to increase. Undercutting of sidewalls in InGaAs has been seen by Adesida *et al.* [3.9] who also report increased undercut with high methane content gas mixtures.

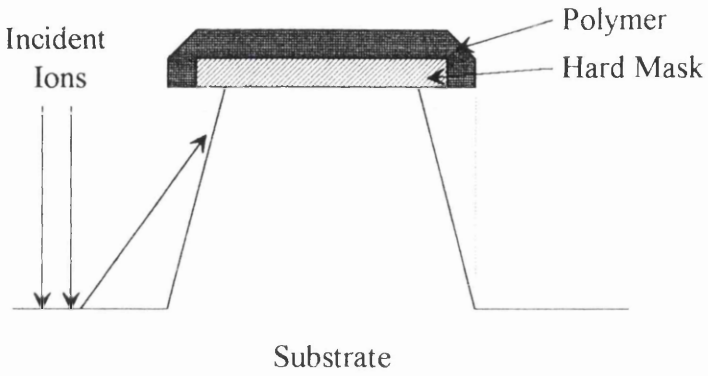

Figure 3.23
Schematic diagram of feature etched using high methane content showing how reflected ions can etch the sidewalls and deposited polymer force out the foot of the sidewall.

Tsutsui *et al.* [3.20] have observed that the amount of undercutting in methane/ hydrogen RIE increases with the area of unmasked etch surface adjacent to the sidewall. The unmasked area acts as a source for scattered ions. An increase in this area will increase the flux of scattered ions that are available and can impinge upon the sidewalls and cause etching. Etch profiles may thus be expected to change between a trench where there is only a small area that can provide scattered ions and ribs where there is a very large adjacent unmasked area. In the study of etch profiles presented in this section etch profiles were studied using widely spaced (>20 μm) rib-like features. The collecting area for scattered ions can therefore be thought of as infinite and no effects due to geometry have been observed.

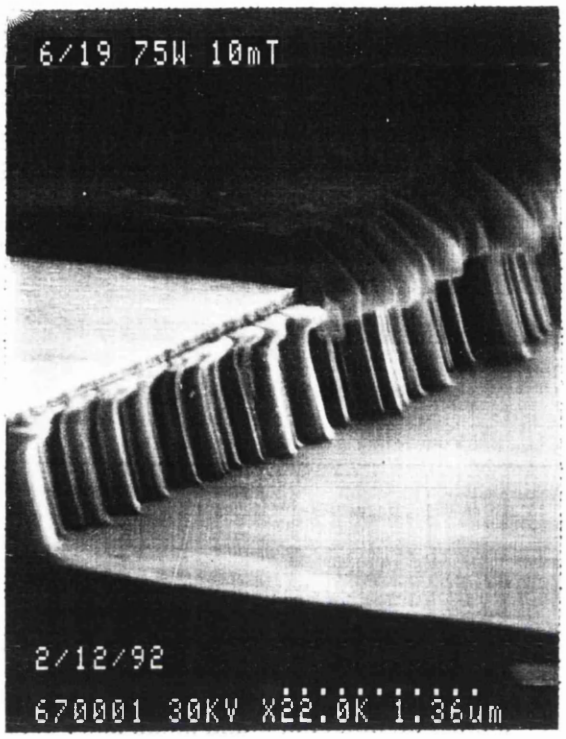

Figure 3.24
InGaAs etched with 6 sccm CH_4, 19 sccm H_2 at 10 millitorr and 75 W showing polymer coating the 200 nm Ti mask.

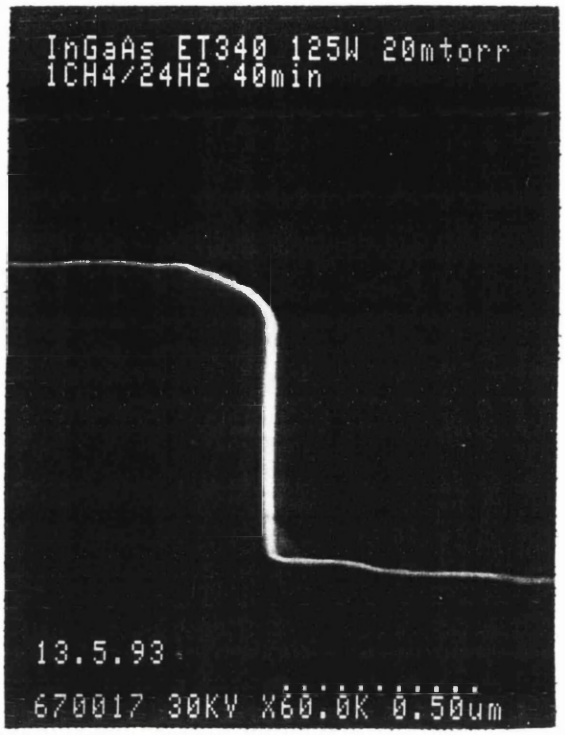

Figure 3.25 (a)

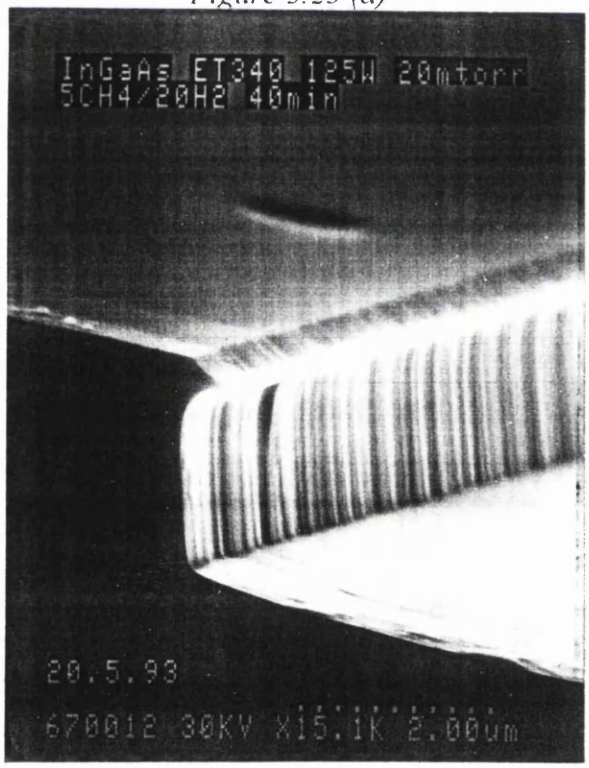

Figure 3.25 (b)

InGaAs etched by (a) 1 sccm CH_4, 24 sccm H_2 and (b) 5 sccm CH_4, 20 sccm H_2 at 20 millitorr.

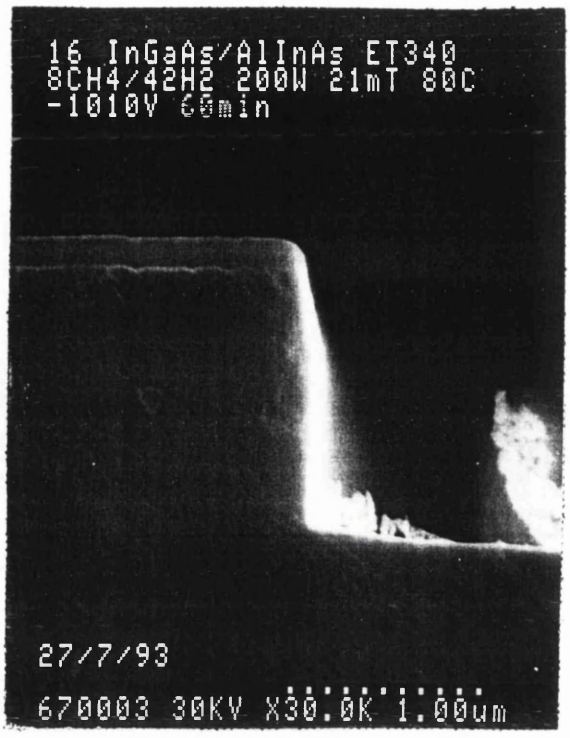

Figure 3.26 (a)

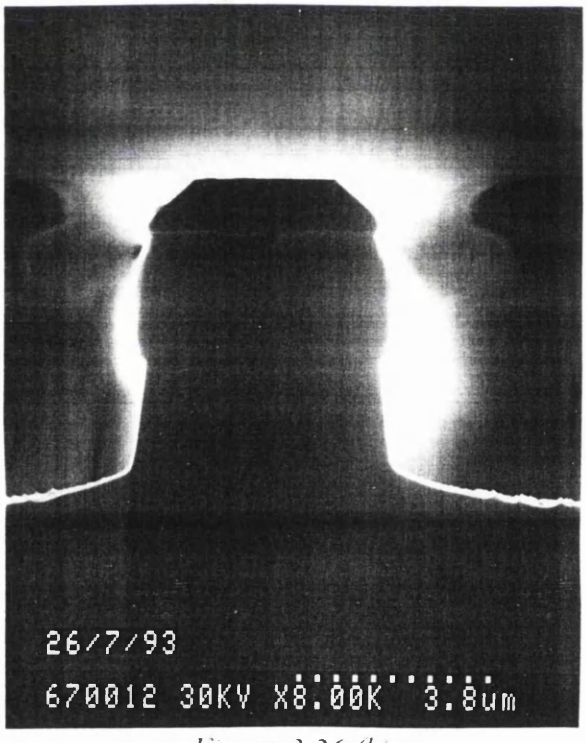

Figure 3.26 (b)

Ridge waveguide laser fabricated in InAlAs (a) etched to the correct depth with slight mask recession and (b) over etched to show the difference in etch profiles between InAlAs and InP under the same process conditions.

3.4.5 CH_4/H_2 RIE for Fabrication of an S-SEED Array

Many of the aspects and behaviour of the methane/hydrogen etch can be brought into context by applying the techniques learnt to device fabrication.
Because of their ability to match the high power available from diode-pumped Nd:YLF and Nd:YAG lasers, InGaAs S-SEED arrays (symmetric self electro-optic effect devices) are of particular interest in digital optical systems when flip-chip bonded to Silicon-CMOS [3.21-3.23]. The SEED is a p-i-n diode, comprising of an undoped multiple quantum well (MQW) layer between a p-doped and an n-doped layer. Application of an external electric field perpendicular to the MQW region can significantly modulate the absorption of the MQW. With the diode reverse biased through a load an optical bistable device will be formed that can be switched by an optical signal. The S-SEED is formed when two such diodes are reverse-biased in series, each diode acting as the other's load. The state of the S-SEED is then able to be switched by an input beam of sufficient intensity.

The fabrication of S-SEED arrays for silicon CMOS flip-chip bonding is rather complex, requiring 10 fabrication stages where the objectives are excellent device performance in high yield arrays. Fabrication of the device requires two separate dry etch stages, the first to define the modulating structure and exposing the n-contact layer, the second etch removes material down to the semi-insulating substrate electrically isolating the device from its neighbours.

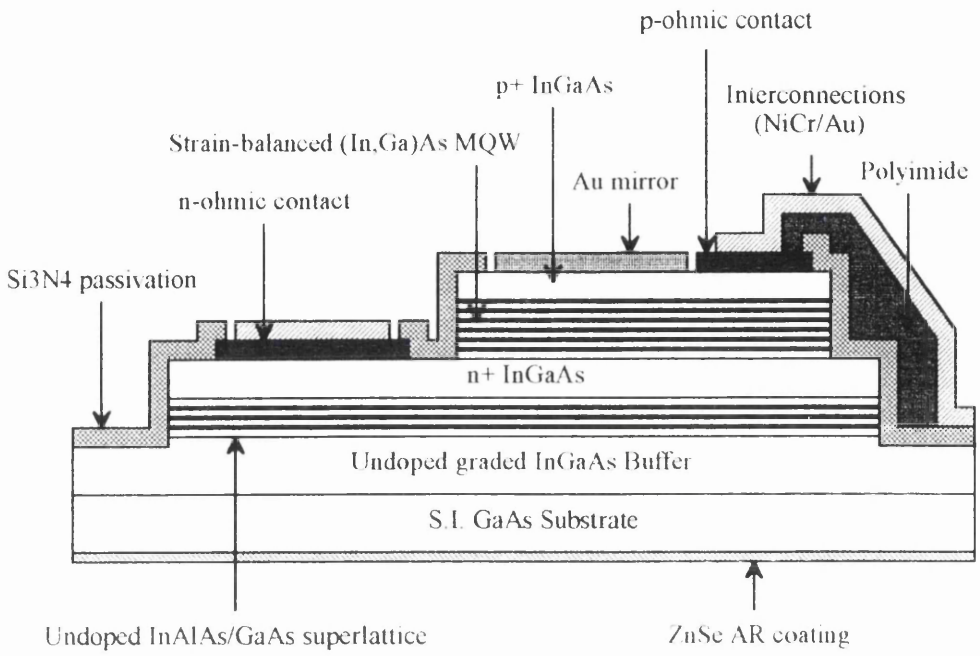

Figure 3.27
Cross-sectional schematic of an S-SEED device

Smooth, clean and uniform etch surfaces are the *sine-qua-non* conditions for the fabrication of high yield arrays. Since the etching steps are the first to be performed defects at this stage may induce failure of the whole S-SEED array. Vertical wall profiles reduce the capacitance of the SEED, increasing switching speed.

The requirements for the etch mask for device fabrication is more stringent than those used for etch tests. The mask must be readily removed without causing degradation of the modulator top surface which at a later as deposited with a NiCr/Au mirror and a p-ohmic contact. During the second-stage a planarisation layer must be incorporated to produce a flat surface suitable for lithography. For these reasons metal-on-polymer (MOP) masks were fabricated from 50 nm NiCr / 100 nm

Au / 150 nm NiCr deposited upon a layer of polyimide. The NiCr provided both a mask for the oxygen etching of the polyimide and a hard mask for the methane/hydrogen etch. Gold has been included to ensure clean lift-off and reduce stress in the NiCr which could cause the metal layer to deform.

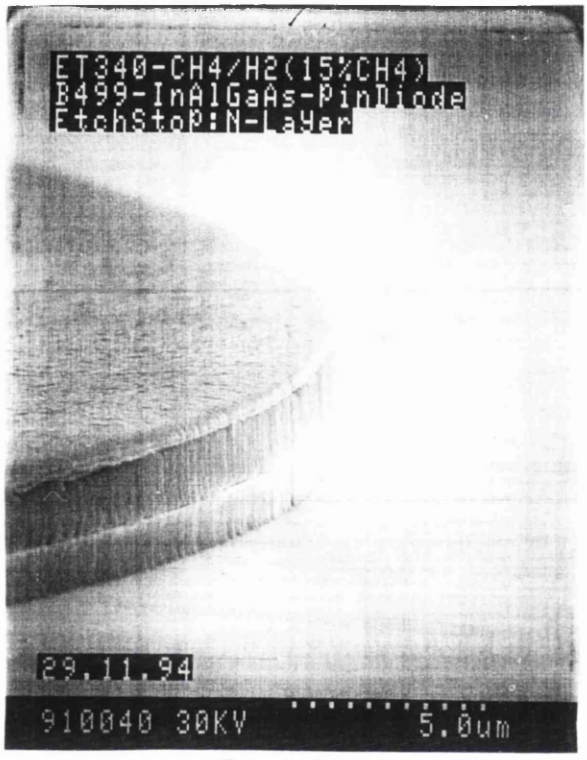

Figure 3.28
First stage etch with MOP mask still in place.

To determine the end-point of the etch accurately so that the MQW region is etched while stopping to leave as much of the underlying p-contact layer intact maskless reflectometry was used during the two-stage etch for SEED fabrication. The theoretical reflectance from an unmasked area of the wafer was calculated and the end of the multiple quantum well layer identified. The theory indicated that the change in reflectance between wells and barriers was large and during device fabrication the quantum wells could be counted and hence the etch stop identified.

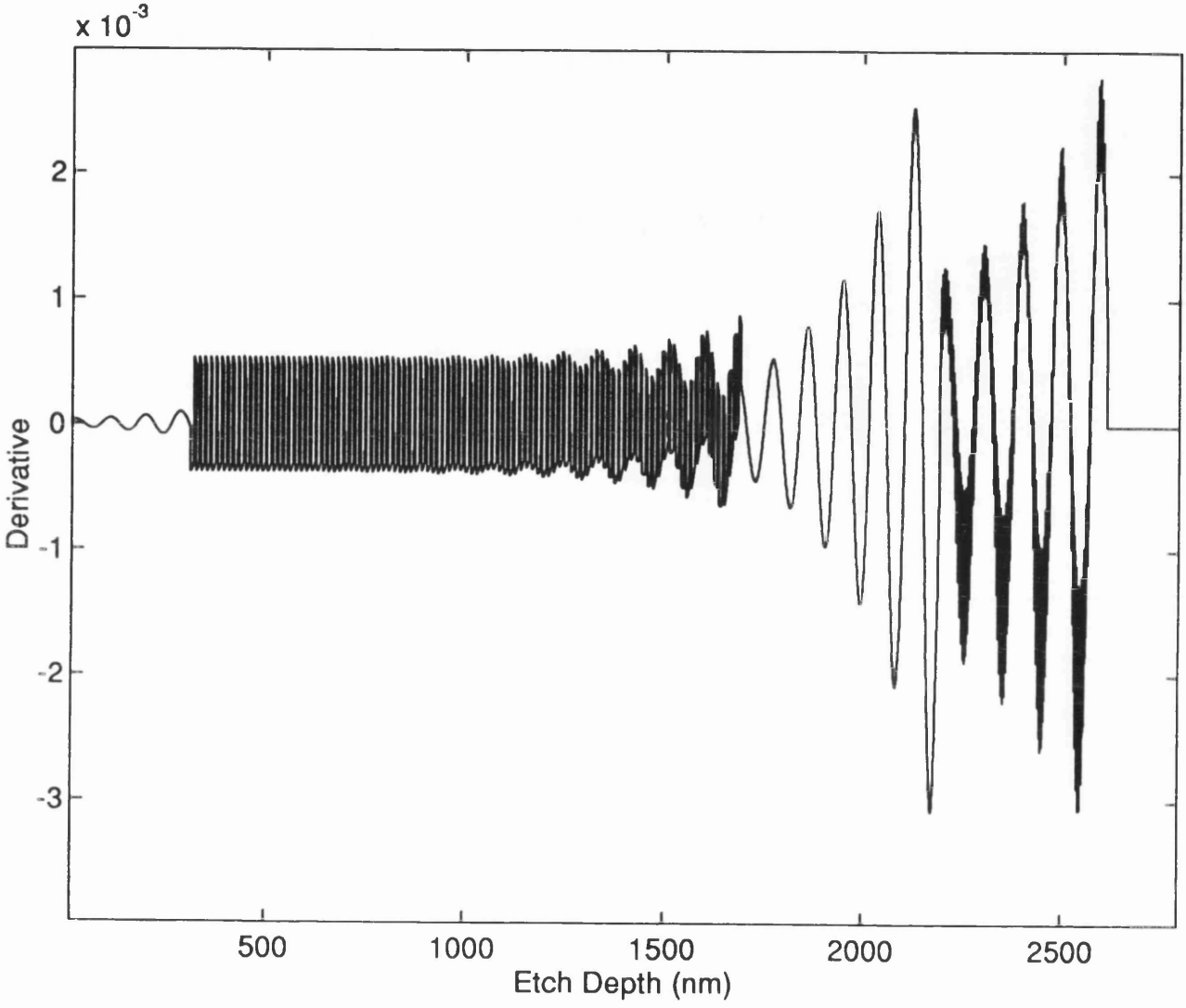

Figure 3.29

First derivative with respect to time of the theoretical reflectance signal for the S-SEED layer structure consisting of 310 nm $In_{0.135}Ga_{0.865}As$ / 100 x (5.7 nm GaAs, 8.1 nm $In_{0.23}Ga_{0.77}As$) MQW / 500 nm $In_{0.135}Ga_{0.865}As$ / 100 x (2.1 nm $In_{0.27}Al_{0.73}As$, 2.1 nm GaAs) SL / 2000 nm graded $In_{0-0.135}Ga_{1-0.865}As$ buffer / GaAs substrate.

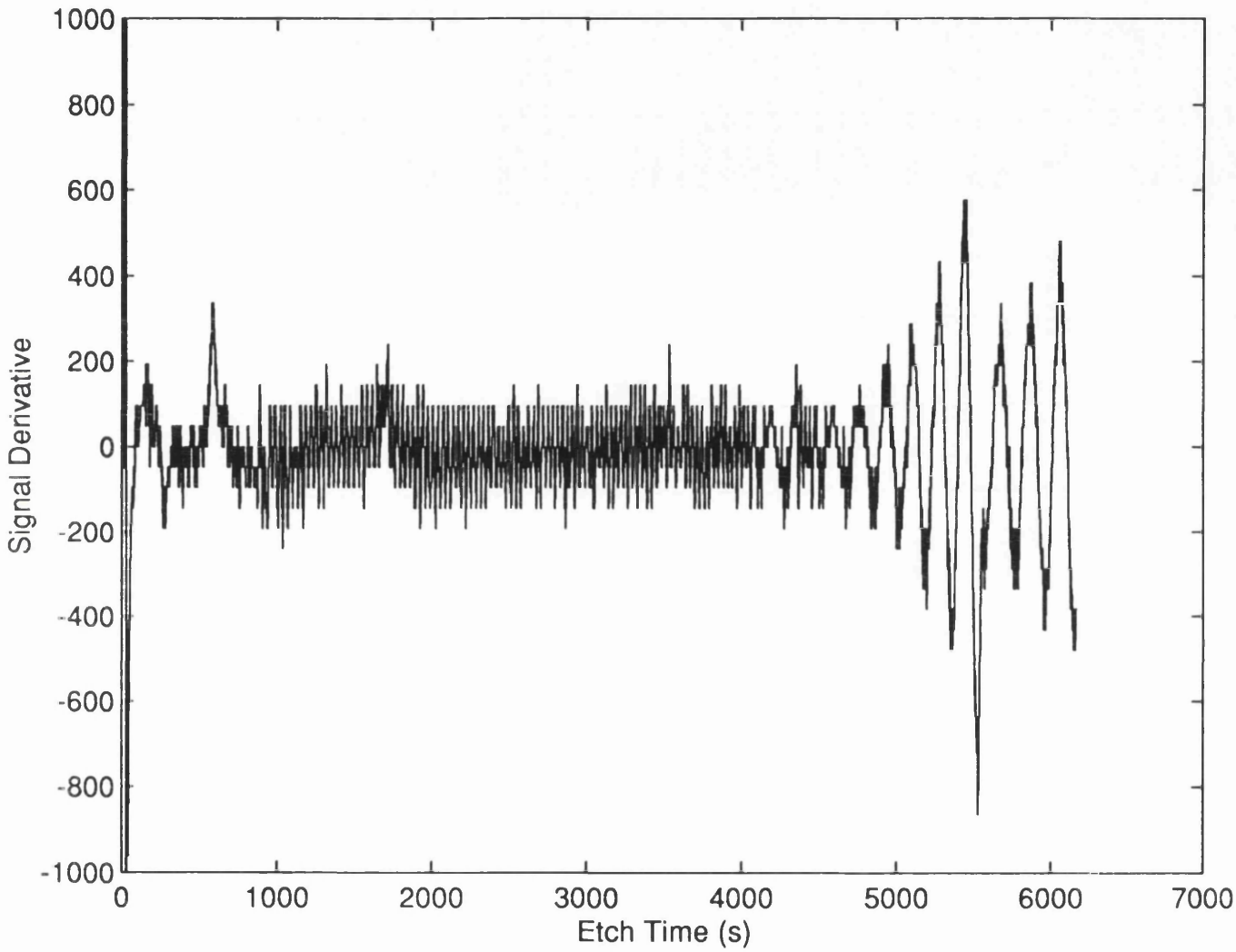

Figure 3.30

First Derivative with respect to time of the experimental reflectance signal from the surface of the S-SEED layer structure during CH_4/H_2 RIE.

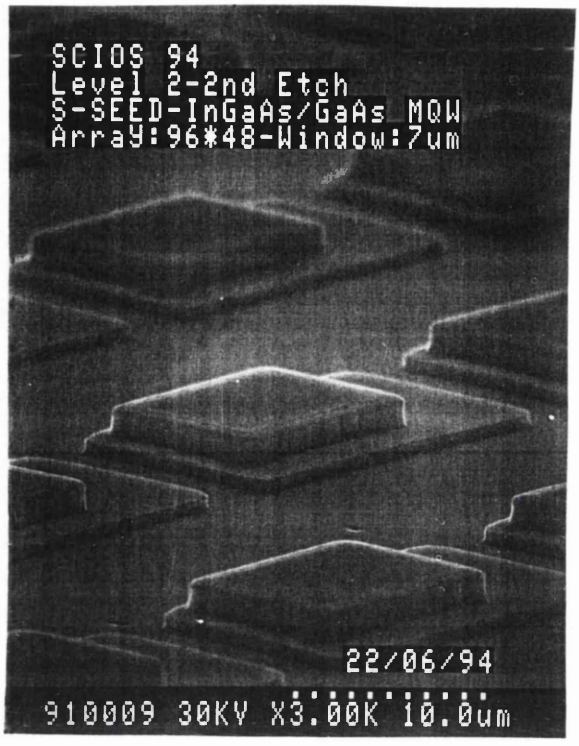

Figure 3.31
Micrograph of S-SEED device after second stage etch

By halting the etch within the InAlAs/GaAs superlattice region it was possible to gain an insight into the uniformity of the etch process on both micro- and macroscopic scales. Investigation of the etch surface showed the presence of two dark rings around each etched feature. These rings were identified as two of the InAlAs layers of the superlattice region. These layers could be seen due to oxidation of aluminium in the layer which produces a dark layer that contrasts with the highly reflective GaAs. The presence of only two rings around the etch features indicates that the etch produced a surface that was smooth and flat between neighbouring devices to within 10 nm. Near identical ring features were observed around all devices over the complete area of the material (6x6 mm) being etched showing a similar uniformity level on the macroscopic scale.

In the second stage etch the super-lattice must be etched completely through to ensure isolation of the device. Again reflectometry was used to identify the end-point and a suitable amount of over-etching allowed. From theory it was just possible in the derivative of the reflected signals to identify each layer of the superlattice. In practice it was impossible to resolve each layer due to noise on the reflected signal. The end of the superlattice was thus identified by the signal received from the buffer layer. The devices whose schematic diagrams are shown in Figure 3.27 were etched using 1 sccm methane and 24 sccm hydrogen at 200 W and 20 millitorr. The two separate etch stages are easily identified in Figure 3.31.

The reflectance signal may also be used to study the linearity of the etch with time whilst etching through a thick epi-layer. Using the example of the S-SEED the etch linearity can be monitored within the 500 nm InGaAs layer that separates the superlattice and the multiple quantum well regions.

Peak Times* (seconds)	Time Difference** (seconds)	Average Etch Rate*** (nm/min)
3631,3778	146 +/- 2	35.8 +/- 0.9
3778,3921	143 +/- 2	36.5 +/- 0.9
3921,4070	149 +/- 2	35.1 +/- 0.9
4070,4220	150 +/- 2	34.8 +/- 0.9

Table 3.1
Reflectometry peak-to-peak times whilst etching InGaAs.

* An error of +/-1 second is present in measuring the reflectance curve peak times.

** The error in the measured peak-to-peak time is the addition of errors in peak times

*** Errors in calculating the average etch time over the peak to peak time interval arrise from arrors in time interval already mentioned, refractive index and illuminating wavelength. For $In_{0.23}Ga_{0.77}As$ the real part of the refractive index is taken as 3.85+/-0.04 and the laser wavelength 679.5+/-0.1nm.

The reflectance signal intensity will rise and fall between maxima and minima for thick epi-layers. For the change in intensity to complete one cycle the epi-layer thickness must change by the thickness $\lambda/2n$ where n is the real part of the refractive index. Measuring the time for the signal to complete the cycle reveals the average etch rate over that time. Comparison of successive peak-to-peak times will reveal average etch rates over these successive cycles. Table 3.1 shows the etch times of five intensity peaks for the reflectance from the surface of the S-SEED whilst etching through the 500 nm InGaAs layer. Good agreement in time differences are observed, showing 4.9% difference between the fastest and slowest etch cycles.

The etch rate of $In_{0.23}Ga_{0.77}As$ deep indicated in Table 3.1 can be compared to the average etch rates of the material within the topmost layer that forms the p-type contact layer. This contact layer is 310 nm thick and from the experimental reflectance data takes 520+/-5 seconds to etch before signal from the MQW region is observed. The etch rate for this layer is thus 35.8+/-0.4 nm/min which is well within the range of rates calculated for the deep layer. The consistency of the etch rate over the 70 minutes of etching leads to the concluded that there is no significant induction time.

3.5 Chapter Summary

Monitoring of the methane/hydrogen plasma has been performed by optical emission spectroscopy. As the methane content of the plasma is increased the intensity of the CH species increases linearly and the intensity of H_2 falls slightly as its relative abundance decreases. Since CH is a cracking product of methane the intensity of the CH peak is taken as a direct indicator of the concentration of methane in the plasma. All peaks observed are seen to increase in intensity as the applied rf power is increased.

OES has also been used as a tool to gauging the cleanliness of the etch chamber; the level of polymer deposited upon the chamber and the rate at which air is leaking in to the vacuum system. Etch rates are seen to fall and the polymer point moves towards regions of lower methane content when the chamber becomes excessively coated with polymer. This polymeric build-up can be removed by cleaning the chamber with an oxygen plasma. The oxygen species react with the polymer forming the volatile CO and CO_2 products which can be pumped away. Monitoring emission lines associated with these products indicates when the chamber has become free from polymer.

When etching semiconductors containing aluminium it is important to remove residual oxygen from the etch chamber prior to the etch. Oxides have been associated with the presence of long induction times. For this reason a hydrogen plasma clean is performed to remove any remaining oxygen.

After cleaning the DC self bias of the cathode will fall as the chamber is again coated with polymer. A steady state is achieved after as long as ten minutes. The final DC bias is related to the applied rf power rather than the composition of the

etch gas, although methane rich plasmas have a slightly lower DC bias than methane rare plasmas.

Energetic ions incident on the surface of the material being etched will lead to the heating of the surface. The highest surface temperatures were observed at the higher DC biases, for example at 75 W a temperature of 112 ^{0}C was achieved but at 175 W a temperature of 154 ^{0}C was recorded. There was no observable difference in surface temperature with gas composition. This is believed to be due to the negligible change in DC bias with gas composition, the ions receiving the majority of there energy from being accelerated across the dark space.

$Al_{0.3}Ga_{0.7}As$ with a 10 nm GaAs cap has been etched using a fixed hydrogen flow of 25 sccm and a range of methane flow and rf powers. With 5 sccm methane, 25 sccm hydrogen etching could only be initiated for rf powers of greater than 50 W. Using a fixed rf power of 150 W etch rates rise with methane content of the gas mixture to a maximum of 18.3 nm/min at 6 sccm methane, 25 sccm hydrogen and then rapidly fall to zero as the polymer point is approached and deposition occurs from the plasma onto the etch surface. Under similar conditions GaAs etches at a rate of 20 nm/min. The induction time is observed to be low, 37 sec when the AlGaAs is capped by GaAs. When no capping material is present oxidation of the surface produces a resistant layer that may take several minutes to remove before etching of the unoxidised AlGaAs can take place.

InGaAs and InAlAs show similar etch rate curves with methane content to AlGaAs. InAlAs however etches at a slower rate and the polymer point found at lower methane contents than InGaAs for all conditions. Selectivities of InGaAs over InAlAs range from 2 at 1 sccm methane, 24 sccm hydrogen at all rf powers to 4.5 at 7 sccm methane, 18 sccm hydrogen at 175 W. Vertical etch profiles are obtained in InGaAs with 1 sccm methane, 24 sccm hydrogen at all rf powers but as the methane

content is increased undercutting of the etch mask becomes evident. The most vertical profiles whilst etching InAlAs are obtainable at the highest rf powers. At lower rf powers the profiles are slightly overcut.

An S-SEED array has been fabricated using 1 sccm methane, 24 sccm hydrogen at 20 millitorr and 200 W. Etch surfaces were extremely smooth showing at the most 10 nm of unevenness at the edges of the devices.

References

[3.1] U. Niggebrugge, M. Klu and G. Garu,
"A novel process for reactive ion etching of InP using CH_4/H_2",
Inst. Phys. Conf. Ser. **79** Chp.6 pp. 367-372 (1985)

[3.2] R. Cheung, S. Thoms, S.P. Beaumont, G. Doughty, V. Law and C.D.W. Wilkinson,
"Reactive ion etching of GaAs using a mixture of methane and hydrogen",
IEEE Electron. Lett. **23** pp. 857-859 (1987)

[3.3] S.J. Pearton,
"Dry etching techniques and chemistries for III-V semiconductors",
Mat. Sci. Eng. B **10** pp. 187-196 (1991)

[3.4] S.J. Pearton, C.R. Abernathy, F. Ren and T.R. Fullowan,
"Dry etching and implant isolation characteristics of $Al_xGa_{1-x}As$ grown by metal organic molecular beam epitaxy",
Semicond. Sci. Technol. **6** pp. 1042-1047 (1991)

[3.5] V.J. Law and G.A.C. Jones,
"Obtaining high etch rates of $GaAs/Al_{0.3}Ga_{0.7}As$ using methane:hydrogen MORIE and organic photoresist masks",
Semicond. Sci. Technol. **4** pp. 833-835 (1989)

[3.6] V.J. Law, G.A.C. Jones, D.A. Ritchie, D.C. Peacock and J.E.F. Frost,
"Selective metalorganic reactive ion etching of molecular-beam epitaxy $GaAs/Al_xGa_{1-x}As$",
J. Vac. Sci. Technol. **B 7** pp. 1479-1482 (1989)

[3.7] A. Semu and P. Silverberg,
"Methane-hydrogen III-V metal-organic reactive ion etching",
Semicond. Sci. Technol. **6** pp. 287-289 (1991)

[3.8] T.R. Hayes, M.A. Dreisbach, P.M. Thomas, W.C. Dautremont-Smith and L.A. Heimbrook,
"Reactive ion etching of InP using CH_4/H_2 mixtures- mechanisms of etching and anisotropy",
J. Vac. Sci. Technol. **B 7** pp. 1130-1139 (1989)

[3.9] I. Adesida, E. Andideh, A. Ketterson, T. Brock and O. Aina,
"Reactive ion etching of submicron structures in InP, InGaAs and InAlAs",
Inst. Phys. Conf. Ser. No. **96** Chp. 6 pp. 425-430

[3.10] J. Werking, J. Schramm, C. Nguyen, E.L. Hu and H. Kroemer,
"Methane/hydrogen-based reactive ion etching of InAs, InP, GaAs and GaSb",
Appl. Phys. Lett. **58** pp. 2003-2005 (1991)

[3.11] S.J. Pearton, W.S. Hobson, F.A. Baiocchi, A.B. Emerson and K.S. Jones,
"Reactive ion etching of InP, InGaAs, InAlAs: Comparison of C_2H_6/H_2 with CCl_2F_2/O_2",
J. Vac. Sci. Technol. **B8** pp.57-67 (1990)

[3.12] M.A. Foad, A.P. Smart, M. Watt, C.M. Sottomayor-Torres and C.D.W. Wilkinson,
"Reactive ion etching of II-VI semiconductors using a mixture of methane and hydrogen",
IEEE Electron. Lett. **27** pp.73-75 (1991)

[3.13] L. Henry, C. Vaudry and P. Granjoux,
"Novel process for integration of optoelectronic devices using reactive ion etching without chlorinated gas",
IEEE Electron. Lett. **23** pp.1253-1254 (1987)

[3.14] J.E. Schramm, E.L. Hu, J.L. Merz, J.J. Brown, M.A. Melendes, M.A. Thompson and A.S. Brown,
"Highly selective reactive ion etch process for InP-based device fabrication using methane/hydrogen/argon",
J. Vac. Sci. technol. **B11** pp. 2280-2283 (1993)

[3.15] S.J. Pearton, U.K. Chakrabarti, A.P. Perley and W.S. Hobson,
"Dry etching of GaAs, AlGaAs and GaSb using electron cyclotron resonance and radio frequency $CH_4/H_2/Ar$ or $C_2H_6/H_2/Ar$ discharges",
J. Electrochem. Soc. **138** pp. 1432-1439 (1991)

[3.16] H. Schmid, F. Fidorra and D. Grutzmacher,
"Endpoint detection for CH_4/H_2 reactive ion etching of InGaAsP hetrostructures by mass spectroscopy",
Inst. Phys. Conf. Ser. No. **96** Chp.6 pp 431-434 (1988)

[3.17] D.L. Melville, J.G. Simmons and D.A. Thompson,
"Identification of volatile products in low pressure hydrocarbon electron clyclotron resonance reative ion etching of InP and GaAs",
J. Vac. Sci. Technol. **B11** pp. 2038-2045 (1993)

[3.18] N.I. Cameron, G. Hopkins, I.G. Thayne, S.P. Beaumont, C.D.W. Wilkinson, M. Holland, A.H. Kean and C.R. Stanley, "Selective reactive ion etching of GaAs/AlGaAs metal-semiconductor field-effect transistors", *J. Vac. Sci. Technol.* **B9** pp. 3538-3541 (1991)

[3.19] S.K. Murad, C.D.W. Wilkinson and S.P. Beaumont, "Selective and nonselective RIE of GaAs and $Al_xGa_{1-x}As$ in $SiCl_4$ plasma", Microcircuit Engineering **23** pp. 357-360 (1994)

[3.20] K. Tsutsui, E. Hu and C.D.W. Wilkinson, "Controlling the profile of nanostructures", *J. Vac. Sci. Technol.* **B11** pp. (1993)

[3.21] D.A.B. Miller, D.S. Chemla, T.C. Daman, T.H. Wood, C.A. Burrus, A.C. Gossard and W. Weigmann, "The quantum well slf-electrooptic effect device- optoelectronic bistability and oscillations, and self-linearised modulation", *IEEE J. Quantum Electronics.* **21** pp. 1462-1476 (1985)

[3.22] D.J. Goodwill, A.C. Walker, C.R. Stanley, M.C. Holland and M. McElhinney, "Improvements in strain-balanced InGaAs/GaAs optical modulators for 1047nm operation", *Appl. Phys. Lett.* **64** pp. 1192-1194 (1994)

[3.23] D.J. Goodwill, F.A.P. Tooley, A.C. Walker, M.R. Taghizadeh, M. McElhinney, F. Pottier, C.R. Stanley, D.G. Vass, I. Underwood, M.W.G. Snook. M.H. Dunn, J. Homg and B.D. Sinclair, "InGaAs S-SEEDs and silicon CMOS smart pixels for 1047-1064nm operation", *IEEE/LEOS Topical meeting on smart pixels* (1994)

Chapter 4

Addition of O_2 or Cl_2 to the CH_4/H_2 Plasma

Chapter Outline

We have seen in the previous chapter that high etch rates can achieved using a high rf power and/or a high content of methane in the gas mixture. The price paid for the greater etch rates with methane rich plasmas is a loss of wall verticality. Small quantities of oxygen and chlorine have therefore been added to the basic methane/ hydrogen gas mixture in order that the wall verticality may be improved.

4.1 The addition of O_2

4.1.1 Introduction

It is only possible to obtain vertical wall profiles in InGaAs when using a gas mixture of 1 sccm methane with 24 sccm hydrogen. For even the high applied rf power of 175 W the etch rate of 25 nm/min may prove to be prohibitively slow for etching of deep (>1 μm) features. Although an increase in the methane content of the gas mixture does increase the etch rate it is at the expense of loss of wall verticality caused by undercutting of the mask and polymer deposition onto the mask.

A method to overcome such difficulties has been developed by several workers [4.1,4.2] who have been able to etch nanostructures into InP with good verticality. A cycle of methane/hydrogen followed by an oxygen etch was employed. The methane/hydrogen etch is performed for as long as possible before a build up of polymer on the mask begins to cause degradation of the wall profile. An oxygen etch is then performed to remove the polymer that has built up. It is postulated that the oxygen plasma etch also has the beneficial role of passivating the sidewall formed during the previous methane/hydrogen etch. Passivation prevents further attack of the walls during the subsequent etch stages. High aspect ratio features have been produced using this procedure but it is complex and time consuming.

It is perhaps preferable to reduce polymer build-up in the first instance and if possible enable passivation of the sidewalls at the same time. The addition of oxygen to the methane/hydrogen gas mixture itself was proposed by M^{c}Nabb *et al.* [4.3] and used by Sugimoto *et al.* [4.4] with the ethane/hydrogen gas mixture. An added benefit was the reduction in the undercutting of the mask. With no oxygen in the gas

mixture polymer coated the mask and the sidewalls were undercut. Increasing oxygen flow first leads to vertical profiles then with excess oxygen the sidewalls become overcut and trenching observed. The etch surface was observed to be very smooth. Oxygen has also been added to methane/hydrogen/argon [4.2]. Its addition has also been used to improve verticality in multilayer material systems [4.5,4.6] and reduce discontinuities in wall profiles produced whilst etching samples comprised from layers of different materials.

The oxygen can play many roles within the plasma. The formation of polymer upon the mask is drastically reduced so eliminating the shadowing caused by the large polymer build-ups that are possible and leading to an improvement in the anisotropy of the etch. Mass spectrometry studies [4.4] have shown that oxygen is involved in the formation of the hydroxyl molecule (OH), carbon monoxide (CO) and carbon dioxide (CO_2) within the plasma and lowering of the number of high molecular weight hydrocarbons, the precursors for polymer formation. The removal of carbon can be related to the diminished rates of polymer deposition. It is believed the oxygen forms a protective passivating layer on reaction with the sidewall that inhibits the sideways etching found with just the methane/hydrogen mixture. Undercutting of the mask is therefore reduced. Little evidence for this mechanism exists but XPS data obtained by Agrawla *et al.* [4.7] whilst etching with HBr suggest that oxygen passivation is responsible for the anisotropy. The oxygen responsible for the passivation is believed to come from residual oxygen or water vapour within the chamber.

4.1.2 Etch Characteristics of InGaAs

4.1.2.1 Etch Rates and Profiles

In order to study the effect of the addition of oxygen to the methane/hydrogen mixture a fixed methane to hydrogen ratio of 5 sccm methane and 20 sccm hydrogen was used at a pressure of 20 millitorr with an applied rf power of 75 W. Without oxygen these etch parameters give an etch rate of approximately 30 nm/min with considerable undercutting and deposition of polymer onto the mask. The amount of oxygen added to the methane/hydrogen mixture has to be carefully controlled; too little and the effects of the oxygen will be minimal, too much and there is the possibility of mask erosion due to sputtering by the massive oxygen ions and the danger of explosion within the vacuum system upon reaction with hydrogen.

When oxygen is added to gas mixture the most noticeable features are a decrease in the polymer deposited onto the mask and an improvement to the wall verticality. The oxygen will be involved in reactions within the plasma itself, reacting with both carbon and hydrogen reducing the ability to form carbon based polymers in the gas phase as the relative concentration polymer precursors are reduced. As well as the lower flux of polymer species to the surface of the mask any polymer that manages to build up on the mask will be subject to attack by oxygen and removed by the formation of volatile products that can be pumped from the etch chamber. Most importantly the amount of undercutting of the mask is seen to be reduced and with the optimum oxygen content almost eliminated. The oxygen must also be involved in the formation of a protective passivating layer upon the sidewalls since the amount of undercut has been dramatically reduced compared to the situation where no oxygen has been added to the gas mixture.

As the amount of oxygen in a mixture of 5 sccm methane and 20 sccm hydrogen is increased the amount of undercut reduces until the most vertical profiles are obtained with 0.5 sccm oxygen. Increasing the oxygen content beyond this level does not produce an improvement in verticality but instead causes the sidewalls to become rough.

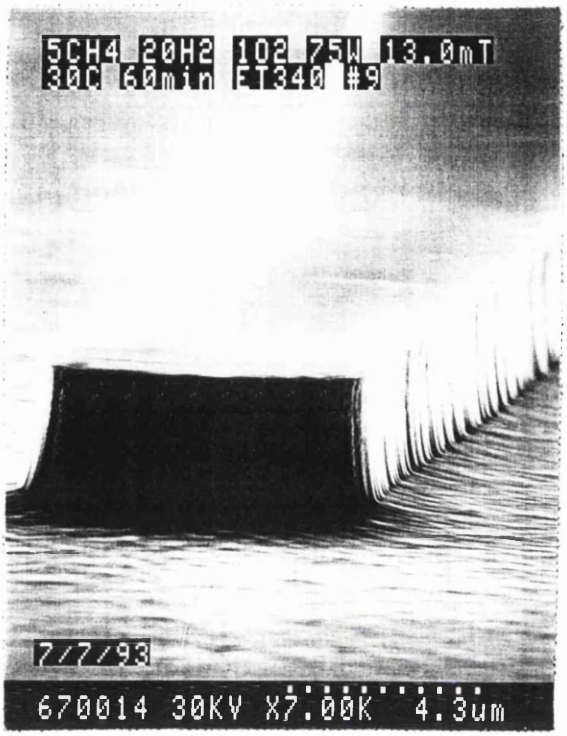

Figure 4.1

Micrograph of InGaAs etched with 5 sccm CH_4, 20 sccm H_2 and 1 sccm O_2 at a pressure of 13 mT and an rf power of 75W using 100nm Ti mask.

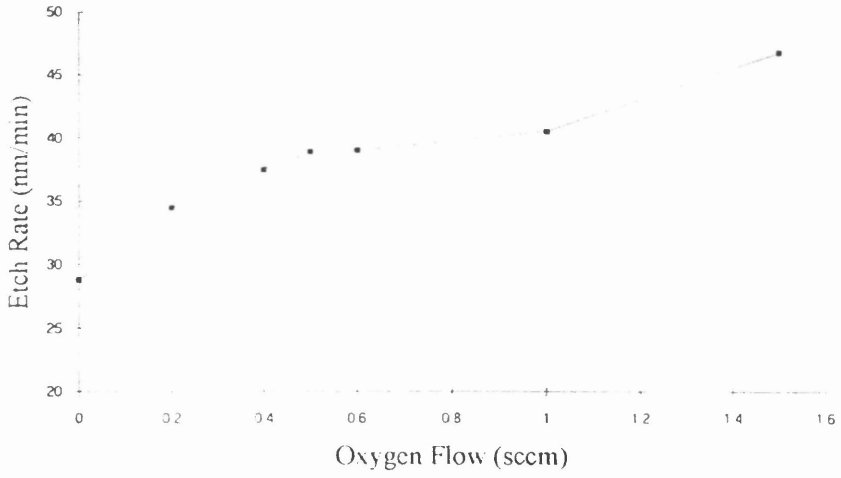

Figure 4.2

Enhancement of InGaAs etch rate with addition of O_2 to 5 sccm CH_4, 20 sccm H_2 at 150 W and 20 millitorr.

A reduction in polymer transport to the etch surface or oxygen reacting and removing inhibitors on the etch surface will reduce the number species present that block the etching mechanism, thus enhancing the effect of the reactive ions at the etch surface resulting in a rise in etch rate. At no time was the quality of the horizontal etch surface seen to degrade, even with oxygen flows of up to 2 sccm.

It was noted in the previous chapter that the walls of the etch chamber quickly become coated in polymer during methane/hydrogen RIE. When the chamber has become heavily coated, this polymer can act as a source of polymeric species resulting in a slowing of the etch and increasing the likelihood that the regime chosen to etch with is now past the polymer point. The addition of oxygen during the etch also has the beneficial effect that this polymer as well as that formed on the mask is deposited at a much reduced rate. As a result much longer etches can be performed or a less rigorous cleaning routine of the chamber followed.

4.1.2.2 The Effect of Etch Pressure

In section 3.4.2 the etch rates of InGaAs were shown to increase with the gas pressure within the reactor chamber. The effect of pressure upon the etch rate of the methane/hydrogen/oxygen gas mixture was studied using 6 sccm methane, 19 sccm hydrogen, 0.5 sccm oxygen with an rf power of 75 W.

At pressures of 20 millitorr and below etch profiles displayed good wall verticality. Etching at 40 millitorr however was shown to lead to inward bowing of the etch wall and a slight increase in polymer deposition onto the mask.

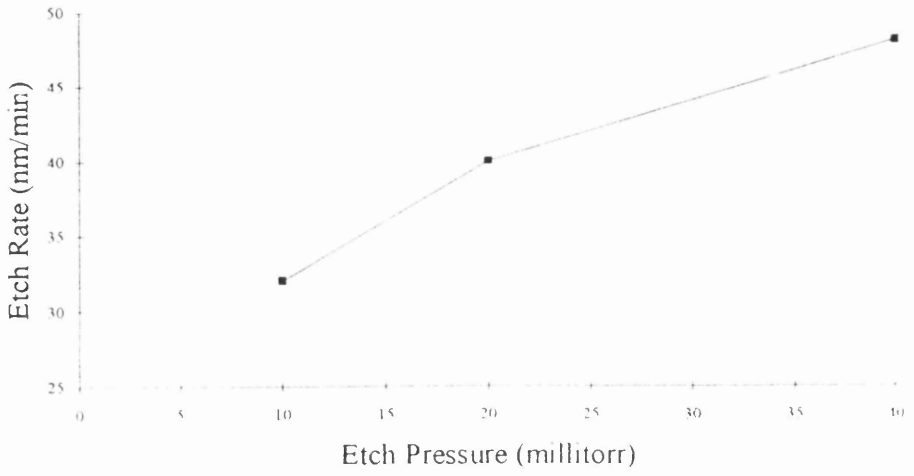

Figure 4.3
Etch rate of InGaAs with pressure.

Figure 4.4
InGaAs etched with $CH_4/H_2/O_2$ at 40 millitorr

4.1.2.3 Mask Considerations

The addition of oxygen is beneficial when etching InGaAs with metal or dielectric mask materials. The presence of oxygen can however be harmful to organic masks such as photoresist or polyimide. Oxygen will etch with these masks in the same way at it would do with the deposited polymer within the chamber. When attempting to etch InGaAs with the bi-layer mask of NiCr upon a polyimide spacer layer it can be seen that the polyimide layer has been etched, (Figure 4.5) undercutting the NiCr upper layer and exposing the top InGaAs surface. When the InGaAs has been exposed to the glow discharge by the removal of the protective layer of polyimide, it can then be etched in the normal manner causing degradation to the top surface. Because the mask has effectively been reduced in dimensions an overcut profile or discontinuity in the etch profile can be produced. Such a result can have a detrimental effect on device performance.

Figure 4.5

Etching of polyimide in bi-level mask with $CH_4/H_2/O_2$

4.1.3 Etch Characteristics of InAlAs

Although the wall profile after etching InAlAs showed no undercutting of the mask it is important to understand how the material will etch when etching multiple layer structure that contain InAlAs. Table 4.1 demonstrates that the addition of oxygen results in two effects. When using a methane flow and rf power that would normally result in polymer deposition, the addition of a small amount of oxygen can prevent these deposits and allow etching, although at a low etch rate.

CH_4 Flow (sccm)	H_2 Flow (sccm)	O_2 Flow (sccm)	RF Power (W)	Etch Rate (nm/min)
5	20	0	75	deposition
5	20	0.5	75	4.7
5	20	0	175	14
5	20	0.5	175	11

Table 4.1
Etch Characteristics of InAlAs with CH_4/H_2 and $CH_4/H_2/O_2$ RIE.

The addition of oxygen to the same methane/hydrogen mixture at high power results in etching but at a reduced rate. The reduction in the etch rate is probably due to the formation of oxides of aluminium. These oxides have a high boiling point thus a low vapour pressure at the temperatures obtainable with RIE. The oxides will then remain on the etch surface where they are formed building up a tough layer that prevents normal etch reactions, resulting in a slowing of the etch rate.

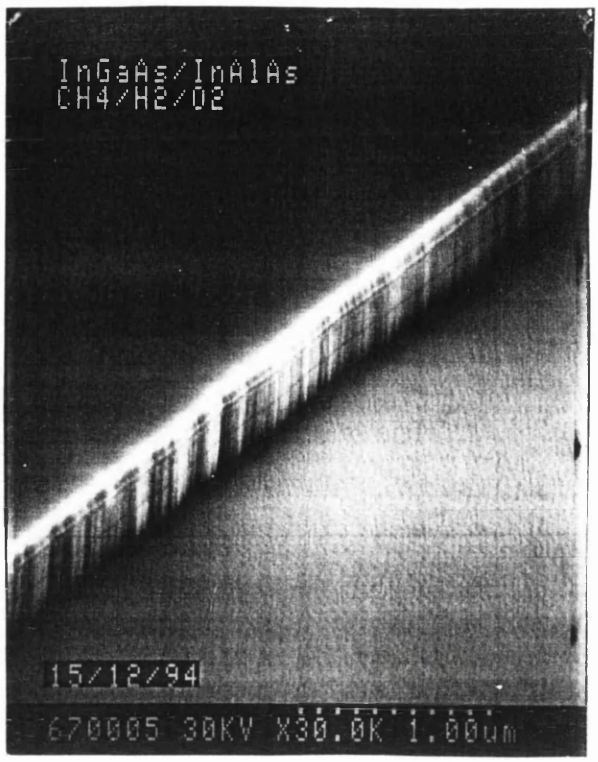

Figure 4.6
InAlAs etched in $CH_4/H_2/O_2$

4.1.4 Optical Emission Spectroscopy of the $CH_4/H_2/O_2$ Plasma

It is clear that the addition of a small amount of oxygen to the methane gas mixture resulted in an improved etch profile and the reduction of deposited polymer upon the etch mask and chamber walls. Analysis of the emission spectra shows that the oxygen added to the gas mixture is involved in the formation of CO and CO_2 species thus removing carbon from the glow discharge. Increasing the amount of oxygen added to the gas mixture leads to the formation of greater numbers of these species. This is consistent with the reduction of polymer in the gas-phase and an improvement to the etch quality due to the lessening of the deposition of polymer.

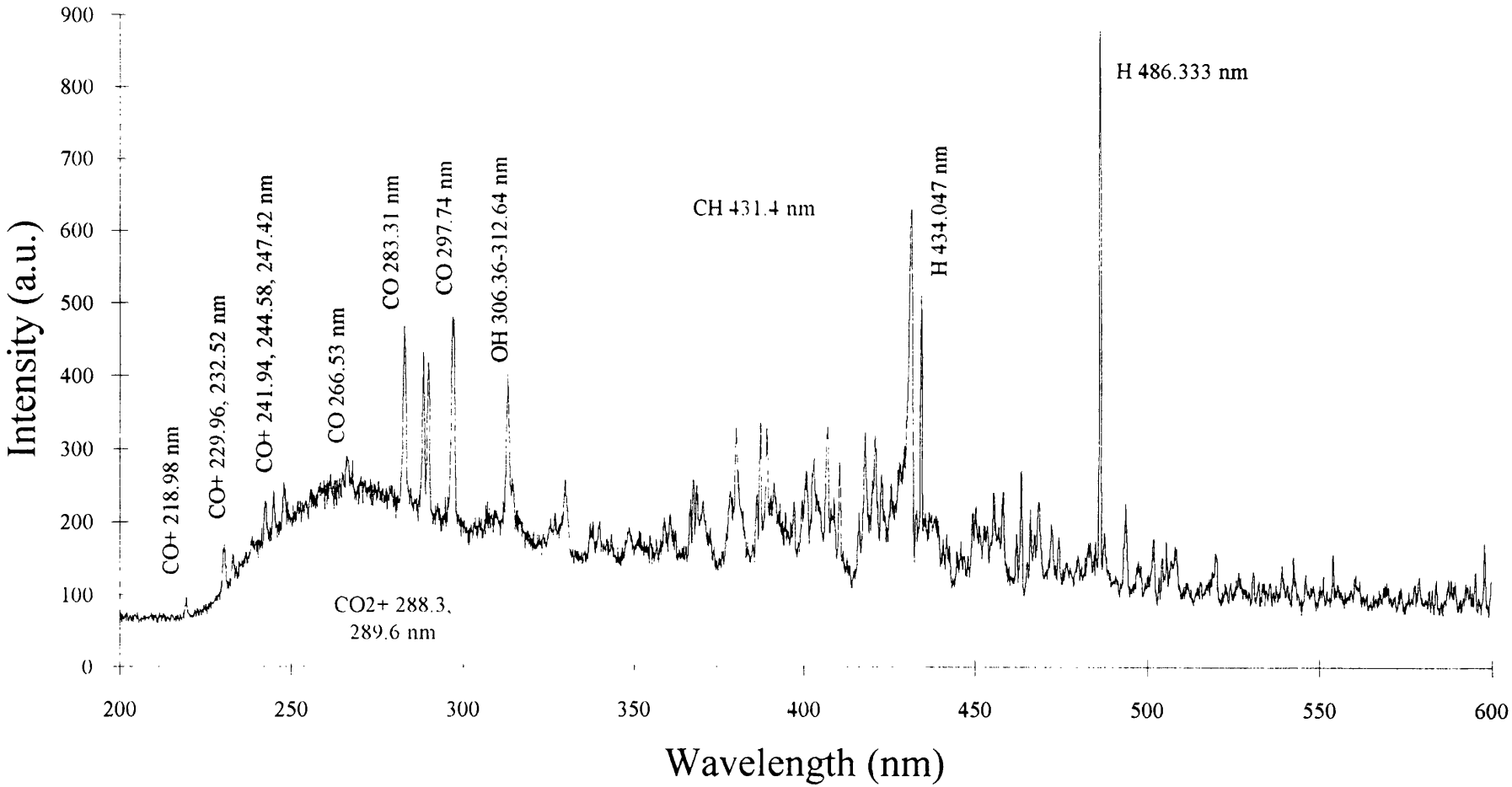

Figure 4.7 OES of 5 sccm CH4, 20 sccm H2, 1 sccm O2 at 20 millitorr and 75 W

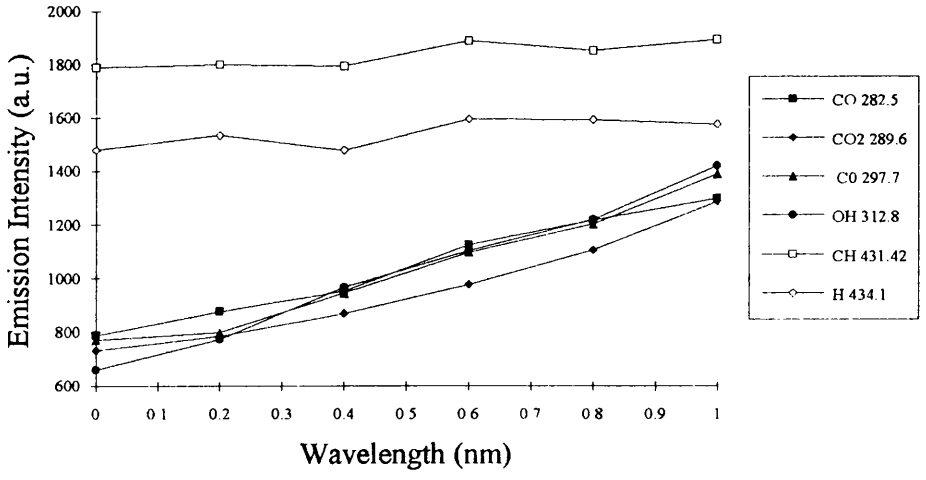

Figure 4.8
Emission peak intensities with the addition of O_2 to the CH_4/H_2 discharge.

4.2 The Addition of Cl_2

4.2.1 Introduction

It was seen in the previous chapter that with high methane content gas mixtures below the polymer point that undercutting of the etch mask can be a serious problem. In this chapter we have shown that the addition of a small amount of oxygen to the gas mixture improves anisotropy by decreasing polymer deposition upon the mask and passivating the sidewalls. The addition of oxygen is however detrimental when etching InAlAs and can cause problem such as etching of the mask when using organic mask materials such as photoresist or polyimide. In order to reduce polymer deposition and passivate sidewalls the addition of chlorine to the methane/hydrogen mixture was investigated.

Chlorine has been added to methane/hydrogen plasmas for ECR etching [4.8] and ion beam etching [4.9] of InP and RIE of GaAs [4.10]. With all etching techniques pure chlorine plasmas produce poor surface morphologies. The addition of methane and hydrogen to chlorine improves the morphology of the etch surface and etch walls.

4.2.2 Etch Characteristics of InGaAs

By varying the methane/hydrogen/chlorine ratio a region in which vertical walls could be produced was identified. Due to the ranges over which the mass flow controllers for the various gases could operate, fine control of the methane flow was the best available option with the other flows being held constant. The etch mask used was 100 nm titanium defined by optical lithography. Etching was performed using an Oxford Plasma Technology system 90 reactive ion etch machine fitted with a loadlock and pumped with a turbo/rotary pump combination.

Using 9 sccm methane and 40 sccm hydrogen at 275W (-505 V) an etch rate of approximately 17 nm/min was achieved. Severe deposition of polymer was found on the etch mask causing the mask to increase in width and force out the base of the feature causing an undercut type of profile. This is similar to the etching behaviour of InGaAs when etched with methane/hydrogen gas mixtures alone with high methane content. By the introduction of 4 sccm of chlorine to the methane/hydrogen (Figure 4.9) gas mixture the etch rate was increased to approximately 27 nm/min. No polymer was found on the mask and etching of the mask itself had occurred, resulting in an overcut profile. By increasing the methane flow to 10 sccm the etch rate again rose to 30 nm/min and polymer deposition upon the mask was again observed (Figure 4.10). The polymer protects the titanium mask from etching by chlorine species within the glow discharge. With far too little methane in the

discharge (8 sccm) and at too low an etch temperature (30 ^{0}C) the mask is completely etched and the etch surface becomes degraded by the presence of patches of what may be indium or indium chlorides.

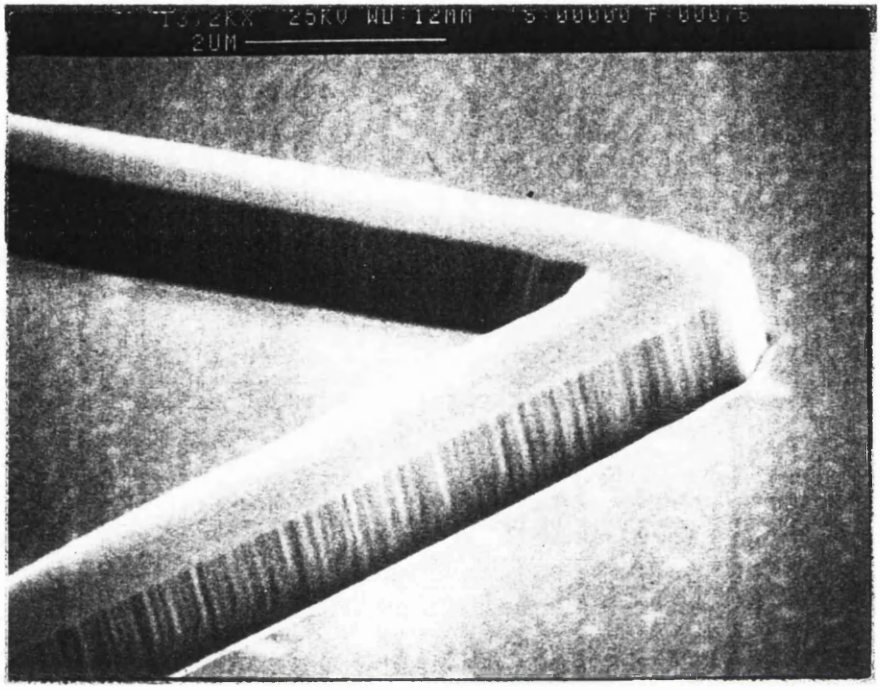

Figure 4.9
InGaAs etched with slightly too little methane.

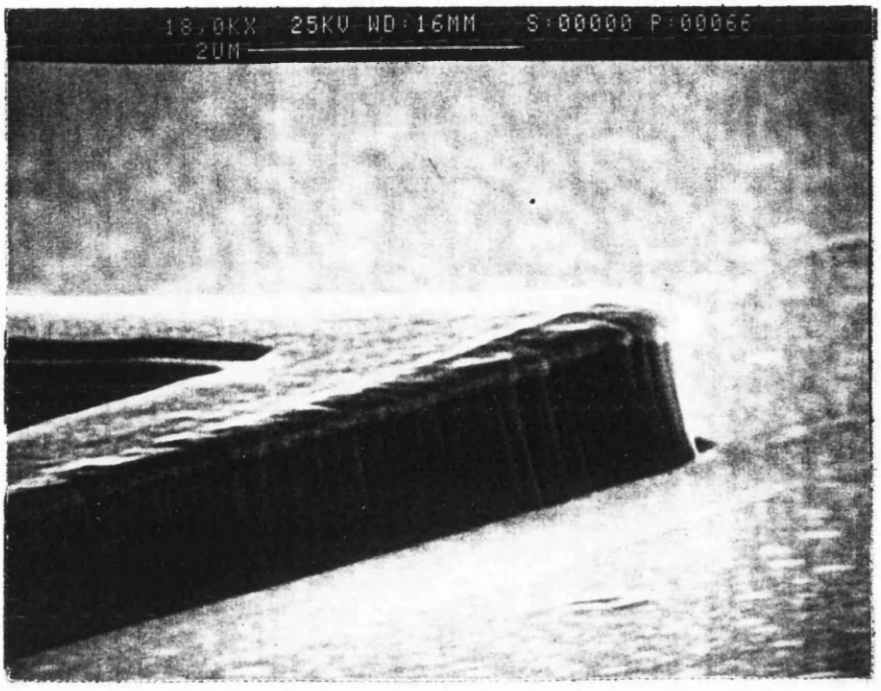

Figure 4.10
InGaAs etched with slightly too much methane

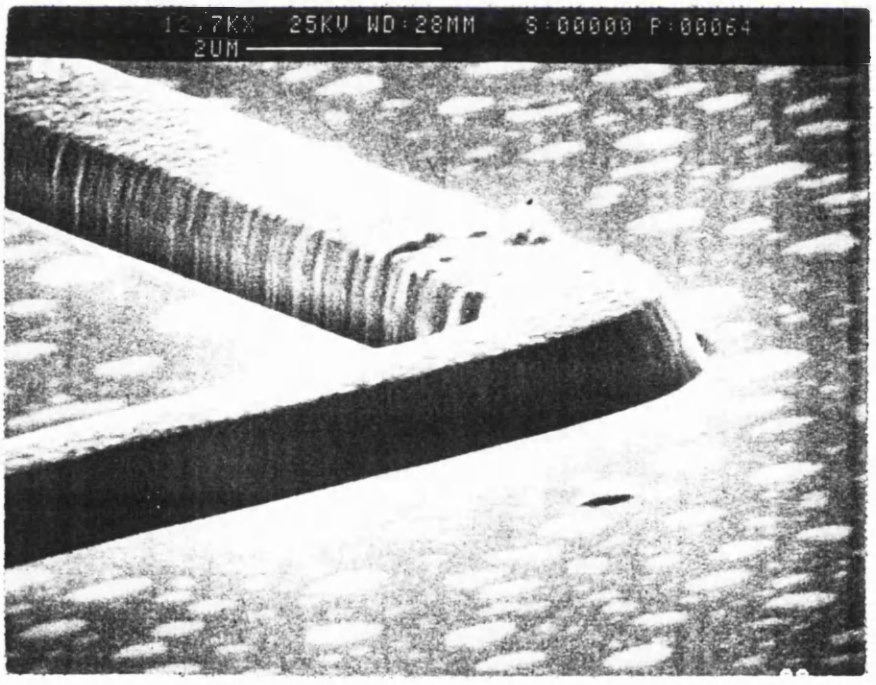

Figure 4.11
InGaAs etched with far too little methane.

The role of the chlorine in the etch process is not well understood. From the evidence that the polymer is reduced and the appearance of trenching at the sidewall/ etch surface boundary suggest that the chlorine may be playing a more physical than chemical role. The mechanism by which chlorine participates in the etch process is such as to enhance the sputtering of the polymer from the mask preventing polymer formation upon the side of the mask which would normally force an overcut profile by shadowing the etch surface.

4.3 Chapter Summary

It has been shown that the addition of oxygen to the methane/hydrogen gas mixture both enhances the etch rate and the verticality of the etched feature. By reacting with carbon within the plasma and polymer which has been deposited upon the etch chamber and mask to form CO and CO_2 the overall rate of polymer deposition and flux of inhibitors to the etch surface is reduced. The oxygen also reacts upon the etched feature sidewalls forming a passivating layer that reduces undercutting of the mask at high methane contents. Increases in etch pressure can however lead to a bowing of the etch wall. Oxygen allows etching to occur with gas mixtures that are normally beyond the polymer point.

Chlorine has also been added to the gas mixture. By enhancing the sputter rate of deposited polymer wall profiles can be improved and etch rates enhanced. With the addition of too much chlorine leads to excessive sputtering and damage to the etch mask. Trenching may also be observed.

References

[4.1] I. Adesida, K. Nummila, E. Andidej, J. Hughes, C. Canneau, R. Bhat and R. Holmstrm, "Nanostructure fabrication in InP and related compounds", *J. Vac. Sci. Technol.*, 1990, **B8,** pp.1357-1360

[4.2] J.E. Schramm, D.I. Babic, E.L. Hu, J.E. Bowers and J.L. Merz, "Anisotropy control in the reactiove ion etching of InP using oxygen in methane/hydrogen/ argon", *Proc. 6th Int. Conf. InP and related materials.*, 1994

[4.3] J.W. McNabb, H.G. Craighead, H. Temkin and R.A. Logan, "Anisotropic reactive ion etching on InP in methane/hydrogen based plasmas", *J. Vac. Sci. Technol.*, 1991, **B9,** pp.3535-3537

[4.4] H. Sugimoto, K. Ohtsuka, T. Isu, H. Tada, T. Miura and T. Shiba, "Reactive ion etching of InP using $C_2H_6/H_2/O_2$", *J. Appl. Phys.*, 1992, **72,** pp.3125-3128

[4.5] S.E. Hicks, C.D.W. Wilkinson, G.F. Doughty, A.L. Burness, I. Henning, M. Asghari and I. White, "Reactive ion etching of low-loss mirrors in InP/ InGaAsP/InP hetrostructures using $CH_4/H_2/O_2$ chemistry", *European Conference on Integrated Optics*, 1993

[4.6] A.L. Burness, P.H. loosemore, S.N. Judge, I.D. Henning, S.E. Hicks, G.F. Doughty, M. Asghari and I. White, "Low loss mirrors for InP/InGaAsP waveguides", *IEEE Electron. Lett.*, 1993, **29,** pp.520-521

[4.7] S. Agarwala, I. Adesida, C. Caneau and R. Bhat, "Selective reactive ion etching of InGaAs/InAlAs hetrostructures in HBr plasma", *Appl. Phys. Lett.*, 1993, **62,** pp.2830-2832

[4.8] C. Constantine, C. Barratt, S.J. Pearton, F. Ren and J.R. Lothian, "Smooth, low-bias plasma etching of InP in microwave $Cl_2/CH_4/H_2$ mixtures", *Appl. Phys. Lett.*, 1992, **61,** pp.2899-2901

[4.9] R. van Roijen, C.W.T. Bulle-Lieuwma and E.A. Montie, "Formation and damage of sidewalls after CL_2/CH_4 based reactive ion beam of InP", *J. Vac. Sci. Technol.*, 1992, **B10,** pp.2188-2191

[4.10] N. Vodjdani and P. Parrens, "Reactive ion etching of GaAs with high aspect ratios with Cl_2-CH_4-H_2-Ar mixtures", *J. Vac. Sci. Technol.*, 1987, **B5** , pp.1591-1598

Chapter 5

Reactive Ion Etching of InGaAs with Halogenated Gases

Chapter Outline

Silicon tetrafluoride ($SiCl_4$) and boron tribromide (BBr_3) have been investigated for their suitability as etch gases for reactive ion etching of InGaAs. To aid desorption of etch product species from the etch surface the temperature of the cathode is raised from room temperature to temperatures as high as 180 ^{0}C.

5.1 Introduction

GaAs, AlAs and AlGaAs can be etched with chlorine (Cl_2), the halogenated gases silicon tetrachloride ($SiCl_4$) and boron trichloride (BCl_3) and chlorofluoro-carbons (CFC) such as dichlorodifluoromethane (CCl_2F_2) also known as Freon 12. These widely used gases produce highly vertical etch profiles that are either selective [5.1,5.2] or non-selective [5.1,5.3] to aluminium containing layers. Rapid etch rates are possible using a low DC bias with minimal damage to the semiconductor.

With GaAs and AlGaAs, the chlorinated etch products have low melting and boiling points suggesting that these species will be very volatile and readily enter the gas phase from where they are pumped away. An etch process using only chlorinated gases is therefore non-selective. The fluorinated etch products have higher melting points are less volatile. It is believed that it is the extremely low volatility of aluminium fluorides relative to other products that is responsible for the high selectivities of GaAs over AlGaAs obtainable with mixed chlorine/fluorine chemistry etching.

The high melting and boiling points of indium chlorides and fluorides however suggest that under the low ion energy conditions that are used to etch GaAs, it may prove difficult to etch indium containing semiconductors with chlorinated gases. Stern *et al.* [5.3] and Pearton *et al.* [5.4] have etched InP under 'normal' operating temperatures with $SiCl_4$ and HCFCs respectively. Normal operating temperatures are taken to mean approximately room temperature prior to striking the plasma. DC biases of 200-400 V were used during the etches, but etch rates were low, wall verticality poor and etch surfaces rough. Using thermodynamic models, McNevin [5.5] predicted that etch rates of InP when etched with chlorine containing gases should rise with temperature, the additional energy available from

the increased temperature at the etch surface aiding desorbtion of the etch products. Etching of InP at elevated temperatures has been shown to be possible [5.6,5.7] with enhanced etch rates and improved wall verticality.

Compound	m.pt. (°C)	b.pt. (°C)
$AlBr_3$	97.5	263.3
$AlCl_3$	190	262
AlF_3	1291 subl	-
AlI_3	191	360
$AsBr_3$	32.8	221
$AsCl_3$	-5.8	130.2
AsF_3	-85	-63
AsF_5	-80	-53
AsH_3	-116.3	-55
AsI_3	146	403
AsI_5	76	-
$GaBr_3$	121.5	278.8
$GaCl_2$	164	535
$GaCl_3$	77.9	201.3
GaF_3	800 subl	c1000
GaI_3	212	345 subl
InBr	200	662 subl
$InBr_2$	235	632 subl
$InBr_3$	436	subl
InCl	225	608
$InCl_2$	235	550-570
$InCl_3$	586 (300 subl)	600
InF_3	1,170	>1200
InI	351	711-715
InI_2	212	-
InI_3	210	-

Table 5.1
Melting and boiling points for group III and V halides at atmospheric pressure.

The data presented in table 5.1 suggests that the use of bromine or iodine containing gases may be more suitable for etching indium since melting points on the whole tend to be lower than those of the indium chlorides. A half-way step between methane/hydrogen RIE and fully halogenated RIE is the use of iodomethane (CH_3I), iodoethane (C_2H_5I) or iodopropane (C_3H_7I) [5.8]. The use of such gases result in an etch processes which maintains the smooth etch surfaces obtainable with methane/ hydrogen but with a slightly higher etch rate. Flanders *et al.* [5.9] have mixed hydrogen iodide (HI) with methane, enabling control of the iodine to carbon and hydrogen ratio within the plasma. It was found that pure iodine resulted in slightly rough InP surfaces. Addition of methane and hydrogen improved the surface roughness. Hydrogen iodide has been mixed with argon [5.10] instead of methane. Etch rates were high, walls highly vertical and surface smooth. Although iodine compounds have proved to be efficient etch gases for InP, the iodine readily attacks the etch chamber and pumping system. Hydrogen iodide is also unstable and can decompose in the bottle.

Less corrosive than iodine compound are the bromides. Hydrogen bromide [5.11] produces a selective etch for InGaAs over InAlAs at a DC bias of -100 V but etch rates are low at 11nm/min for InGaAs. Pure bromine etches InP extremely fast at 2 μm/min [5.12] at 10 ^{0}C but wall profiles are undercut and etch surfaces rough. The addition of nitrogen improves wall verticality and raising the temperature to 40 ^{0}C reduces surface roughness.

The use of boron tribromine (BBr_3) as a gas suitable for RIE has been demonstrated whilst etching aluminium [5.13]. Thermodynamic models [5.14] predict that boron tribromide should produce higher etch rates than boron trichloride plasmas under the same conditions of flow, temperature etc. Boron tribromide benefits also from having no hydrogen attached to the molecules so etching may lead

to less loss of carriers. The topic of loss of carriers due to donor species passivation by hydrogen will be discussed at length in chapter six.

5.2 RIE of InGaAs with $SiCl_4$

Using the highly anisotropic etch developed by Murad et al. [5.1] for etching GaAs (a flow rate of 12 sccm silicon tetrachloride with an etch pressure of 8 milliTorr) the etch behaviour of InGaAs was investigated over a range of rf powers and cathode temperatures. Etching was performed in the Plasma Technology µp80 reactive ion etching machine. A silicone oil recirculator and heater unit were used to control the temperature of the cathode. The InGaAs samples were again grown by MBE.

RF Power (W)	Table Temp. (Celcius)	Etch Rate (nm/min)
15	100	3
15	100	4.3
15	125	10
15	150	12
15	175	18.6
30	100	12
30	125	19.3
30	150	28
30	175	44
50	125	32.5
100	125	45
100	175	250

Table 5.2
Etch rates with rf power and cathode temperature for InGaAs when etched with 12 sccm $SiCl_4$ at 8 millitorr.

Etch rates increase with cathode temperature following the predicted trends of the thermodynamic model. With increased rf power there is a corresponding increase of the DC bias and hence the ion bombardment energy. The increased ion bombardment will enhance desorption rates from the surface and raise etch rates. Using an Arrhenius plot, the etch data can be displayed in such a way so that information may be gained about the chemical reaction taking place at the surface during etching.

Fitting a straight line to the data obtained for rf powers of 15 and 30W yields activation energies of 0.2656 and 0.3097 eV. The activation energies are in good agreement showing that is possible that the same chemical reaction is occuring at both 15 W and 30 W rf power.

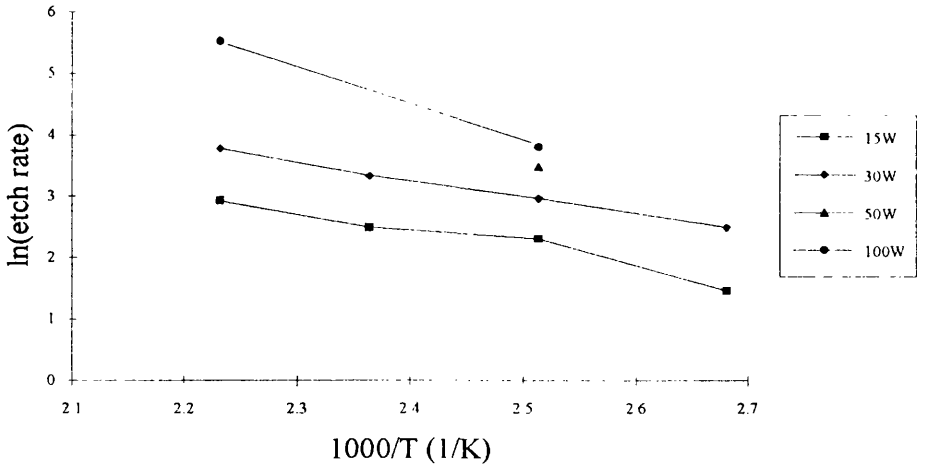

Figure 5.1
Arrhenius plot for SiCl4 RIE of InGaAs. Temperatures are those of the hot oil bath not the those of the etch surface itself.

The temperatures indicated in Figure 5.1 are those of the oil circulating through the cathode. In chapter 3 we saw that the surface temperature of the sample being etched can be raised by ion bombardment. The temperatures here of the surfaces were not measured by fluoroptic thermometry, but the linearity of the etch data with cathode temperature indicates that the effect of ion bombardment is to raise the surface temperature by a fixed amount dependant upon the rf power used.

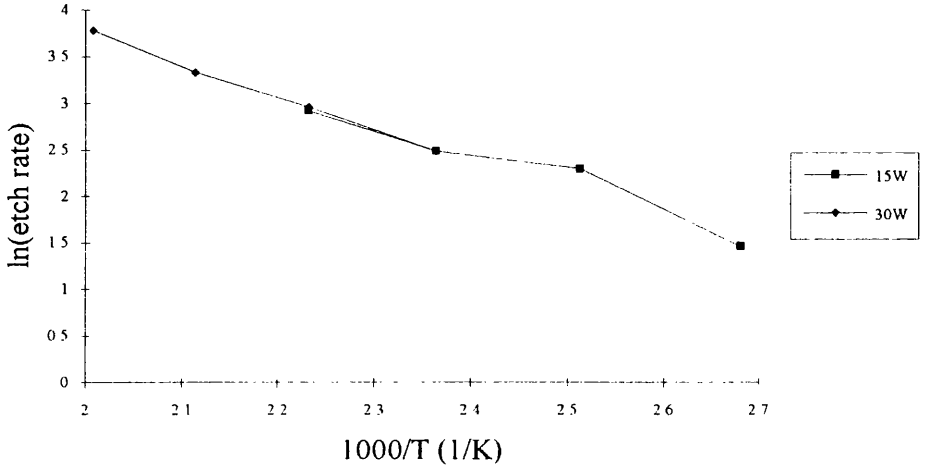

Figure 5.2
Etch rate data for etching at 15 and 30W with the temperatures at 30W adjusted upwards by 50 ^{0}C.

An etch rate of 12 nm/min was obtained at 15W with a cathode temperature of 150 ^{0}C and at 100 ^{0}C using 30 W rf power. Assuming that increasing the applied rf power from 15 to 30 W raises the surface temperature by 50 ^{0}C the etch rate data can be replotted.

The replotted data shows in a more convenient manner how the activation energy is the same at these two rf powers. Fitting a straight line to the replotted data yields an activation energy of 0.2782 eV. It is meaningless to estimate the rate

constant R_0 since even after replotting the data we do not know the true surface temperature.

If the data obtained at an rf power of 100 W is true and accurate the slight change in slope of the plot would suggest that a change of activation energy and thus chemical reaction has occurred. Using 100 W rf power with a cathode temperature of 175 ^{0}C the etch is seen to form extremely vertical wall profiles. The etch surface in InGaAs is however very rough a problem that can be encountered with fast etch rates. When the etch is allowed to continue, so that the etch surface enters the underlying InAlAs buffer layer, a dramatic improvement in the roughness of the surface is seen. Etching within the InAlAs layer occurs at a rate of only 1 nm/min, a selectivity of 250:1. The roughness of the surface is thus improved as the etch front enters the InAlAs and slows down allowing InGaAs spikes to be etched away with only a small advance of the InAlAs etch front.

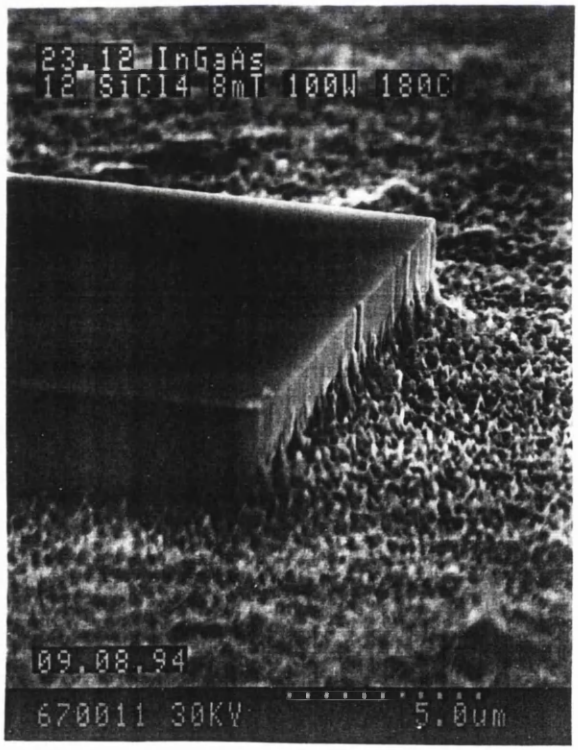

Figure 5.3

Micrograph of InGaAs etched with $SiCl_4$ at 100W and 180 ^{0}C

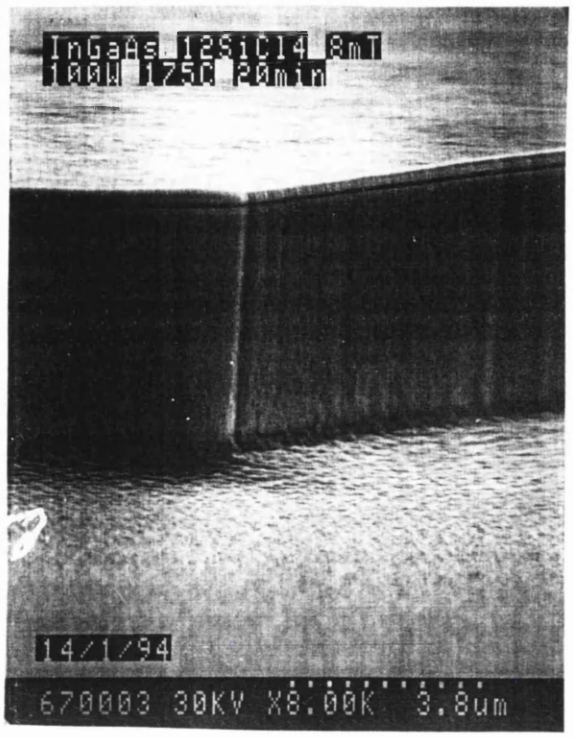

Figure 5.4
100W, 175 ^{0}C $SiCl_4$ etch where the etch surface has entered the InAlAs layer

5.3 RIE of InGaAs with BBr_3

A brief study of the suitability of boron tribromide as an etch gas for InGaAs was undertaken in the Plasma Technology µp80 machine. Using a flow rate of 12 sccm an etch pressure of 12 millitorr was produced.

Figure 5.5 has too few data points for any hard and fast conclusions to be drawn. In a similar manner to etching with $SiCl_4$ etch rates rise with temperature with the etch rate at 175 ^{0}C departing markedly from the lower etch rates observed at lower temperatures. A change of surface chemical reaction is suggested at high

temperature. Micrographs of the etched surface show poor sidewall quality and rough etch surfaces at temperatures of 125 and 150 ^{0}C.

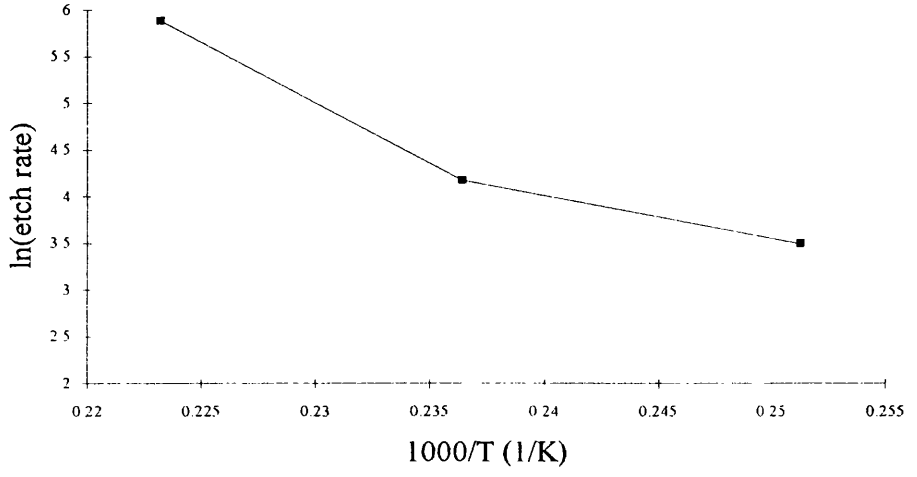

Figure 5.5
Arrhenius plot for InGaAs etched with 12 sccm BBr_3 at 12 millitorr and using an rf power of 100 W.

Etching at 175 ^{0}C however produces undercut wall profiles and relatively smooth etch surfaces considering the etch rate. Undercutting of the mask is characterised by the presence of two distinct planes. These planes are crystallographic planes and are formed by chemical etch that preferentially etches along specific crystal planes. Lowering the gas flow and etch pressure has no effect upon the amount of undercut but improves the roughness of the etch surface.

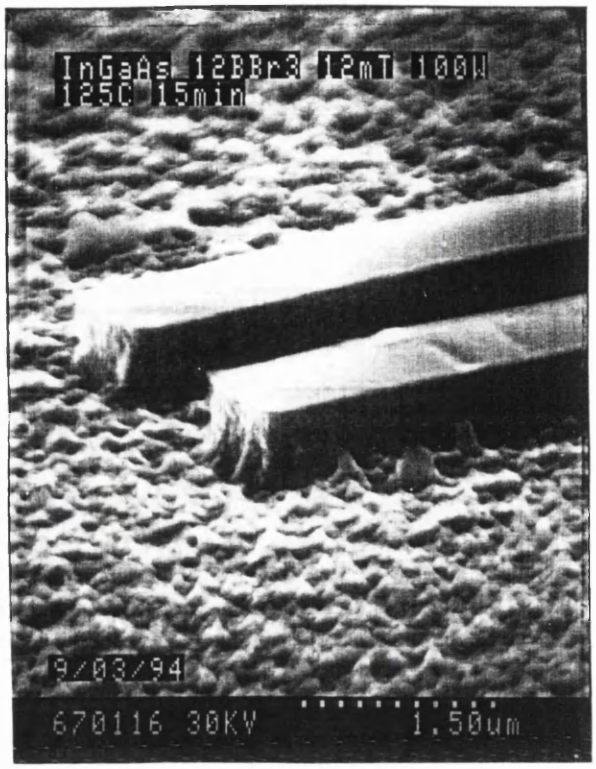

Figure 5.6

InGaAs etch with BBr_3 at 125 ^0C.

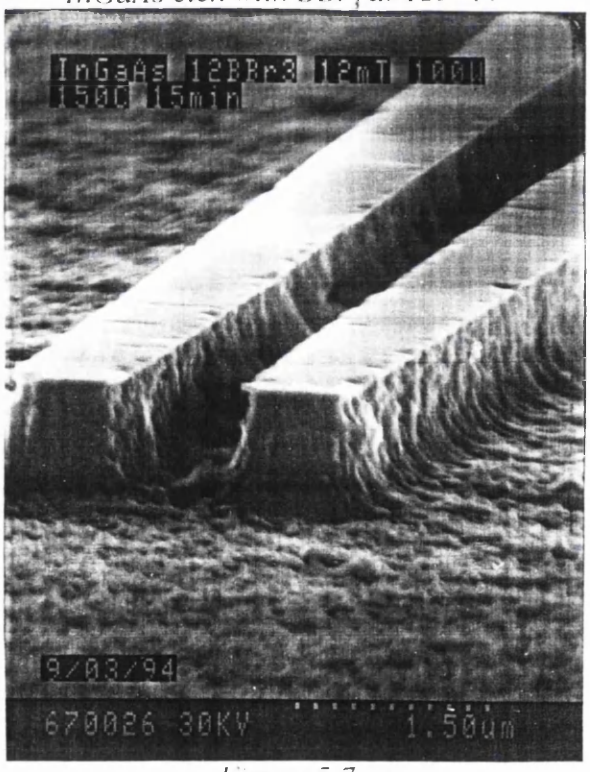

Figure 5.7

InGaAs etched with BBr_3 at 150 ^0C

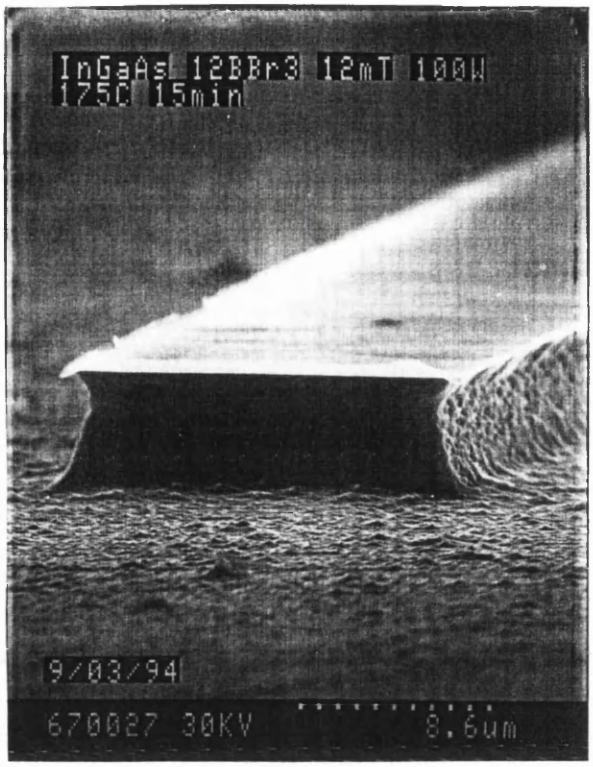

Figure 5.8
InGaAs etched with BBr_3 at 175 °C.

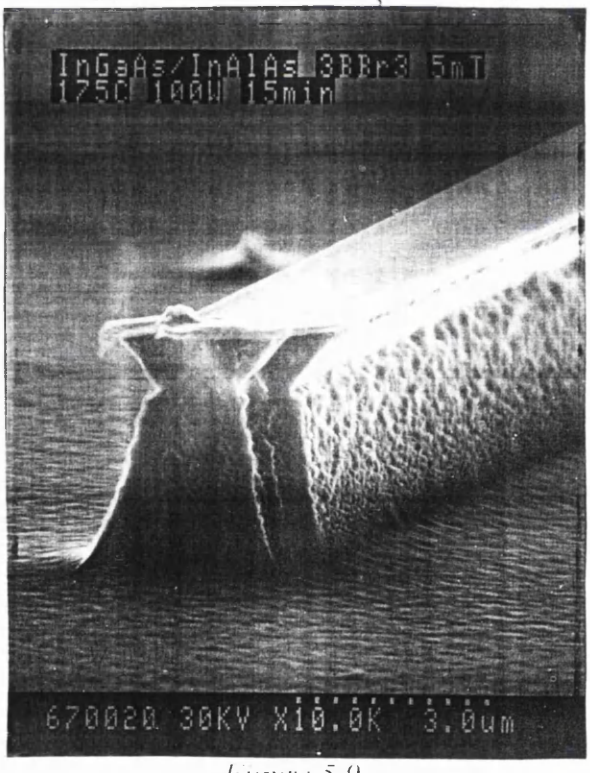

Figure 5.9
InGaAs etched with BBr_3 at 175 °C at low flow rate and pressure.

The optical emission spectra of BBr_3 was obtained using a flow rate of 8 sccm at 150W.

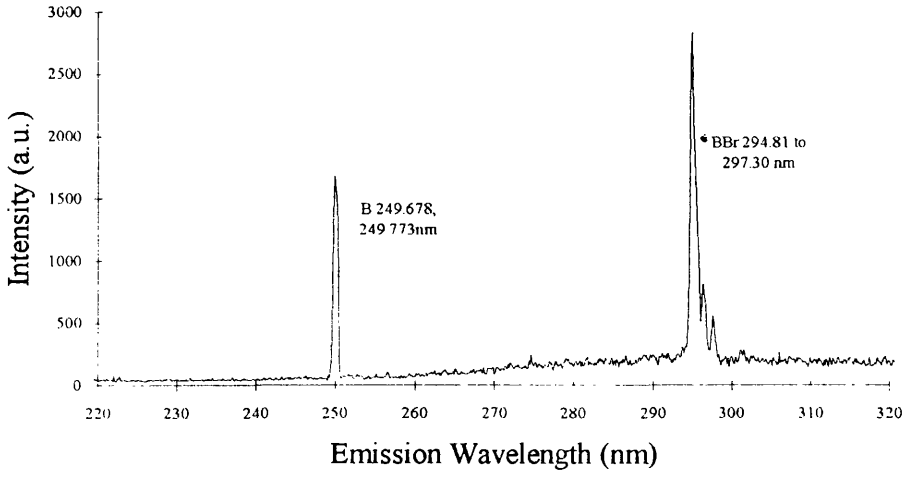

Figure 5.10
Optical emission spectra for BBr_3.

The spectra of Figure 5.10 is typical of plasmas of BBr_3 over the full range of power, flow and pressure available. The most prominent features are two bands related to atomic boron and a complex set of bands from BBr. No etch products such as $InBr_x$ have been observed.

5.4 Chapter Summary

RIE of InGaAs has been investigated using the gases silicon tetrachloride and boron tribromide at elevated cathode temperatures. With both gases etch rates are observed to increase with temperature as the extra energy available at the surface enhances reaction rates and promotes desorption from the surface. An Arrhenius plot of 1000/T verses the natural log of the etch rate gives a chemical activation energy of 0.28 eV at rf powers of 15 and 30 W. A change in the slope of the Arrhenius plot

suggests that a change of chemical reaction may take place at an rf power of 100 W and a oil bath temperature of 175 ^{0}C with both gases. RIE with $SiCl_4$ produces a vertical etch with a rough etch surface and BBr_3 a non-vertical etch with undercut wall profiles with a less rough etch surfaces. RIE with $SiCl_4$ can produce selectivities as high as 250:1 for InGaAs/InAlAs systems.

References

[5.1] S.K. Murad, C.D.W. Wilkinson and S.P. Beaumont, "Selective and nonselective RIE of GaAs and $Al_xGa_{1-x}As$ in $SiCl_4$ plasma", *Microcircuit Engineering*, 1994, **23,** pp.357-360

[5.2] N.I. Cameron , G. Hopkins, I.G. Thayne, S.P. Beaumont, C.D.W. Wilkinson, M. Holland, A.H. Kean and C.R. Stanley "Selective eactive ion etching of GaAs/AlGaAs metal-semiconductor field-effect transistors", *J. Vac. Sci. Technol.*, 1991, **B9,** pp.3538-3541

[5.3] M.B. Stern and P.F. Lio, "Reactive ion etching of GaAs and InP using $SiCl_4$", J. *Vac. Sci. Technol.*, 1983, **B1,** pp.1053-1055

[5.4] S.J. Pearton, W.S. Hobson, U.K. Chakrabarti, G.E. Derkits and A.P. Kinsella, "Use of hydrogenated hydrofluorocarbon mixtures for reactive ion etching of In-based III-V semiconductors", *J. Vac. Sci. Technol.*, 1990, **B8,** pp.1274-1284

[5.5] S.C. McNevin, "Chemical etching of GaAs and InP by chlorine: The thermodynamically predicted dependence on Cl_2 pressure and temperature", *J. Vac. Sci. Technol.*, 1986, **B4,** pp.1216-1226

[5.6] D.G. Lishan and E.L. Hu, "Chlorine and HCl radical beam etching of III-V semiconductors", *J. Vac. sci. technol.*, 1990, **B8,** pp.1951-1955

[5.7] J. Schneider, M. Moser and K. Affolter, "Low loss corner mirrors in InP/InGaAsP/InP for integrated optics etched with chlorinated gases", *Proc. 6th Int. Conf. Indium phosphide and related materials*, 1994

[5.8] U.K. Chakrabarti, S.J. Pearton, A. Katz, W.S. Hobson and C.R. Abernathy, "Dry etching of III-V semiconductors in CH_3I, C_2H_5I and C_3H_7I discharges", *J. Vac. Sci. Technol.*, 1992, **B10,** pp.2378-2385

[5.9] D.C. Flanders, L.D. Pressman and G. Pinelli, "Reactive ion etching of indium compounds using iodine comtaining plasmas", *J. Vac. Sci. Technol.*, 1990, **B8,** pp.1990-1993

[5.10] S.J. Pearton, U.K. Chakrabarti, A. Katz, F. Ren and T.R. Fullowan, "High-rate, anisotropic dry eyching of InP in HI-based discharges", *Appl. Phys. Lett.*, 1992, **60,** pp.838-840

[5.11] S. Agarwala, I. Adesida, C. Caneau and R. Bhat, "InAlAs/InGaAs hetrostructure FETs processed with selective reactive-ion-etching gate-recess technology", *Appl. Phys. Lett.*, 1993, **62,** pp.2830-2832

[5.12] K. Takimoto, K. Ohnaka and J. Shibata, "Reactive ion etching of InP with Br_2-containing gases to produce smooth, vertical walls: Fabrication of etched facet lasers", *Appl. Phys. Lett.*, 1989, **54,** pp.1947-1949

[5.13] A. Landauer Keaton and D.W. Hess, "Aluminium etching in boron tribromide plasmas", *J. Vac. Sci. technol.*, 1985, **A3,** pp.962-966

[5.14] S.C. McNevin, "A thermochemical model for the palsma etching of aluminium in BCl_3/Cl_2 and BBr_3/Br_2", *J. Vac. Sci. Technol.*, 1990, **B8,** pp.1212-1222

Chapter 6

Assessment of Damage due to Reactive Ion Etching

Chapter Outline

In this chapter we discuss the changes to semiconducting materials brought about during methane/hydrogen etching. Schottky contact assessment of etched AlGaAs is performed and a qualitative judgement made as to the extent and nature of the induced damage. Raman spectroscopy is used to study the change in surface depletion layer thickness for GaAs at low and high DC bias for hydrogen plasmas alone and at high DC bias for hydrogen and methane/ hydrogen plasmas. This technique has also used for studying InGaAs etched under normal methane/hydrogen plasma conditions but photoluminescence of the etched surface is needed to establish the presence of a possible surface modification. The surface composition of the as-grown and etched InGaAs is established using XPS. The suitability of two differing HEMT structures for methane/hydrogen RIE gate recessing is investigated again at low DC bias. Finally the damage created on the sidewalls of wires etched in InGaAs are estimated by the fabrication of narrow conducting wires.

6.1 Introduction

Whilst a material is being etched the surface is subjected to bombardment by energetic ions, neutral species and photons. These ions as well as being directly involved in the etch mechanism, transfer energy and momentum into the crystal lattice of the semiconductor or can themselves penetrate the surface and enter the bulk. The transfer of energy to the surface can cause displacement of atoms within the lattice or if the ionic species penetrate the surface they may chemically react with the atoms of the lattice or capture free charge from the semiconductor. The general trend of such damage is to degrade the quality of the lattice, remove free carriers and alter the electrical and optical characteristics of the material near to the surface.

In general the following may occur. (1) Modification of the near surface crystalline structure by ion bombardment, (2) changes in stoichiometry of the surface due to differential chemical effects, (3) the introduction of traps and (4) passivation of donors and deep centres by hydrogen. Materials etched using a methane/hydrogen plasma are particularly susceptible to passivation of donors by ionic hydrogen. GaAs [6.1-6.4], AlGaAs [6.5] and InP [6.6,6.7] have been studied using a variety of methods and show a general trend of increased hydrogen penetration with DC bias. A low DC bias may generate the same degree of passivation but because the ions do not penetrate as far the overall damage is less. Low DC self biases have been employed to great effect in ECR etch machines [6.8-6.9]. The typical penetration depths found cannot be explained by conventional projection of ions into the crystal lattice but other mechanisms such as a knock-on replacement collisions [6.10] or channelling [6.11] must be evoked. Annealing of the etched samples at temperatures greater than 300 ^{0}C restores most of the free carriers.

6.2 Schottky Contact Damage Assessment of AlGaAs

6.2.1 Theory of the Schottky Contact

A Schottky contact is formed when a metal and semiconductor are brought into intimate contact. To achieve the required intimacy of the contact and for contamination free bonding of the metal to the surface of the semiconductor, the metal is evaporated under high vacuum typically, in the region of 10^{-6} mbar onto an oxide free surface.

When the metal and semiconductor are brought into contact electrons will flow from the conduction band of n-type semiconductors onto the surface of the metal which is at the lower potential. The flow of electrons can be seen as the result of the Fermi levels in each material adjusting so as to come into equilibrium with each other. Negative charge builds up on the surface of the metal until the electric field generated is strong enough to counter the flow of electrons onto the metal surface.

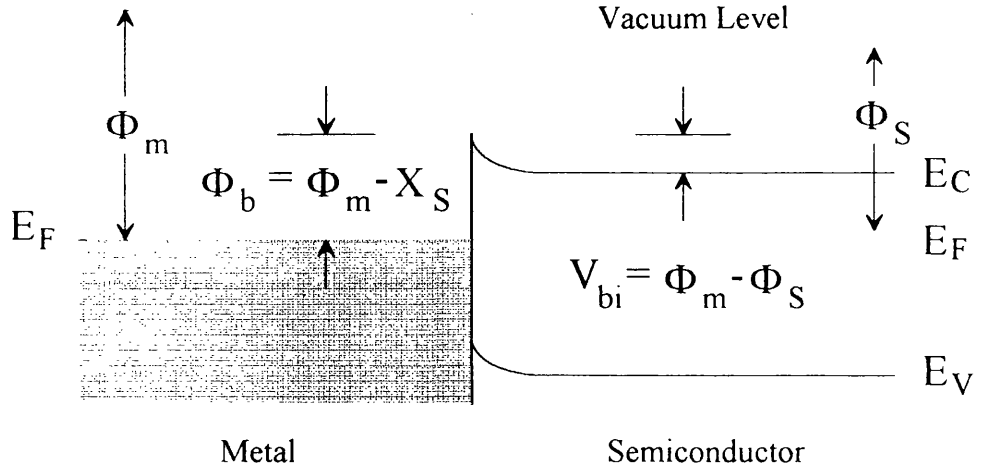

Figure 6.1
The complete Schottky contact.

The transfer of electrons from semiconductor to the metal leaves the semiconductor with a net positive charge creating a depletion region in the semiconductor forming a potential barrier to electron flow.

The Fermi level in the metal can still be considered to be flat since the electrons are confined to the Debye layer of the metal's surface. The height of the potential barrier seen by the electrons in the semiconductor is the difference between the Fermi energy of the metal , Φ_M and the energy of the bottom of the conduction band, X_S of the semiconductor. If the semiconductor is externally positively biased with respect to the metal the electrons of the semiconductor will move to a lower energy state, the bands move towards the vacuum level. The potential barrier at the interface seen by these electrons will thus be V_{bi}-V_{ext} where V_{ext} is the applied voltage. If a negative bias is applied the size of the barrier increases when viewed from the semiconductor. Electrons in the metal will see that the potential barrier remains equal to the difference between the Fermi energy of the metal and the bottom of the conduction band of the semiconductor for all externally applied voltages.

In practical semiconductors the surface is a region of incomplete bonding for the surface atoms. These 'dangling bonds' introduce surface states which may be occupied by electrons from the conduction band. In Gallium Arsenide these surface states are found within the band gap and are so dense that the Fermi level becomes 'pinned' at the centre of the band-gap. A surface barrier of 0.6 eV for GaAs [6.12] and AlGaAs of 0.74 eV [6.13] when going from the semiconductor to metal is produced. This barrier height is found to be largely independent of the type of metal used to form the contact.

The pinning of the Fermi level near the mid gap point results in a surface depletion region in which the density of free carriers is low relative to that deep within the bulk of the material. From Poisson's equation, Chandra *et al.* [6.14] were able to show that d_0 the natural surface depletion depth can be expressed by

$$d_0 = \left[\frac{2\varepsilon_r \varepsilon_o (V_b - kT/q)}{q(N_D - N_A)} \right]^{\frac{1}{2}} \qquad \text{(eqn. 6.1)}$$

Where ε_r is the relative static dielectric constant of the semiconductor, ε_0 the permitivity of free space, V_b the surface barrier potential and $(N_D\text{-}N_A)$ the net donor density, q the charge of electron, k the Boltzman constant and T the absolute temperate.

Four current transport processes have been identified for forward biased Schottky contacts. These are;

(i) emission of electrons over the barrier
(ii) quantum mechanical tunnelling through the barrier
(iii) recombination of electrons and holes in the neutral (bulk) region
(iiii) recombination within the depletion layer

It is believed that thermionic emission of electrons over the barrier is the current limiting process for the Schottky diode, with the current flow being described by the diode equation:

$$I = I_0 \exp\left(\frac{eV}{nkT}\right)\left[1 - \exp\left(\frac{-eV}{kT}\right)\right] \qquad \text{(eqn. 6.2)}$$

where V is the applied external voltage, n the ideality factor which is equal to unity for a perfect diode and greater than unity when there is recombination within the

depletion layer. When n > 1 current flow is no longer described by the thermionic emission theory and tunnelling through the barrier and recombination become significant. However for the ideal diode, I_0 the saturation current is given by;

$$I_0 = A.A^{**}T^2 \exp\left[\frac{-e(V-V_{bi})}{kT}\right] \qquad \text{(eqn. 6.3)}$$

where A is the effective area of the contact, A** Richardson's constant modified to account for the electron effective mass, electrons reflected above the barrier and phonon scattering of electrons between the top of the barrier and the surface of the metal and V_{bi} the surface built in barrier.

If the externally applied potential V > 3kT/e then eqn. 6.2 can be approximated by

$$I = I_0 \exp\left(\frac{eV}{nkT}\right) \qquad \text{(eqn. 6.4)}$$

A fuller description of all aspects relating to Schottky contacts can be found in reference 6.15. Plotting voltage (V) across the diode against the natural logarithm of the current (ln I) passed will yield information upon the ideality factor and the saturation current.

6.2.2 Schottky Contacts on Etched $Al_{0.3}Ga_{0.7}As$

In chapter 3 the etch rates of $Al_{0.3}Ga_{0.7}As$ were established using either a constant applied rf power of 150 W over a range of methane/hydrogen ratios or for a constant ratio of methane:hydrogen ratio of 5:25 over a range of rf powers. Using the gas mixture 6 sccm methane with 25 sccm hydrogen samples consisting of 1μm of $Al_{0.3}Ga_{0.7}As$ doped with silicon to give a free carrier density of $3x10^{17}$ cm^{-3} were

etched over a range of rf powers for the fixed time period of 10 minutes. The AlGaAs had been grown by MBE upon an N^+ GaAs substrate with 10 nm GaAs grown upon the top surface to prevent oxidation. Prior to etching the back surface of the GaAs substrate was deposited with 14 nm Au / 14 nm Ge / 14 nm Au / 11 nm Ni / 240 nm Au [6.16]. Half the samples were annealed prior to etching the remainder after etching. The contacts were annealed at 380 ^{0}C for 60 seconds in a reducing atmosphere of 95% argon, 5% hydrogen. At each rf power two samples were etched for a period of three minutes, one for which the ohmic contact had been annealed before etching and the other for which annealing of the ohmic contact took place after the etch.

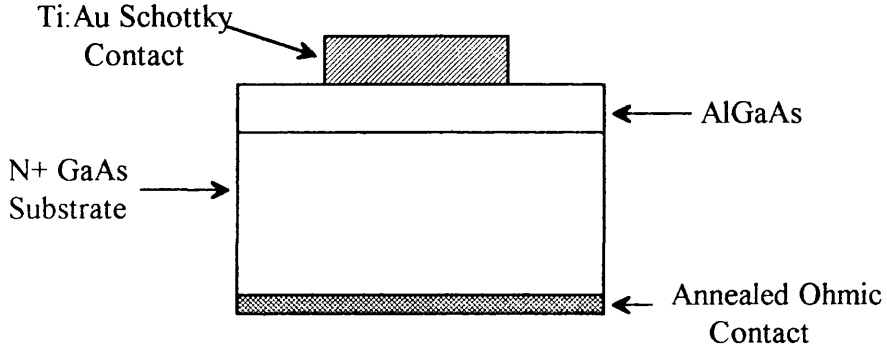

Figure 6.2
Schematic cross-section of Schottky diode.

A control sample was prepared that would not be dry etched. To give a truer comparison of damage between RIE AlGaAs and unetched AlGaAs the GaAs cap had to be removed from the control sample to expose an AlGaAs surface onto which the Schottky diode would be formed. The cap was removed using the selective wet etch 8:2:250 NH_3 :H_2O_2 :H_2O for 30 seconds. All samples had the native surface oxide layer removed by using 1:1 HCl:H_2O for 30 seconds, rinsed with RO water and blown dry with dry nitrogen before being loaded into the vacuum chamber for Schottky contact evaporation. 100 μm diameter Schottky contact were formed by

lift-off of 33 nm Ti and 160 nm Au evaporated through Shipley S1400-17 photoresist. Titanium is used as the first layer of the contact to ensure good adhesion to the semiconductor surface and gold used to provide a thick, soft layer suitable for probing.

Once fabricated, the contacts were characterised using a Hewlett Packard HP4145B semiconductor parameter analyser. To prevent irreversible damage of the Schottky contacts the current flow through the contacts was limited to 10 mA. The ideality factor, barrier height and reverse breakdown voltage where measured for the Ti/Au contacts. Here the reverse breakdown voltage is defined here as the voltage for which a reverse current of 10 μA will flow.

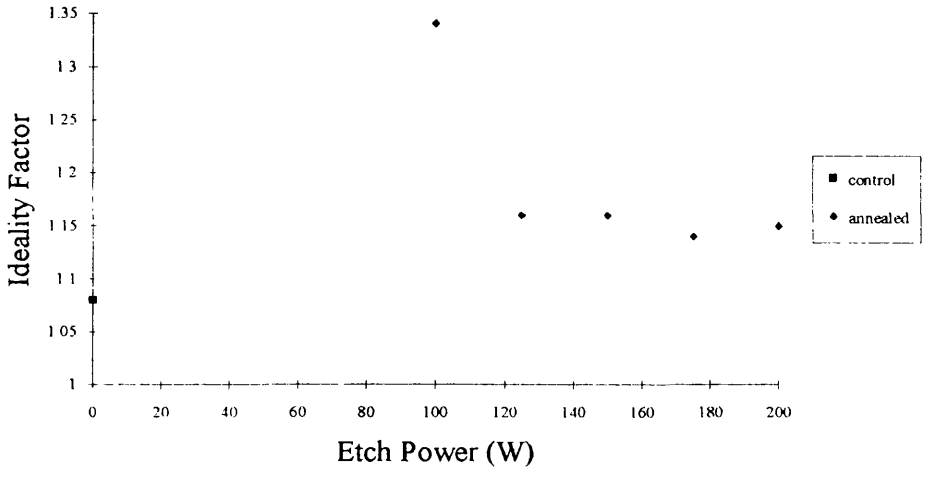

Figure 6.3
Ideality factor of Ti/Au Schottky contacts on AlGaAs.

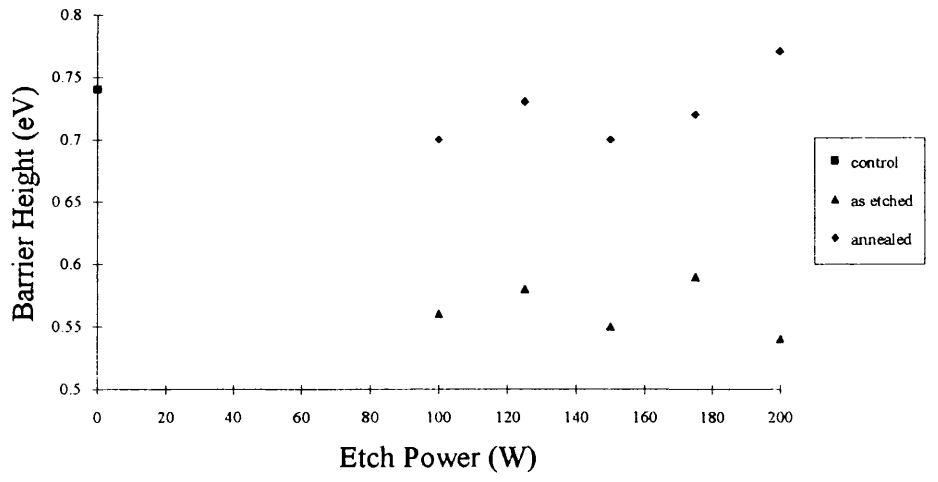

Figure 6.4
Barrier Height of Ti/Au Schottky contacts on AlGaAs.

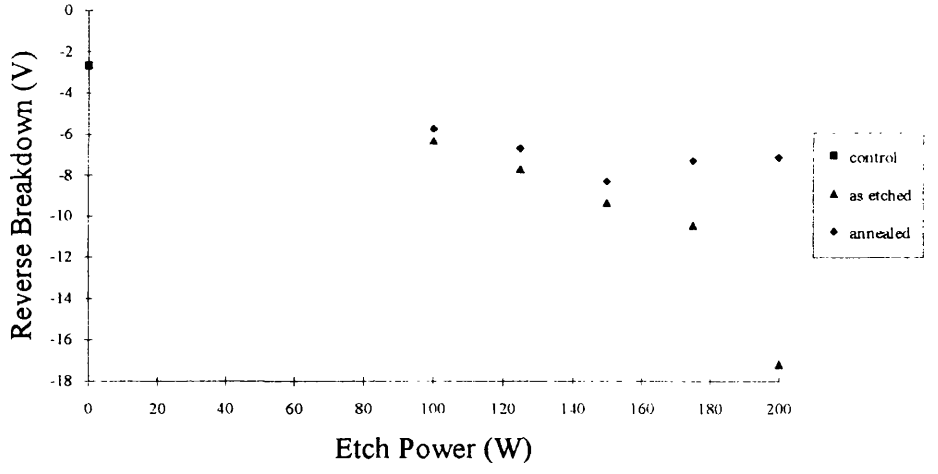

Figure 6.5
Reverse Breakdown Voltage of Schottky contacts on AlGaAs.

The Schottky contact parameters obtained for AlGaAs etched with methane/hydrogen show considerable changes compared to those obtained from the unetched control samples. The ideality factor of the control contact is low at 1.08, but upon etching the value rises sharply to the extent that only after annealing does

the ideality factor come within the range $1 < n < 2$. Of the annealed samples those etched at the highest rf powers show the best (lowest) values of ideality factor. Higher rf power give rise to higher etch rates for any given gas mixture. At these higher etch rates surface damage that could allow non-thermionic emission processes to occur is removed more efficiently than at lower etch rates.

If the surface was not etched, ion bombardment (neglecting chemical effects such as hydrogen donor passivation) would create a damaged surface layer in which the crystal lattice had been destroyed and an 'amorphous' layer created. The depth of this layer would be dependant upon the incident ion energy (rf power), the higher ion energies creating greater damaged layer thickness. If the surface was now allowed to be etched then the self terminating thickness of the amorphous layer would not be reached due to this layer also being etched. If the high powered etch produces etching at a higher rate proportional to the amorphous layer thickness than a low power etch, the resulting amorphous layer will be of greater thickness at low powers than at high powers. So although the high power etch has the potential to produce more damage it is in fact the low power etch that is responsible for the greater amount of surface damage.

This efficient removal of this surface damage can also be seen in the results obtained for the barrier heights of the contacts. Although it is not so clear as the ideality factor, the barrier height is lowered to a greater degree at low rf powers. The low rf power and associated etch rate introduce more surface states leading to a lowering in Fermi level pinning. The greater removal rates of surface damage at high rf powers maintains the surface state density closer to that of the control .

For both the as-etched and annealed samples the reverse breakdown voltage increases with rf power. The reverse breakdown voltage is a measure of the width of the depletion layer at the semiconductor surface. Breakdown occurs when the barrier

width under reverse bias becomes small, allowing carriers to tunnel through the barrier and thus a current to flow. For any given barrier height, a greater depletion layer will require a higher applied voltage to reduce the barrier width to that suitable for tunnelling.

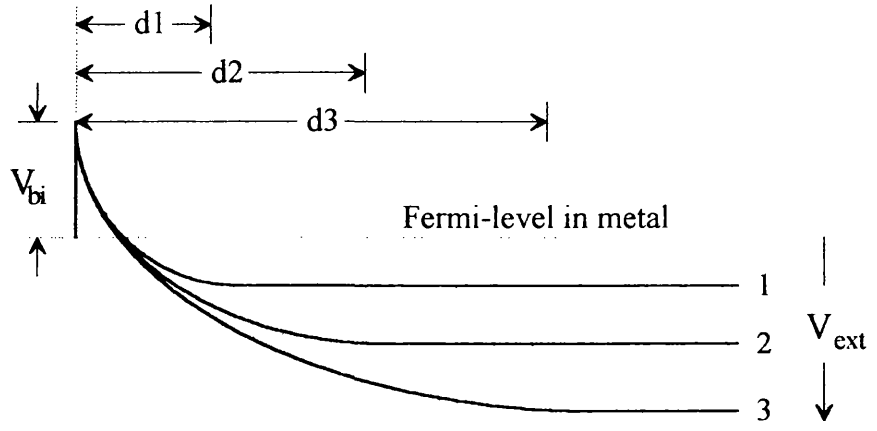

Figure 6.6
How an increase in externally applied bias voltage modifies the position of the conduction band for Schottky contacts of differing depletion widths to obtain the same barrier width and hence reverse current.

The increase in the depletion layer width is due to the increased energy of the hydrogen ions (from the higher rf power used), that are incident upon the surface of the sample during etching. These ions will be able to penetrate further into the material and so passivate donors at greater depths increasing the depletion layer width.

In forward bias the enhanced depletion layer will also lessen the probability of tunnelling through the barrier. Since recombination rates in the neutral region will remain constant the increase in ideality factor can only be explained by an increase in recombination within the depletion region.

6.3 Raman Spectroscopy

6.3.1 Background Theory

6.3.1.1 General

Scattering of laser radiation can occur within semiconductors resulting in an energy shift of the scattered light. Scattering occurs in undoped material by the production or absorption of a phonon (a quantised lattice vibration) and additionally in doped material by interaction with plasmons. Since the density of phonons in the semiconductor is normally low at room temperature compared to the density of photons from the laser the probability of light being scattered by absorption of a phonon is very slight. Normal scattering processes are therefore via the formation of a phonon. The formation of a phonon requires an exchange of energy (photon momenta approximate to zero) resulting in a lowering to the energy of scattered radiation compared with that of the incident radiation.

The advantage of Raman spectroscopy over DC electrical damage characterisation techniques such as Schottky diodes is that it is a non-destructive, contactless method that by changing the wavelength of excitation can probe different surface depths. In the experiments presented within this section an Ar^+ ion laser operating at a wavelength of 514.5 nm was used.

6.3.1.2 Binary Semiconductors

Binary materials such as GaAs [6.17-6.20] and InP [6.21,6.22] have been extensively studied by Raman spectroscopy. The Raman spectra of undoped GaAs contains two main features, these being associated with interactions of the transverse

optical (TO) and the longitudinal optical (LO) phonons producing scattering peaks at 269 cm^{-1} and 291cm^{-1} respectively. For a given scattering geometry, selection rules determine which scattering processes are observable. For GaAs in the backscattering configuration only the LO mode is observed, the TO mode being forbidden by symmetry. If the crystallographic structure of the surface is damaged for example by dry etching, then the selection rules may be broken and the TO phonon mode can be observed with the backscattering configuration.

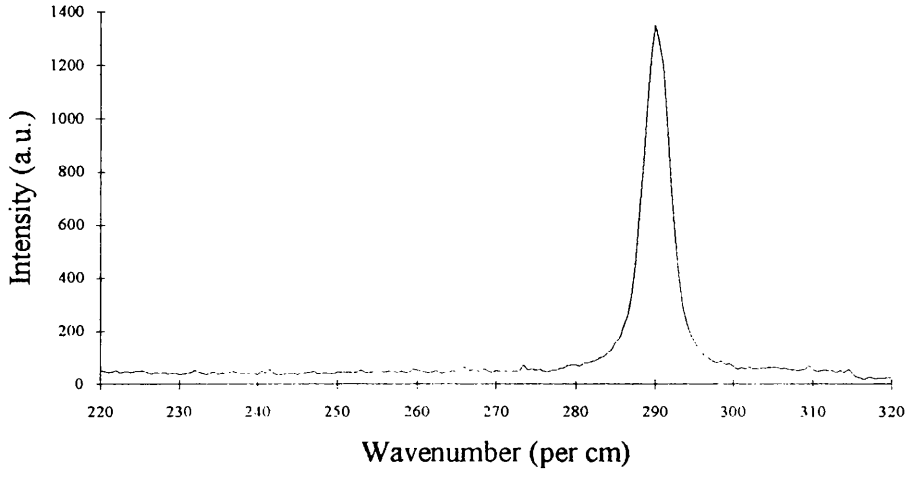

Figure 6.7

Raman spectra of undoped GaAs in backscattering configuration showing a scattering peak from the allowed LO phonon. Scattering from the forbidden TO phonon is not observed indicating good crystal quality.

In doped GaAs coupling of the phonon to the plasmon produce two new modes, a low frequency mode L_1 and a high frequency mode L_2. The frequencies of these two plasmon-phonon coupled modes can be found by solving the Drude expression [6.23] for the dielectric function of the system,

$$\varepsilon(\omega) = \varepsilon_\infty \left(\frac{\omega^2 - \omega_L^2}{\omega^2 - \omega_T^2} - \frac{\omega_P^2(q)}{\omega^2} \right) = 0 \qquad \text{(eqn 6.5)}$$

Where ε_∞ is the high frequency dielectric constant, ω the angular frequency of the incident radiation with, ω_L and ω_T the frequencies of the LO and TO phonons respectively and $\omega_P(q)$ the wave vector dependant plasma frequency given by,

$$\omega_P^2(q) = \frac{Ne^2}{\varepsilon_0 \varepsilon_r m^*} + 0.6q^2 v_f^2 \qquad \text{(eqn. 6.6)}$$

Where N is the free carrier density, e the electric charge, ε_0 the vacuum dielectric constant ε_r the static dielectric constant, m* the effective mass of the charge carriers, v_f the Fermi velocity and where q is the wave vector of the plasmon-phonon mode for the backscattering configuration. q=2vn where v is the wave vector of the illuminating light and n the refractive index of the material at v.

The low frequency plasmon-phonon mode L_1 is therefore only slightly dependant on carrier concentration and approaches the frequency of the TO mode for heavily doped GaAs at room temperature. The high frequency mode L_2 is however strongly dependant upon the doping concentration and is located close to the plasma frequency. Measurement of L_2 can give an independent assessment of the carrier concentration.

The presence of a surface depletion layer in doped semiconductors will allow for scattering by both LO and plasmon-phonon modes to be observed. Assuming that the depletion layer has an abrupt junction with the bulk doped region then,

$$I(LO) = I_0(LO)(1 - e^{-2\alpha d}) \qquad \text{(eqn. 6.7)}$$

Where I(LO) is the measured intensity of the LO phonon mode, I_0(LO) the intensity of the LO phonon mode from undoped material, α the absorption coefficient of the semiconductor at the illuminating radiation and d the depth of the surface depletion layer. Since the depletion layer thickness is inversely proportional to the doping concentration the intensity of the LO phonon will decrease with increasing doping levels.

The intensity of the L_1 phonon peak will be proportional to the difference between the measured intensity of the LO phonon peak in the doped material and the intensity in undoped material then,

$$\frac{I(LO)}{I(L1)} = \beta(e^{2\alpha d} - 1) \qquad \text{(eqn. 6.8)}$$

Where β is the scattering constant given by,

$$I_0(LO) - I(LO) = \beta I(L_1) \qquad \text{(eqn. 6.9)}$$

The scattering constant can be found by analysis of a control sample of known doping concentration and depletion layer thickness.

6.3.1.3 Ternary Semiconductors

In the binary material system of GaAs two phonon modes, LO and TO are possible in the undoped material. The ternary material systems such as AlGaAs and InGaAs are alloys of two such binary materials. In the case of InGaAs the two constituent materials are GaAs and InAs and Raman spectroscopy of the alloy reveals that four phonons are possible [6.23,6.24]. These have been prescribed to

'LO-' and 'TO-like' modes resulting from each of the constituent binary materials. The precise energy of the four phonon scattering modes are determined by the mole fraction of the alloying materials.

Phonon	GaAs [6.25]	InAs [6.26]	$In_XGa_{1-X}As$ [6.27]
GaAs-like LO	291.9	-	$290-18.6x-32.4x^2$
GaAs-like TO	268.6	-	$265.1-5.3x-29.0x^2$
InAs-like LO	-	238.6	$234.9-7.7x+8.92x^2$
InAs-like TO	-	217.3	$233.7-16.5x$

Table 6.1
Raman shifts (cm^{-1}) due to scattering by optical phonons at 300K for the binary materials GaAs and InAs and the ternary alloy $In_xGa_{1-x}As$.

The expressions for the wavenumbers of the InGaAs alloy are plotted in Figure 6.8. Under the condition for lattice matching of $In_xGa_{1-x}As$ to InP i.e. x = 0.53 the four phonon scattering peaks should be found at 224.96 (InAs-like TO), 233.32 (InAs-like LO), 254.14 (GaAs-like TO) and 271.99 cm^{-1} (GaAs-like LO).

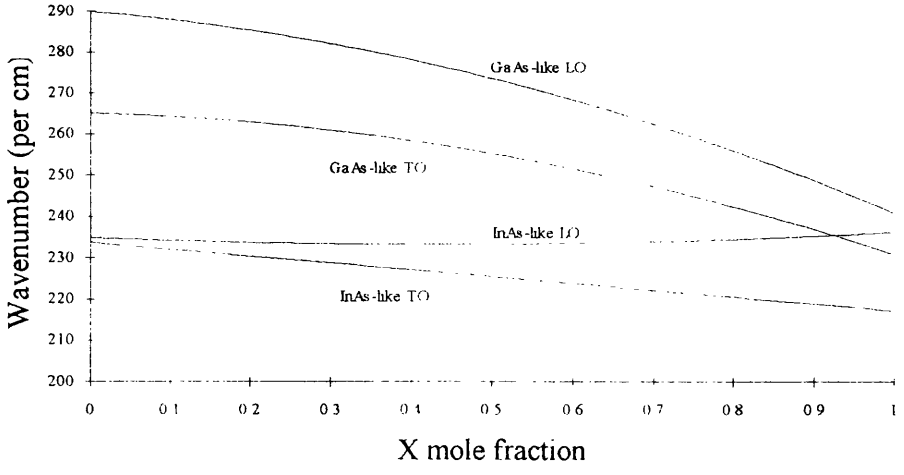

Figure 6.8
Frequencies of optical phonons in $In_xGa_{1-x}As$ at 300K [6.27].

The Drude expression for the dielectric function for binary systems (eqn. 6.4) becomes extended by one term to describe ternary materials such that,

$$\varepsilon(\omega) = \varepsilon_\infty \left(\frac{\omega^2 - \omega_{L_{GaAs}}^2}{\omega^2 - \omega_{T_{GaAs}}^2} \times \frac{\omega^2 - \omega_{L_{InAs}}^2}{\omega^2 - \omega_{T_{InAs}}^2} - \frac{\omega_p^2(q)}{\omega^2} \right) \qquad \text{(eqn. 6.9)}$$

In the backscattering geometry four scattering peaks should be observed. The LO and LO-plasmon coupled modes of GaAs and the LO and LO-plasmon coupled modes of InAs.

6.3.2 H_2 and CH_4/H_2 Plasma Treatments of GaAs

1μm of GaAs doped with silicon to give a free carrier concentration of 4.4×10^{18} cm^{-3} upon an undoped GaAs buffer grown by MBE upon semi-insulating GaAs substrate was used to study the effect of a number of plasma treatments to the extent of the surface depletion layer. Spectra from undoped and doped GaAs control samples were taken, the undoped spectra being obtained from the semi-insulating substrate of the wafer. The undoped control sample shows only one peak in the spectra at $291cm^{-1}$ (see Figure 6.7), the LO phonon. Doped samples show two phonon peaks, the LO as seen in the undoped sample and the other phonon peak at $268cm^{-1}$, the phonon-plasmon peak L_1.

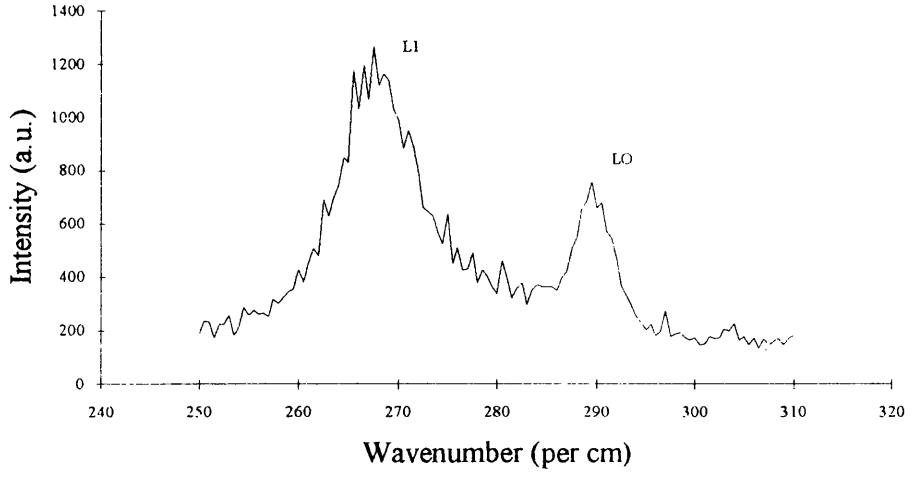

Figure 6.9
Raman spectroscopy of the n^+ GaAs control sample.

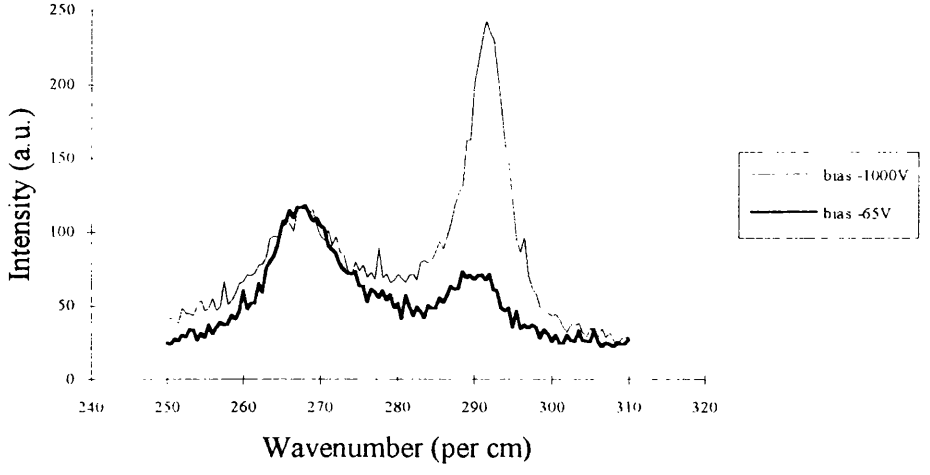

Figure 6.10
The effect of DC bias of hydrogen plasma upon Raman spectra of n^+ GaAs.

When the doped GaAs is exposed to a H_2 or CH_4/H_2 plasmas, H^+ ions will enter into the GaAs and passivate silicon donors to a depth that equals the maximum penetration depth of the ions. The surface Depletion depth will thus change in dimensions with the energy of the bombarding ions. By exposing the GaAs to

hydrogen plasma of differing DC bias it is possible to see the change in depletion depth with ion energy.

A high bias plasma exposure was performed upon the Electrotech Plasmafab 340 RIE machine. With 25 sccm H_2 at 20 millitorr with 170 W a DC bias of -1000 V was produced. A DC bias of -65 V was obtained upon the Plasma Technology μp80 RIE machine with 20 sccm H_2, 200 millitorr and 15 W. All samples were exposed to the plasma for 5 minutes.

The sample exposed to the high DC bias shows a considerable increase to the intensity of the LO phonon peak relative to the L_1 phonon peak indicating a large increase to the depletion depth. Exposure to the lowest DC bias plasma results in a small relative change to the peak intensities showing that little change to the depletion layer hence passivation of carriers has occurred.

DC Bias (-V)	Intensity L_1 (a.u.)	Intensity LO (a.u.)	I(LO)/I(L_1)	Depletion Depth (nm)
Control	1,178	256.5	0.22	13.7
65	1,215	543.6	0.45	25.2
88	1,919	824.9	0.43	24.4
107	2,146	1,217	0.57	30.3
165	1,595	1,069	0.67	34.3
1,000	1,304	1,732	1.33	54.6

Table 6.2
Change in surface depletion depth due to DC bias during hydrogen plasma exposure.

Exposure of the surface to a hydrogen plasma results in the worst possible case of induced damage. The hydrogen exposure results in continual bombardment of the surface leading to eventual saturation of the material and saturation of donors.

Etching with methane/hydrogen also produces hydrogen ion bombardment of the surface but because the surface is continually being etched, passivated material is also etched. The etching of the surface does not allow saturation to occur and should create less damage at the surface.

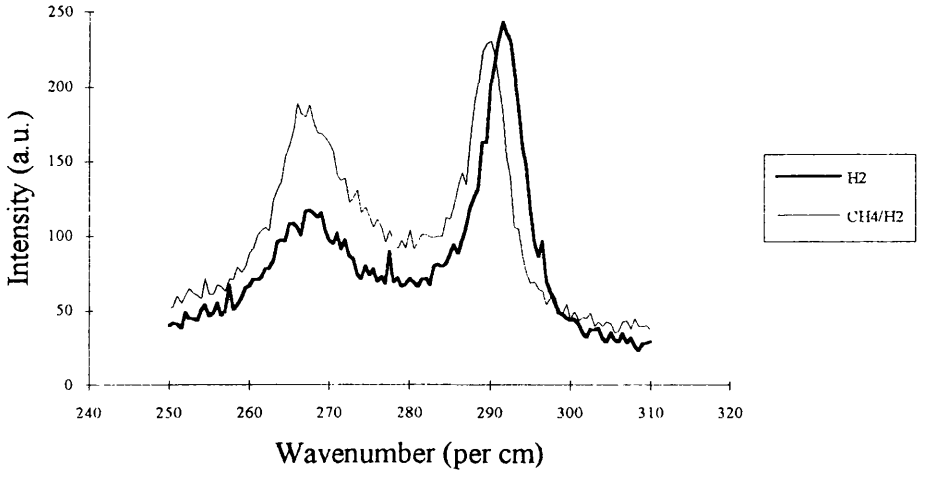

Figure 6.11
Change in Raman spectra of n⁺ GaAs for H_2 plasma treatment and CH_4/H_2 etch at a DC self bias of -1000V.

Two samples of the doped GaAs were exposed to plasmas at -1000V DC bias. The first plasma was of hydrogen only and the second constituted a 3 sccm methane, 22 sccm hydrogen mixture. Raman spectroscopy of the two samples shows that the intensity of the LO peak relative to the L_1 peak is lower when methane is added to the gas mixture.

Treatment	Intensity L_1 (a.u)	Intensity LO (a.u.)	I(LO)/I(L_1)	Depletion depth (nm)
Control	1,178	256.5	0.22	13.7
-1000V H_2	1,304	1,732	1.33	54.6
-1000V CH_4/H_2	1,664	1,462	0.88	41.6

Table 6.3
The effect of treatment method upon surface depletion depth.

The presence of methane and hence etching of the surface reduce the surface depletion depth by means of continually removing passivated material. The depletion depth is still many times greater than that found in the unetched sample. Provided etching could be initiated by the addition of a little methane at the low DC biases used in this experiment, a reduction in these depletion depths could be expected.

6.3.3 CH_4/H_2 RIE of InGaAs

Samples suitable for Raman studies were grown by MBE. The material consisted of 1 μm $In_{0.53}Ga_{0.47}As$ doped with silicon to a carrier density of $5x10^{18}$ cm^{-3} with a 500 nm undoped $In_{0.52}Al_{0.48}As$ buffer upon an InP substrate. Samples were etched with various methane/hydrogen mixtures for 5 minutes in the Electrotech plasmafab 340 RIE machine. Again excitation was at 514.5 nm at an ambient temperature of 300K.

The unetched control sample shows the presence of the four scattering peaks, the maxima of which occur at 227, 242, 254 and 265 cm^{-1}. Upon exposure of the surface to the methane/hydrogen plasma the Raman spectra is seen to change. The most noticeable feature of the spectra from the etched samples is the lowering of the GaAs-like LO phonon peak relative to all other peaks. If damage is being done to the material by the etch process one would expect the two TO peaks to rise in intensity

relative to the two LO peaks as either symmetry rules are broken or as surface depletion is enhanced. The results obtained here are at odds with these expectations and another mechanism must be responsible for the observed changes. Such a mechanism is discussed in Section 6.4. Information can however be gained form looking at the high frequency phonon-plasmon scattering peak L_2. The position of the L_2 peak is strongly dependant on the free carrier density of the semiconductor and will thus change position if a loss or enhancement of carriers is experienced. Shen and co-workers [6.28] have used this method to investigate the doping levels of GaAs.

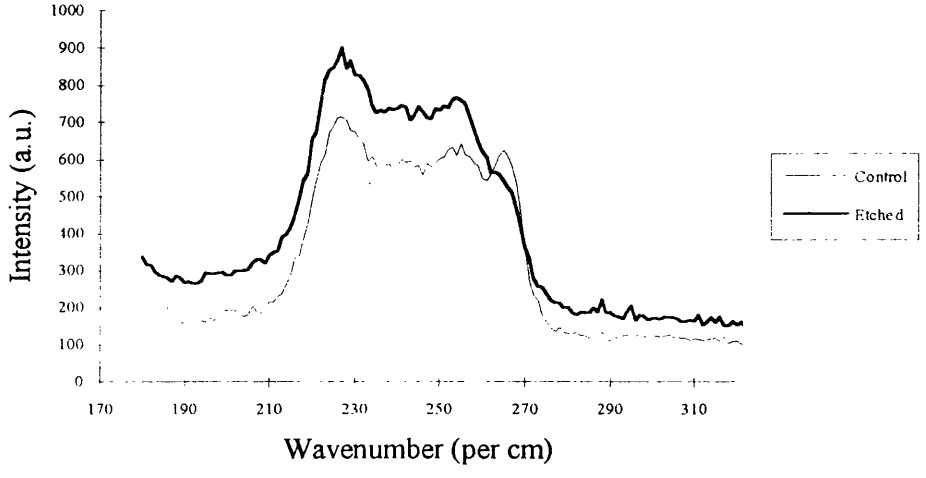

Figure 6.12
Raman Spectra of InGaAs showing the relative decreases of the GaAs-like LO phonon after etching with 5 sccm CH_4, 20 sccm H_2 at 20 millitorr and 75 W.

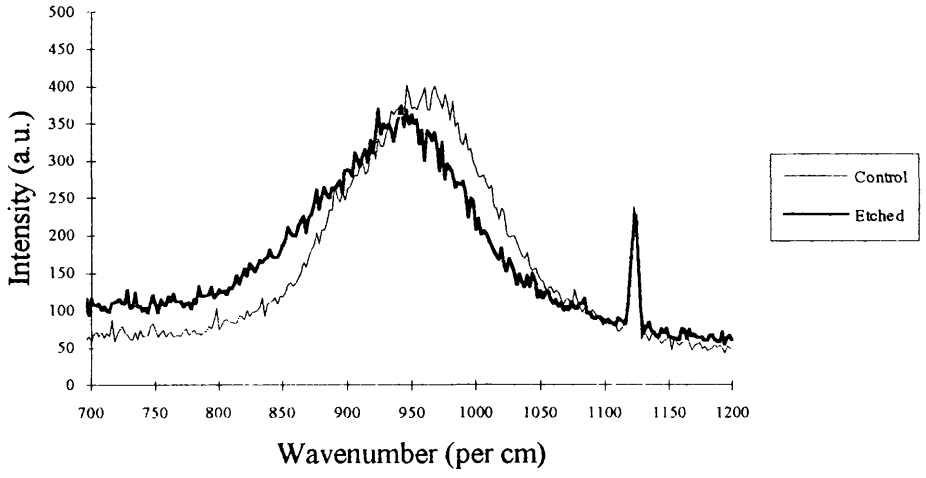

Figure 6.13
Raman spectra of InGaAs showing high energy L_2 plasmon-phonon scattering peak.

After etching the L_2 peak is seen to shift slightly towards lower energies indicating a loss of carriers. The peak observed at a wavenumber of 1122 cm^{-1} is due to one of the plasma lines of the laser used to illuminate the sample.

6.4 Photoluminescence

6.4.1 Photoluminescence Theory

Incident laser radiation with photon energy greater than the band-gap can create electron-hole pairs in a non-equilibrium state by the absorption of photons. To regain equilibrium direct recombination of the pair may occur resulting in the emission of a photon of energy equal to the band-gap. In the presence of damage recombination via a non-radiative centre is possible, a process by which a photon is not emitted.

The greatest rates of electron-hole pair generation are at the semiconductor's surface. As the intensity of the illuminating light reduces with distance into the bulk of the material, generation rates will also reduce. Photoluminescence is therefore a surface technique limited to probing depths equal to the absorption length of the illuminating light.

An electron in the conduction band and hole in the valence band can experience a mutual attractive force. This system is named an exciton. If an exciton is free to move through the crystal the electron and hole must have the same velocities. A free hole can combine with a neutral donor to form a positively charged excitonic ion with the hole moving in the electrostatic field of a 'fixed' dipole determined by the instantaneous position of the electron. This is termed a bound exciton. The electron and hole of an exciton can combine radiatively with an energy lower than the band-gap energy by an amount equal to the exciton binding energy. Photo-luminescence studies of bulk InGaAs have shown that the prime features of photoluminescence spectra result from bound excitons [6.29]. Low temperatures (9K) have been used to ensure narrow luminescence line widths.

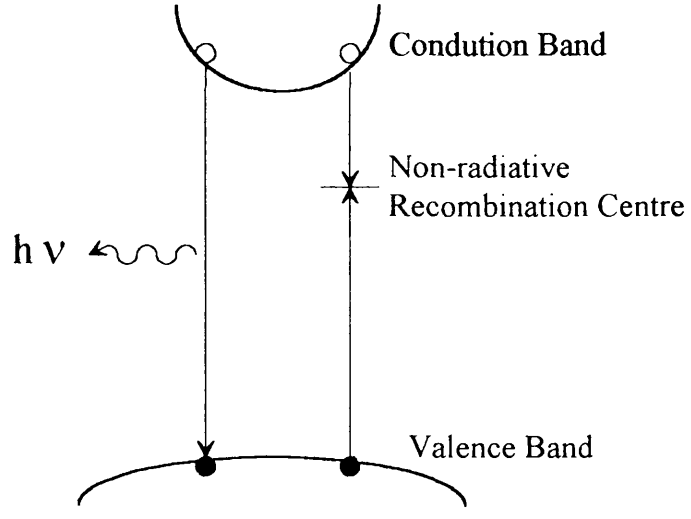

Figure 6.14
Schematic of radiative and non-radiative processes near the band-gap minima.

6.4.2 Photoluminescence of CH_4/H_2 Etched InGaAs

Photoluminescence test samples consisted of 5 μm undoped $In_{0.53}Ga_{0.47}As$ with a 500 nm $In_{0.52}Al_{0.48}As$ buffer layer upon InP substrate. Etching was performed using the Electrotech Plasmafab 340 RIE machine. The sample was illuminated using the 632.8 nm line of a HeNe laser.

The unetched control sample shows a particularly strong peak at 1536 nm (0.807 eV) corresponding to luminescence from the bound exciton. Etching of the InGaAs sample results in a second broader luminescence peak at 1597 nm (0.776 eV) and a shift of 0.027 eV of the bound exciton peak to 0.803 eV. Photo-luminescence studies of as-grown InGaAs [6.30, 6.31] can show similar peaks. The presence of this peak has been explained by consideration of an InAs surface quantum well [6.32] formed by segregation during growth. Clearly the unetched InGaAs sample did not show surface segregation, but it is believed that etching process creates an indium rich surface or an InAs surface QW.

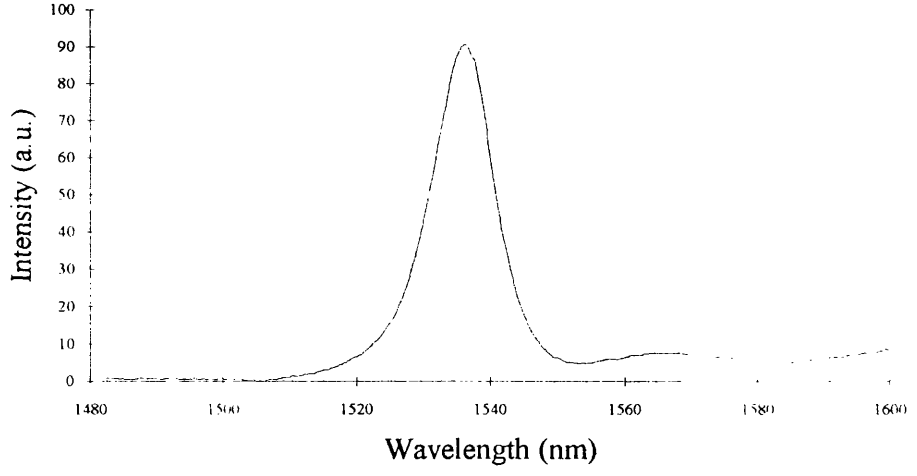

Figure 6.15
Photoluminescence spectra from unetched InGaAs.

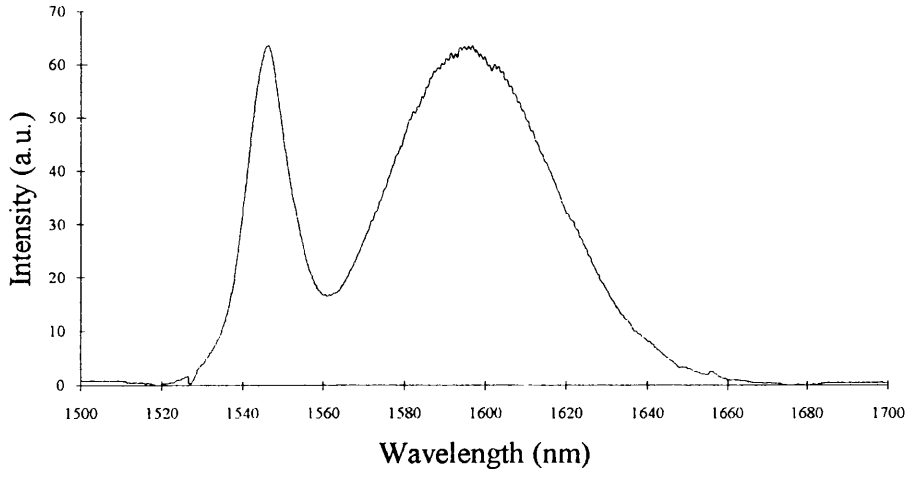

Figure 6.16
Photoluminescence spectra from InGaAs etched with 5 sccm CH_4, 20 sccm H_2 at 20 millitorr and 75 W rf power.

It is known that etching InGaAs with methane/hydrogen gas mixtures can lead to the formation of indium droplets [6.33] upon the etch surface and has been shown using XPS (X-ray Photoelectron Spectroscopy) that InP and InGaAsP show indium enrichment [6.34] upon the surface after similar methane/hydrogen etches. The indium rich surfaces form because of the differing volatilities of the etch products.

Product Species	m.pt. (^{0}C)	b.pt. (^{0}C)
$Al(CH_3)_3$	15	126
$Ga(CH_3)_3$	-15.7	56
$In(CH_3)_3$	88.4	136
AsH_3	-116.3	-62.5
PH_3	-132.5	-87.8

Table 6.4
Melting and boiling point for primary etch products formed during CH_4/H_2 RIE.

The melting and boiling point data can be used as a guide to understand the ease with which a product will desorb from the etch surface. To be accurate, data should be obtained under the appropriate ion bombardment. Table 6.4 demonstrates that trimethyl- gallium will desorb from the surface more readily than trimethylindium resulting, over time in an indium rich surface.

The presence of the indium rich surface is consistent with the observed fall in intensity of the GaAs-like LO phonon peak for Raman spectroscopy of etched InGaAs. As the etch surface becomes richer in indium the GaAs-like LO phonons become less likely and the TO phonons more likely as long range crystallographic order is destroyed at the surface.

6.5 X-ray Photoelectron Spectroscopy

6.5.1 Introduction

X-rays incident on a material can be absorbed and may eject core electrons form the parent atom. These photoelectrons if they have sufficient energy to overcome surface potentials and scattering losses may then be emitted from the surface of the material. Because the precise electron energy levels of the atom will depend on the chemical environment of that atom, the energy of the emitted electron will be a unique indicator of the chemical composition of the material irradiated.

The depth to which materials can be probed by XPS is approximated by;

$$d \sim 3\lambda.\cos(\theta) \qquad \text{(eqn. 6.10)}$$

Where λ is the elastic mean free path of the photoelectrons within the material and θ the angle between the material's surface normal and the direction of the incident x-rays. This angle is referred to as the take-off angle (TOA) and is the angle between the surface normal and the incident direction of the x-rays.

6.5.2 XPS of CH_4/H_2 etched InGaAs

Three samples of InGaAs were prepared for XPS. These were; the control, an as-grown sample, sample C1 etched with 1 sccm CH_4, 24 sccm H_2 at 20 millitorr and 75 W for 5 minutes and sample C5 etched with 5 sccm CH_4, 20 sccm H_2, 0.5 sccm O_2 at 20 millitorr and 75 W for 5 minutes. Photoelectrons ejected from a 1 mm^2 area of the samples were collected in a hemispherical analyser at take-off angles of 0 and 60^0.

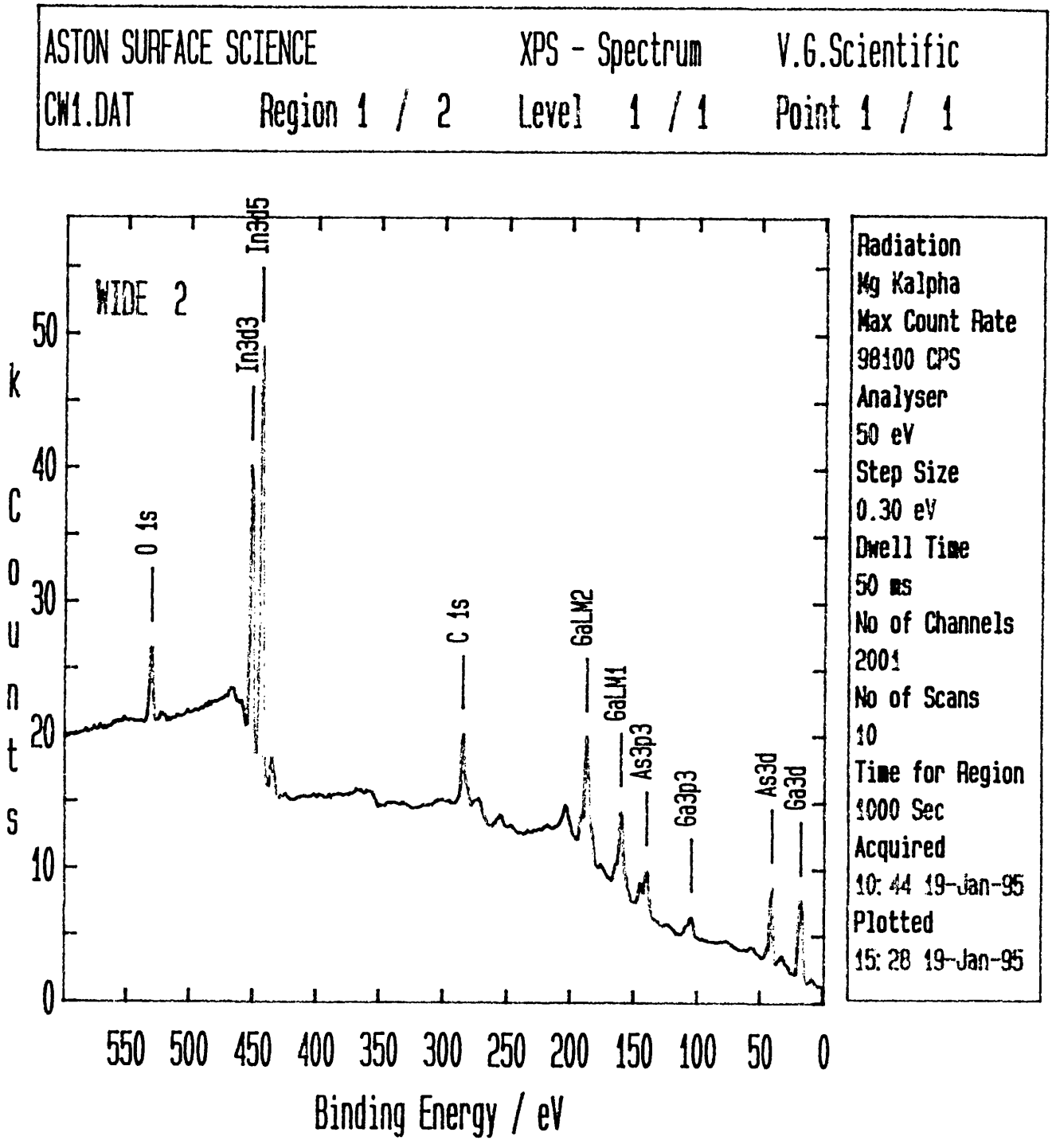

Figure 6.17

XPS of InGaAs over the range of binding energies 0-600 eV.

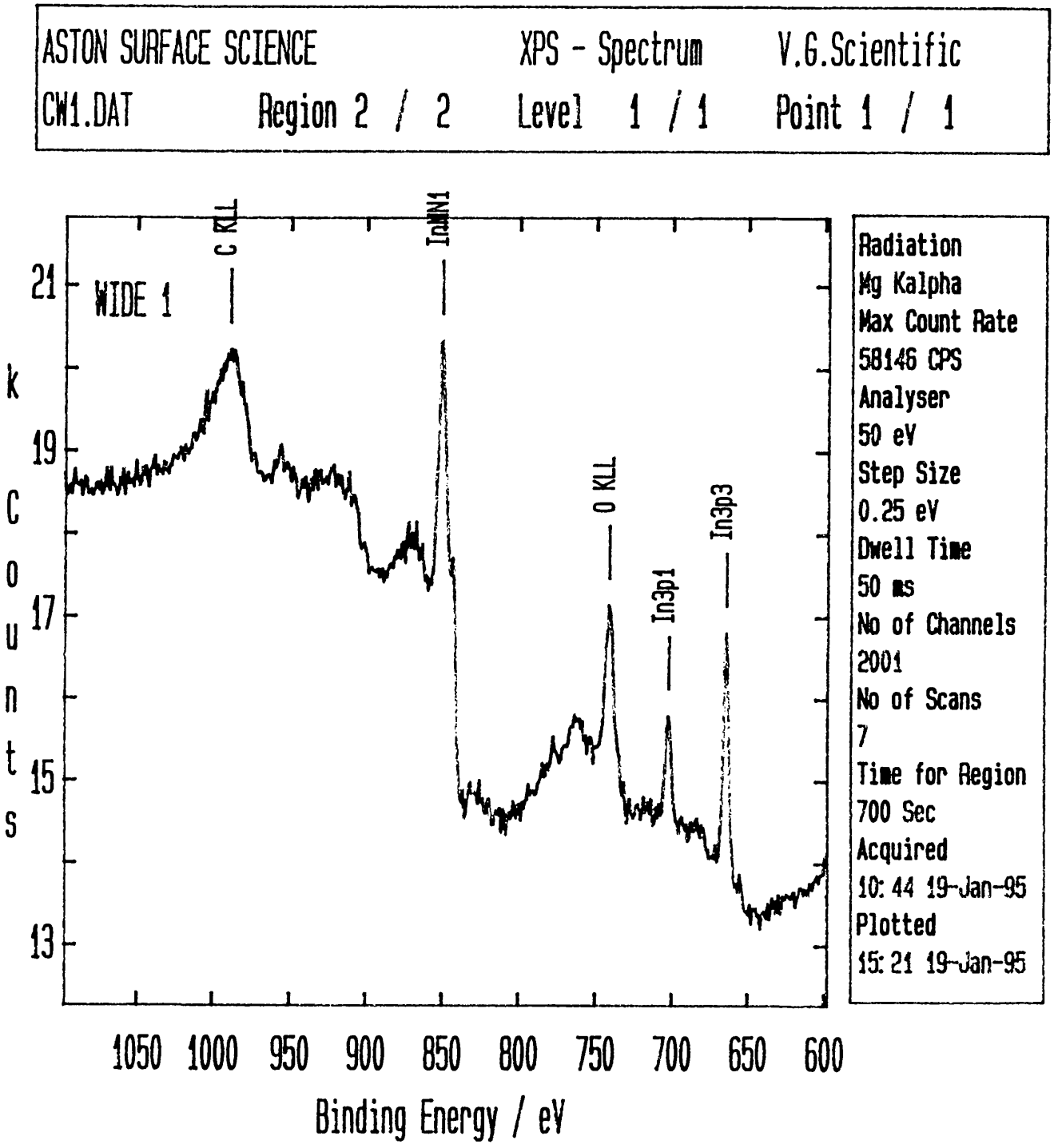

Figure 6.18

XPS of InGaAs over the range of binding energies 600-1100 eV.

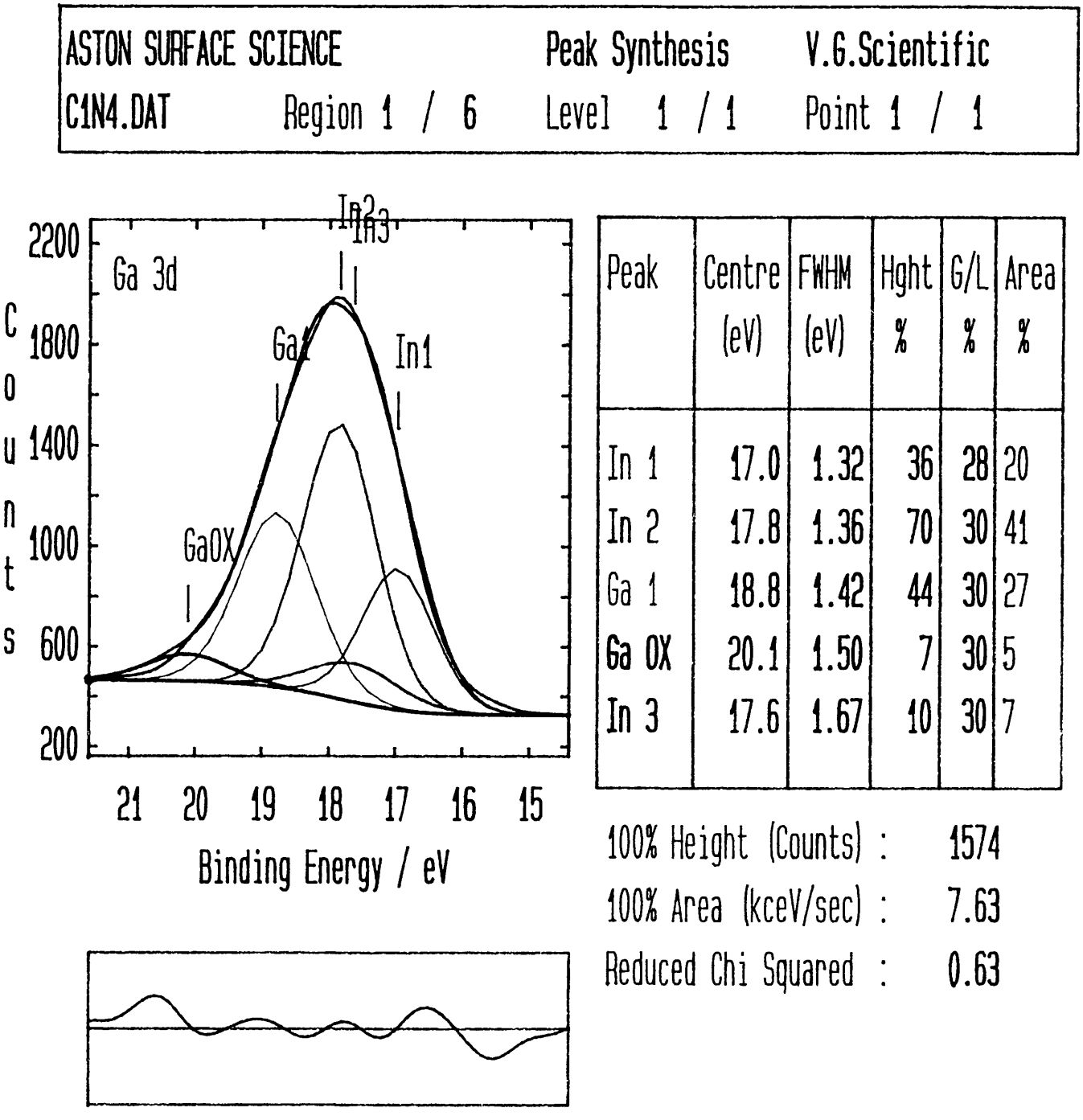

Figure 6.19

Curve fitting in the region of the Ga 3d and In 4d peaks to establish relative abundances of Ga and In.

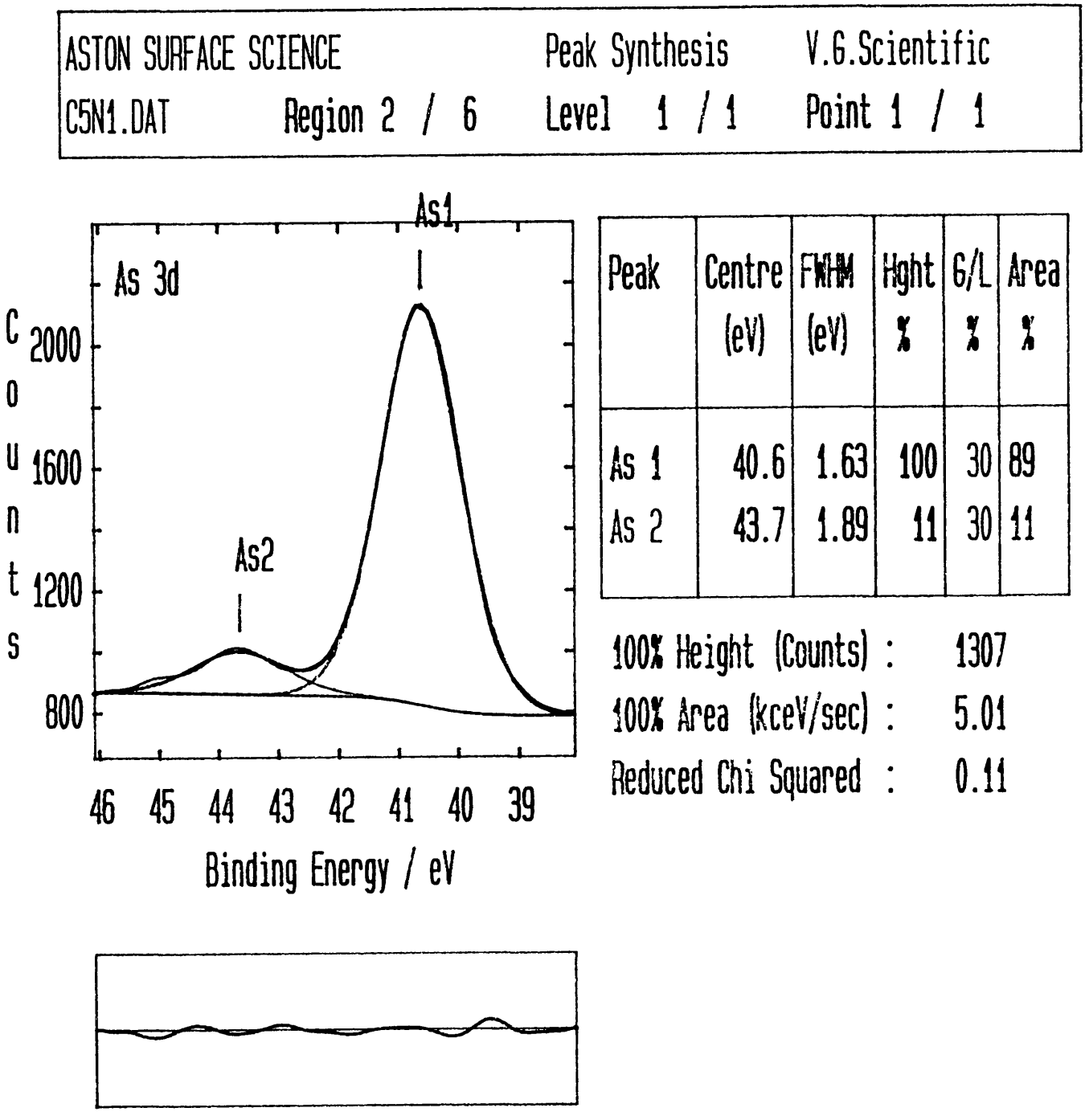

Figure 6.20

Splitting of the As 3d peak due to elemental As and oxides of As.

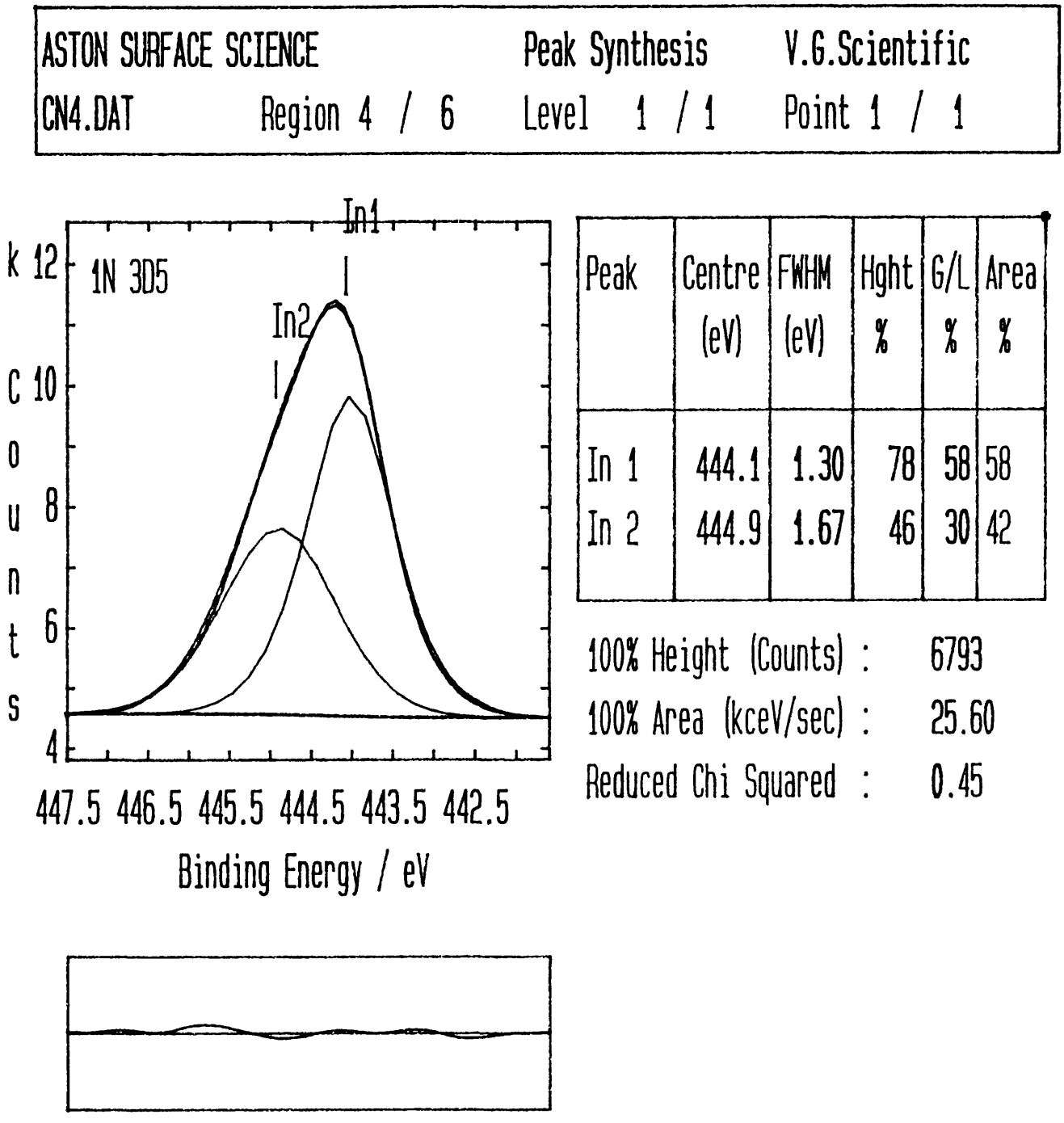

Figure 6.21

Peak fitting of In 3d5/2 peak to show elemental In and oxides of In.

Sample	TOA	Relative abundance As=1.00				In:Ga
		C 1s	In 3d5/2	O 1s	Ga 3d	
Control	0	1.23	0.84	0.92	0.69	1.22
Control	60	2.38	0.93	1.41	0.96	0.97
C1	0	1.56	1.59	1.07	0.35	4.57
C1	60	4.27	2.01	1.68	0.74	2.7
C5	0	1.86	1.41	1.15	0.47	2.99
C5	60	4.23	1.5	1.71	0.85	1.76

Table 6.5
Atomic ratios normalised to As for the three InGaAs samples.

Sample	TOA	In %	Ga %	As %
Control	0	33.2	27.2	39.5
Control	60	32.2	33.3	34.5
C1	0	54.2	11.8	34
C1	60	53.5	19.8	26.7
C5	0	49	16.4	34.7
C5	60	44.8	25.4	29.9

Table 6.6
Relative amounts of the three elements In, Ga and As.

Analysis shows that in the unetched control sample has more indium than gallium in the bulk but at the surface this ratio is reduced. There is less arsenic at the surface than within the bulk. Etching the sample enhances the amount of arsenic depletion and shows an increase in indium content relative to gallium. Probing only the surface reveals more gallium than when greater depths are probed. The use of the methane/hydrogen/oxygen etch results in a less indium rich surface and less arsenic depletion than when using the methane/hydrogen etch.

Sample	TOA	As	As oxide
Control	0	86	14
Control	60	74	26
C1	0	88	12
C1	60	82	18
C5	0	89	11
C5	60	77	23

Table 6.7
Proportion of oxides of arsenic against all other forms of arsenic.

Sample	TOA	In	In oxide
Control	0	78	22
Control	60	58	42
C1	0	62	38
C1	60	26	74
C5	0	62	38
C5	60	33	67

Table 6.8
Proportion of indium oxides against all other forms of indium.

The As 3d and In 3d5/2 peaks are split due to different bonding of the As or In atoms. Both As and In show there to be more oxide at the surface than deeper down. No conclusions should however be drawn form Tables 6.7 and 6.8 with regards to the effect of oxygen in the etch gas mixture. All samples had been exposed to the air for several weeks so natural surface oxidation will mask the effect of the etch.

6.6 The Transmission Line Model

6.6.1 The Transmission Line Model method

The specific contact resistance and the sheet resistance of the semiconductor between a pair of ohmic contacts can be established using the transmission line model (TLM) [6.35, 6.36]. The total resistance between two adjacent ohmic contacts can be described in terms of the resistance of each contact, R_C and the resistance of the sheet, r_S connecting the two contacts. Thus

$$R = 2R_C + r_S\left(\frac{l}{w}\right) \qquad \text{(eqn. 6.11)}$$

Where R is the total resistance, l the inter-contact separation and w the width of the contact. Plots of inter-contact separation against total resistance will yield a straight line of gradient r_S/w and an intercept upon the resistance axis of $2R_C$.

The test structure consists of a series of identical ohmic contacts arranged in a line formed upon a conducting epi-layer on a semi-insulating substrate. The contacts are oriented so that their long side is perpendicular to the line joining the centres of all the contacts and are separated such that a range of inter-contact distances are available to be investigated. All the thin conducting epi-layer is removed by either wet or dry etching except for the region between adjacent ohmic contacts. The current flow is thus limited to between neighbouring contacts and will be as uniform as possible.

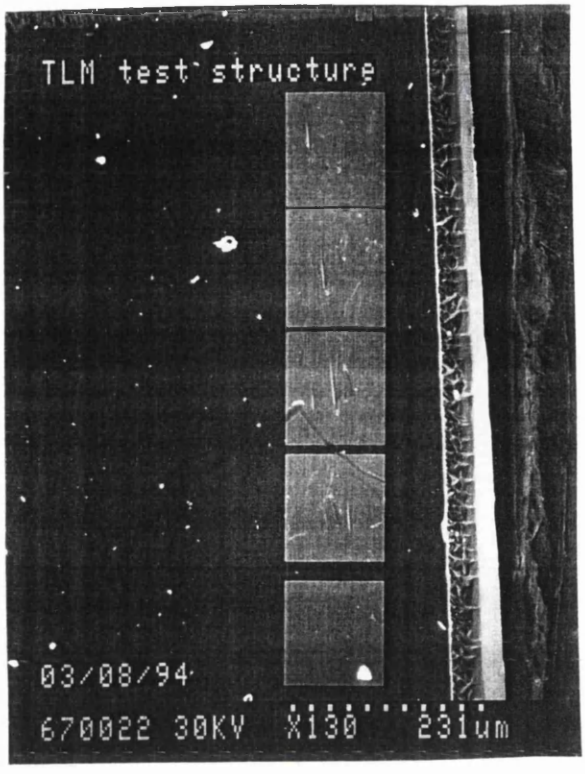

Figure 6.22

Micrograph of TLM test structure used in this study

6.6.2 Hydrogen Exposed Pseudomorphic HEMT Structures

The pseudomorphic HEMT structure, CAS9 was used for preliminary studies of low bias hydrogen plasma damage. Hydrogenation of the TLM test structures at a DC bias -65 V was performed using the Plasma Technology μp80. TLM test patterns were exposed to the plasma for a range of times and the inter-contact resistance measured using a Hewlett Packard 4145A semiconductor parameter analyser.

Layer	Material
Cap	40nm $2.5x10^{18}$ Si doped GaAs
Schottky/ Supply Layer	30nm $2.5x10^{18}$ Si doped $Al_{0.3}Ga_{0.7}As$
Spacer	2nm undoped $Al_{0.3}Ga_{0.7}As$
Channel	12nm undoped $In_{0.3}Ga_{0.7}As$
Buffer	1μm undoped GaAs
Substrate	semi-insulating GaAs

Table 6.9
Material structures of CAS9 as used for TLM measurements.

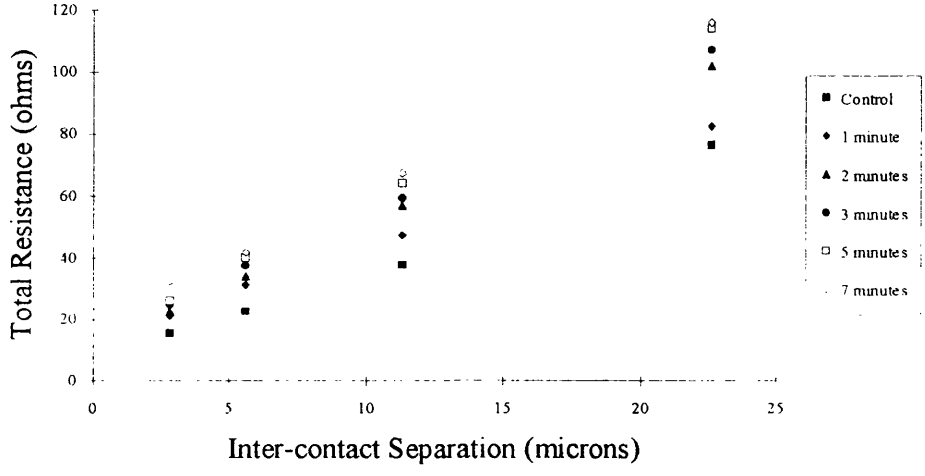

Figure 6.23
Total inter-contact resistance with hydrogen plasma exposure time for CAS9.

Straight lines were fitted to the data presented in Figure 6.23 using a least squares method and from which the sheet resistance was calculated. The sheet resistance increases after an initial period of 1 minute and after 5 minutes reached a maximum at which it remained.

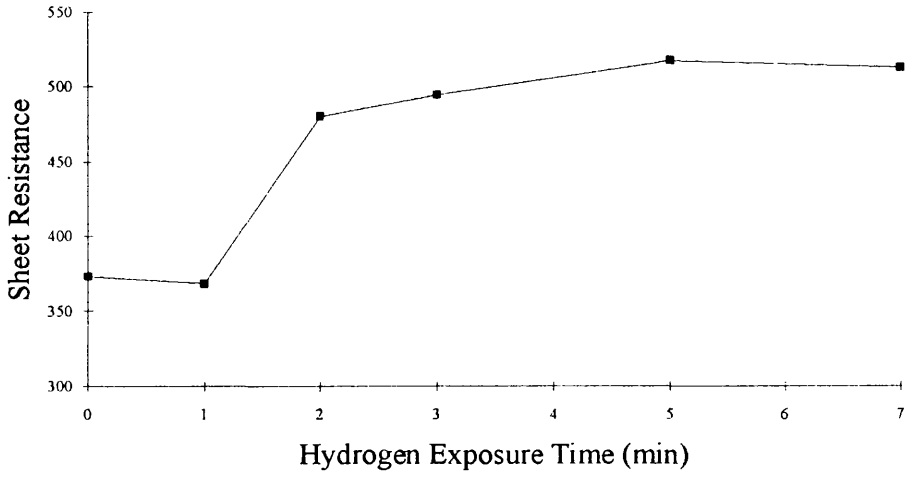

Figure 6.24
CAS9 sheet resistance with time.

The value at which the sheet resistance saturates is 1.38 times the value of the control sample. The data of Figure 6.23 also yields information about the specific contact resistance. It has already been stated that the intercept on the resistance axis is twice the contact resistance. From the experiment the contact resistance is seen to increase with hydrogenation time.

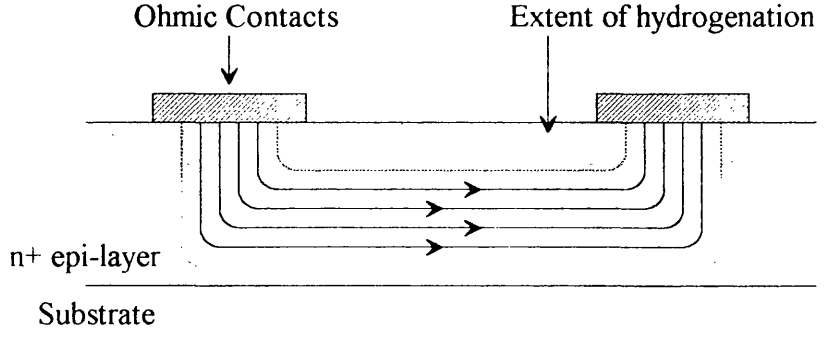

Figure 6.25
Schematic showing the effect of hydrogenation on current flow between ohmic contacts.

Hydrogen will readily penetrate the semiconductor in the direction of ion bombardment, perpendicular to the surface, but scattering processes within the material can result in passivation of donors in material that is masked from direct ion bombardment. Figure 6.25 illustrates how hydrogen can be scattered underneath ohmic contacts. The material under the contact is protected from direct ion bombardment. The contact is reduced in dimensions crowding current giving rise to the measured increase in specific contact resistance.

The layer structure as it is contains 70 nm of highly doped material in the topmost two layers. To increase the sensitivity of the structure to hydrogen passivation the 40 nm GaAs layer was removed using a $SiCl_4/SiF_4$ selective etch that has been shown to induce very little damage [6.37]. Removal of this layer resulted in a loss of 57% of the number of donors and increased the sheet resistance from 373 to 616 Ω/□.

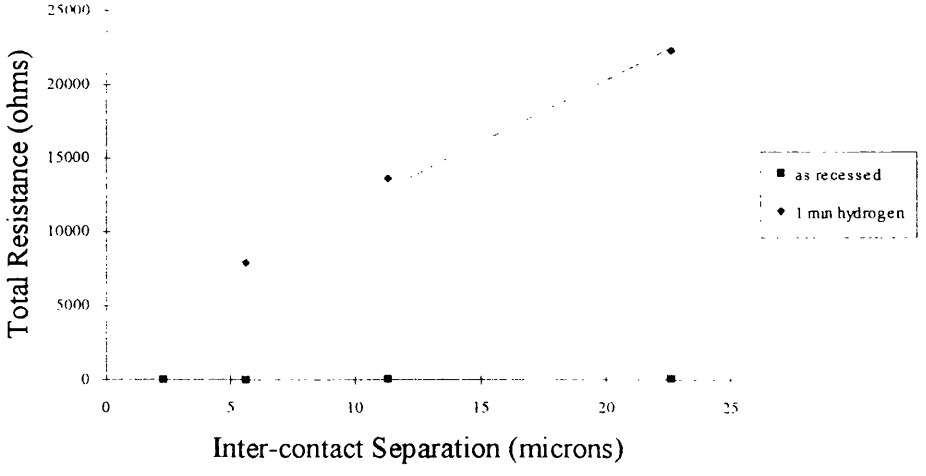

Figure 6.26
Total inter-contact resistance before and after 1 minute H_2 plasma. The GaAs cap has been removed using $SiCl_4/SiF_4$ selective etch..

Exposing the recessed test pattern to just 1 minute of hydrogen plasma was sufficient to cause enough passivation of the donors to effectively destroy conduction through the sample. The sheet resistance was now 100 KΩ/□.

6.6.3 Band Structure modelling

Modelling of the band structure using a 1-dimensional Poisson solver [6.38] was undertaken to try and understand how surface passivation was effecting the sheet resistance. Using the full layer structure with GaAs cap in place the effect of the hydrogen plasma was modelled. By assuming that after exposure a surface layer was produced that was fully passivated leaving no active donor species, an undoped surface layer was introduced into the model.

Layer	Material
Undoped surface layer	25nm undoped GaAs
Remaining doped cap	15nm $2.5x10^{18}$ Si doped GaAs
Schottky/ Supply Layer	30nm $2.5x10^{18}$ Si doped $Al_{0.3}Ga_{0.7}As$
Spacer	2nm undoped $Al_{0.3}Ga_{0.7}As$
Channel	12nm undoped $In_{0.3}Ga_{0.7}As$
Buffer	1μm undoped GaAs
Substrate	semi-insulating GaAs

Table 6.10
Example of layer structure used for band structure modelling. The original 40 nm cap has been split into 25 nm of undoped material and 15 nm of GaAs with the original doping density.

As the thickness of the undoped surface layer is increased the sheet resistance is seen to increase. The majority of conduction occurs in the channel so an increase in sheet resistance strongly reflects a loss of carriers.

In the experiment sheet resistance was observed to saturate at 1.38 times the initial control value. For the model to produce an increase in sheet resistance of this value an undoped layer with a thickness of 23 nm must be employed (see Figure 6.27).

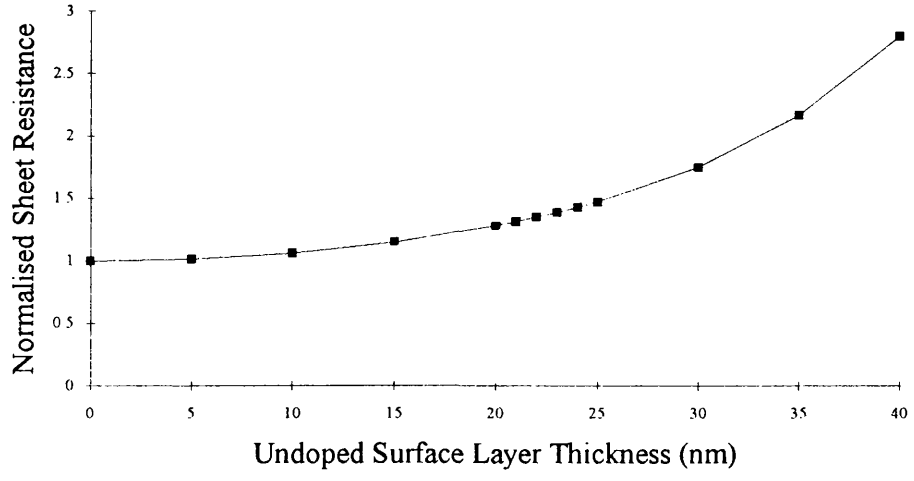

Figure 6.27
Change in sheet resistance with thickness of undoped GaAs surface layer for CAS9.

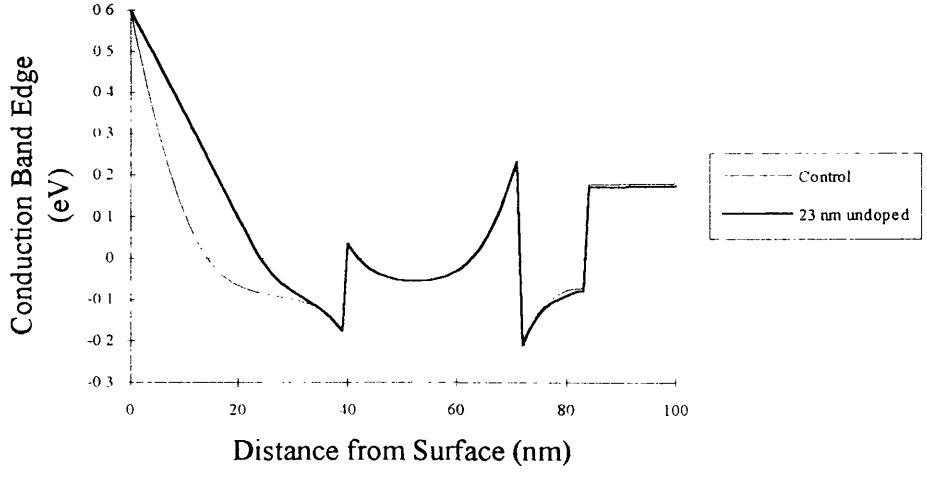

Figure 6.28
Position of conduction band edge relative to Fermi level for CAS9 before hydrogen plasma exposure and with a 23 nm undoped surface layer.

The band structure has been calculated for structures before and after plasma exposure. The presence of the natural surface depletion layer can clearly be seen in the control sample. After exposure to the hydrogen plasma a 23 nm thick undoped layer has been modelled. The electric field due to the surface pinning is found within this undoped layer.

6.7 Van der Pauw Measurements

6.7.1 The Hall Effect and Van der Pauw's Method

The Hall effect is manifest when a conductor carrying a uniform, parallel electric current is placed in a magnetic field. The magnetic field acts upon the charge carriers producing a charge separation orthogonal to the direction of current flow and the magnetic field. The magnitude of the charge separation induced voltage, commonly referred to as the Hall Voltage, V_H is given by;

$$V_H = \frac{B.I}{q.n.t} \qquad \text{(eqn. 6.12)}$$

where B is the magnetic field strength, I the current passed through the layer, q the charge of the current carrier, n the charge density and t the thickness of the epi-layer. The Hall voltage is often written with reference to the Hall Coefficient R_H,

$$V_H = R_H.\frac{B.I}{t} \qquad \text{(eqn. 6.13)}$$

where R_H=1/nq. Knowledge of the Hall coefficient thus yields information on the carrier density, n of the semiconductor. The Hall mobility, μ_H is related to the Hall coefficient through;

$$R_H = \frac{\mu_H}{\rho} \qquad \text{(eqn. 6.14)}$$

where ρ is the sheet resistivity. The sheet resistance R_{SH} is related to the sheet resistivity by

$$R_{SH} = \rho t \qquad \text{(eqn. 6.15)}$$

The Hall method was extended by Van der Pauw [6.39] to cover semi-conductor layers of arbitrary shape and non-uniform current density. Using four ohmic contacts on the periphery of the layer, current is passed between two contacts and the induced voltage measured between the remaining pair yielding values for R_H and ρ. The carrier concentration, Hall mobility and sheet resistance can now be found.

6.7.2 Van der Pauw Measurements on δ-doped HEMT Structures

Raman spectroscopy and TLM measurements have shown that the depletion depth due to hydrogen ion bombardment at a DC bias of -65 V leads to an increase in the surface depletion layer to approximately 25 nm. To try and set an upper bound on the extent to which hydrogen has penetrated the semiconductor Van der Pauw measurements were made upon the pseudomorphic HEMT layer A777, the structure of which is shown in Table 6.11.

This layer structure is particularly sensitive to damage because of the nature of the supply layer. If hydrogen can penetrate as far as the supply layer then conduction will be quickly lost, but if hydrogen is unable to penetrate to the layer no change is conduction will be observed. To increase further the sensitivity the GaAs capping layer was removed using the 'damage-free' $SiCl_4/SiF_4$ etch process. At the

doping level of $1x10^{18}cm^{-3}$ the depletion the cap is fully depleted hence its removal has no effect upon the sheet characteristics. The Schottky contact layer was then exposed to the hydrogen plasma at -65V.

Layer	Material
Cap	20nm $1x10^{18}$ Si doped GaAs
Schottky	25nm undoped $Al_{0.3}Ga_{0.7}As$
Supply	2 monolayers undoped GaAs / $5x10^{12}$ Si δ-doping / 3 monolayers undoped GaAs
Spacer	5nm undoped $Al_{0.3}Ga_{0.7}As$
Channel	10nm undoped $In_{0.3}Ga_{0.7}As$
Buffer	p-doped GaAs
Substrate	GaAS

Table 6.11
A777 material description.

Van der Pauw measurements made after hydrogen plasma exposure show a fall in Hall mobility and carrier concentration leading to a rise in sheet resistance. This degradation of the sheet is however slight.

The slight change to the properties of the sheet show that only a few very energetic hydrogen ions are able to penetrate the through the 25 nm AlGaAs layer and passivate donors. This clearly demonstrates that an upper limit of 25 nm can be set for the penetration of hydrogen ions at a DC bias of -65 V.

H_2 Plasma Time (minutes)	Hall Mobility (cm^2/Vs)	Sheet Concentration (10^{12} cm^{-2})	Sheet Resistance ($\Omega/\square$)
control	6,647	1.83	514.6
0.5	6,655	1.82	516.7
1	6,633	1.81	521.9
3	6,609	1.71	553.4
5	6,551	1.63	586.1

Table 6.12
Material characteristics with H_2 plasma exposure time using a DC bias of -65V.

Bringing together the conclusions drawn about hydrogen passivation of GaAs from Raman Spectroscopy, TLM measurements and Van der Pauw measurements will allow for a more detailed picture of hydrogen penetration and passivation at a DC self bias of -65 V. Both Raman Spectroscopy and the band structure modelling of TLM results use an abrupt transition from passivated to unpassivated material. The transition point is thus at a thickness that has the same effect as the true distribution.

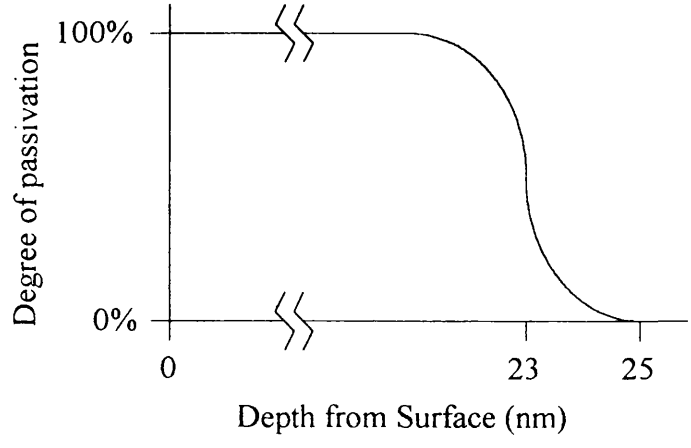

Figure 6.29
Schematic of hydrogen donor passivation with depth.

Van der Pauw data on δ-doped MESFET structures revealed that an upper limit for hydrogen penetration can be set at 25 nm. This represents the limit of deep penetration tail on the passivation curve of Figure 6.29.

6.8 Sidewall Damage to n^+- InGaAs Wires

6.8.1 Conduction of Narrow Wires

The previous sections have considered RIE induced damage to the etch surface only. Damage induced in the exposed sidewalls of an etched feature can be just as important a factor as damage to the etch surface. During an etch the etch surface is subjected to ion bombardment and as we have seen damage is introduced and after a given time will saturate. The sidewalls of features created during the etch are also subjected to ion bombardment. The ions that strike the sidewall may be some of those ions that directly cross the dark space, may have been scattered in the dark space or have been reflected from the etch surface or scattered from the mask. The overall flux of ions to the sidewalls will thus be less than that experienced at the etch surface, the rate of damage introduction will then be lower but because once the sidewall is formed it is ideally no longer etched, damage can build up to its maximum value.

The technique of using narrow conducting wires [6.40] is used to assess the extent of damage to sidewalls etched into InGaAs during methane/hydrogen RIE. At a semiconductor/air interface such as the as-grown wafer surface where no damage is present the natural width of the depletion layer, d_0 is given by eqn. 6.1. As we have seen the introduction of damage will increase the depletion layer thickness. The thickness of the depletion layer at the sidewall, d_S is thus greater than d_0.

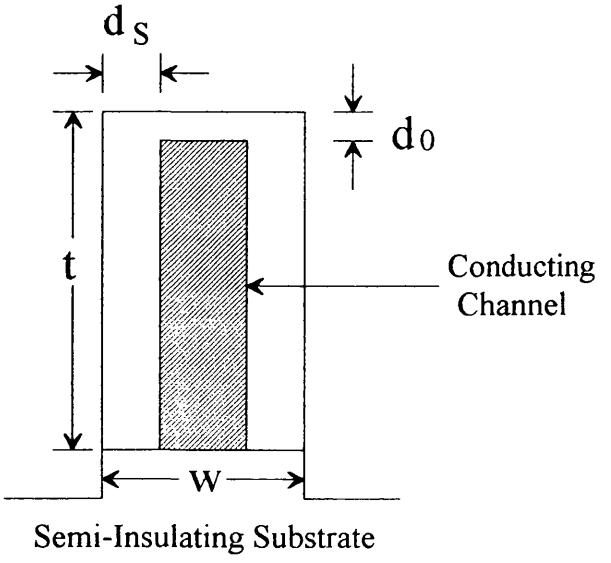

Figure 6.30
Schematic of wire cross-section showing natural surface and the enhanced sidewall surface depletion due to ion bombardment.

A set of etched wires of different widths will have the same sidewall depletion layer thickness. However the conducting core width will follow the overall width of the wire. Reducing the width of the wire will reduce the width of the conducting core reducing the conductance of the wire and when the wire is sufficiently narrow the conducting core will be reduced to zero thickness. The wire width is now equal to twice the sidewall depletion thickness. By extrapolating conductance measurements obtained from a set of wires to the point of zero conductance the sidewall depletion thickness can be found.

To investigate the sidewall damage of InGaAs the conductance of wires fabricated by methane/hydrogen RIE was measured. The wafer consisted of 50 nm $5x10^{18}$ cm^{-3} silicon doped $In_{0.53}Ga_{0.47}As$ / 500 nm undoped $In_{0.52}Al_{0.48}As$ / n+ InP substrate grown by MBE. In design it is only the 50 nm InGaAs epi-layer that

conducts, with the wider band gap InAlAs layer providing a barrier to current transport into the substrate.

6.8.2 Wire Design

The extremely small dimensions of the wires require the use of electron-beam lithography. Three elements are needed in wire fabrication, ohmic contacts, alignment markers and the wire mask itself. To reduce the level of complexity ohmic contacts and alignment markers could be formed using the same lithographic stage and a second lithographic stage used to define the wires. Positioning of the wires is achieved by using a series of alignment markers (20 μm x 20 μm) equally spaced on the perimeter of the overall design. Patterns were generated using the commercial design and simulation program Wavemaker.

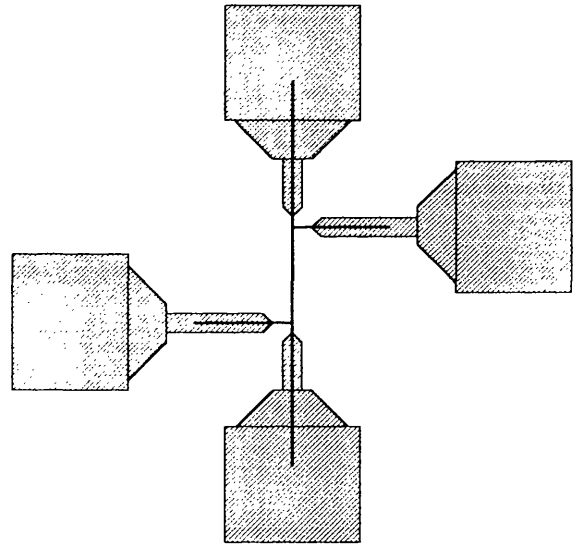

Figure 6.31
Detailed view of wire (heavy line) and ohmic contacts (shaded).

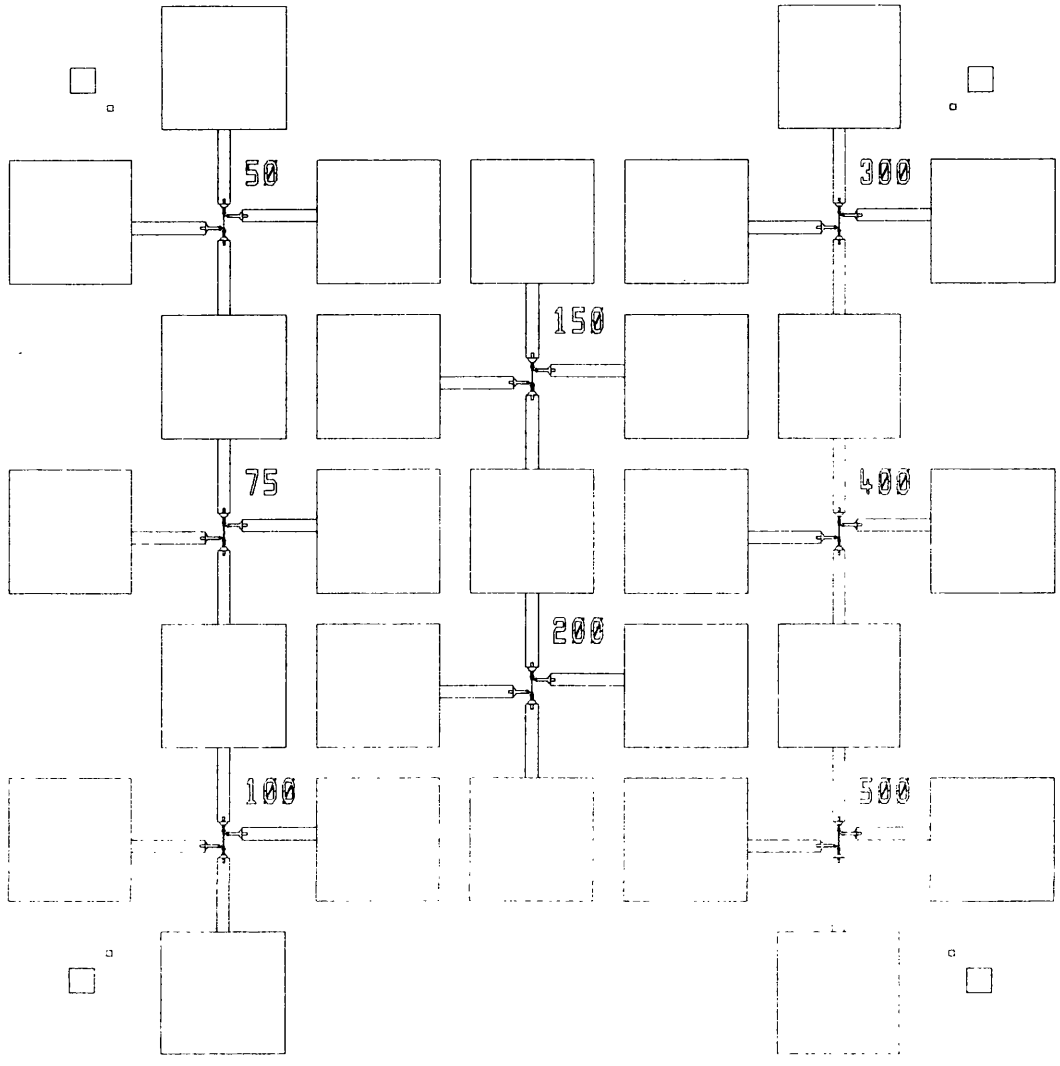

Figure 6.32
Wavemaker design of 8 wires showing alignment markers, ohmic contacts and wires.

6.8.3 Ohmic Contacts

The ohmic contact is the means by which current can be passed through the wire and voltages measured. Two ohmic contact recipes were investigated. The first ohmic contact was 14 nm Au / 14 nm Ge / 14 nm Au / 11 nm Ni / 240 nm Au, the same ohmic contact recipe used in Schottky contact studies of etched AlGaAs. Patterning of the contacts was performed by lift-off in warm acetone. The electron-beam bi-layer resist consisted of 15% BDH in chlorobenzene baked for 4 hours then spun coated with 4% Elv in xylene and baked overnight. The exposure doses at a beam voltage of 50 KV were 300 $\mu C/cm^2$ with a 400 nm spot size for features greater than 1 μm and 400 $\mu C/cm^2$ with a spot size of 160 nm for features less than 1 μm. After the pattern was written development was carried out using 1:1 MIBK:IPA at 23 ^0C for 60 seconds. Once developed the sampled was rinsed with IPA and blown dry with nitrogen.

After ohmic contact fabrication samples were etched removing the highly doped InGaAs epi-layer surrounding the ohmic contacts and etching into the undoped InAlAs buffer. Prior to annealing at 380 ^0C for 60 seconds in the reducing atmosphere inter-contact resistance was extremely high but after annealing considerable conductance between the contacts was observed. It is believed that 'spiking' of the contact allows for connections to be made with the substrate. The implication for the fabrication of InGaAS wires is that there is the possibility of considerable parallel conduction through the substrate that will swamp any conduction through the wire. Micrographs taken of cross-sections through the ohmic contact shows spiking of the ohmic contact into the substrate which being N-doped will provide a low resistance path for parallel conduction.

Another ohmic contact developed specifically for InGaAs HEMTs [6.41, 6.42] was investigated for suitability as a contact for wires. The contact consisted of 10 nm Ni / 50 nm Ge / 80 nm Au with annealing being performed at 340 ^{0}C for 40 seconds in a Rapid Thermal Annealer. To test the ohmic contact the n+ InGaAs epi-layer was removed on both annealed and unannealed samples. Prior to annealing a large inter-contact resistance was found. Little change in the resistance between the ohmic contacts was observed after annealing showing that no contact to the substrate had occurred.

6.8.4 Wire Exposure Tests

The narrow widths of the wires requires the use of a high resolution resist. Again to aid with lift-off a bi-level resist was used. The first layer was 4% BDH in xylene baked at 180 ^{0}C for 5 hours and the second 2.5% Elv in xylene baked over night. Spot size of 15 nm was used to achieve the desired wire widths. The samples were developed in 1:3 MIBK:IPA at 23 ^{0}C for 30 seconds.

Designed Wire Width (nm)	Exposure Dose ($\mu C/cm^2$)
50	950
75	900
100	850
150	800
200	650
300	650
400	500
500	500

Table 6.13
Exposure dose for wires with 15 nm spot size.

6.8.5 Wire Mask Materials

Due to the small widths of the wires needed for this study the resists used only allow for a maximum wire-level mask thickness of 60 nm. This thickness of mask must be able to withstand the high DC bias experienced when etching with methane/hydrogen gas mixtures and after etching the mask must be completely removed to allow accurate measurement of wire width and conductance.

Initial wire-level masks were fabricated using 30 nm NiCr. Although the effectiveness of NiCr to etch deep features with methane/hydrogen and halogenated gas chemistries has previously been demonstrated, problems were experienced when it was attempted to remove the metal. NiCr is normally removed in a solution of HCl with water. After etching with methane/hydrogen, solutions of $HCl:H_2O$ of ratios as high as 1:1 could not remove the mask even after being heated to 50 ^{0}C and agitating in an ultrasonic bath. The wet etch also chemically attacks the ohmic contacts and of the semiconductor surface itself.

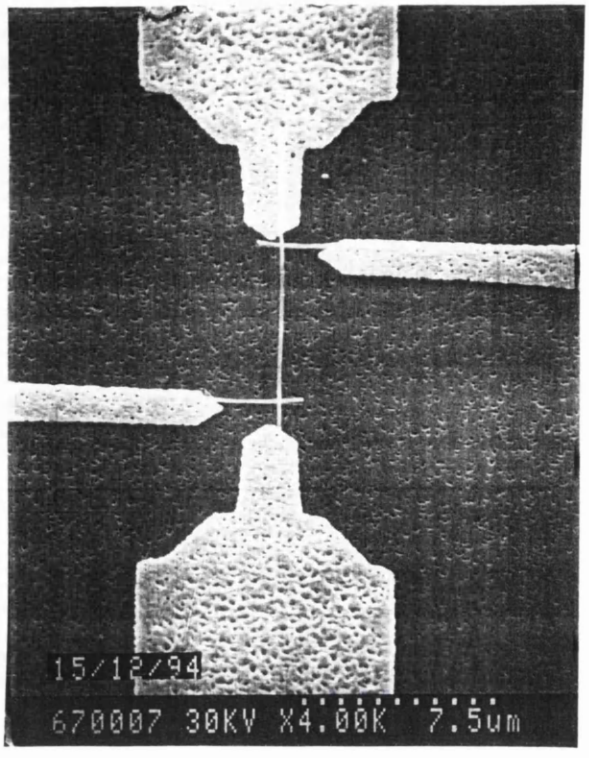

Figure 6.33
Micrograph of post 1 HCl : 1 H_2O etch for wire mask removal

Strontium fluoride (SrF_2) is a masking material that has been used during dry etching with $SiCl_4$ [6.37, 6.43]. The additional benefit of SrF_2 is that it can be readily removed in water or very dilute HCl but is insoluble in organic solvents such as acetone so can be patterned by lift-off. 30 nm SrF_2 was evaporated as the wire-level etch mask. CH_4/H_2 plasmas were however found to sputter all the SrF_2 after only 1 minute.

To exploit the durability of NiCr at high DC biases and the ease with which SrF_2 can be removed, a final wire-level etch mask was fabricated by first depositing 30 nm SrF_2 than 30 nm NiCr. Lift-off was then performed in the normal manner. This bi-level mask structure was found to withstand the high DC bias used to etch with

methane/hydrogen gas mixtures and then could easily be removed by rinsing with 1:20 $HCl:H_2O$ for 3 minutes which etches the SrF_2 allowing the NiCr to float-off.

6.8.6 Conductance Measurements of Etched Wires

The conductance of etched wires was established using a four point probe technique with the Hewlett Packard 4154B semiconductor parameter analyser. This technique allows for current source and voltage measurement to be separated so minimising measurement errors due to cable resistance. The probes of the analyser, simultaneous measurement units (SMU) are either designated as current sources or voltage probes.

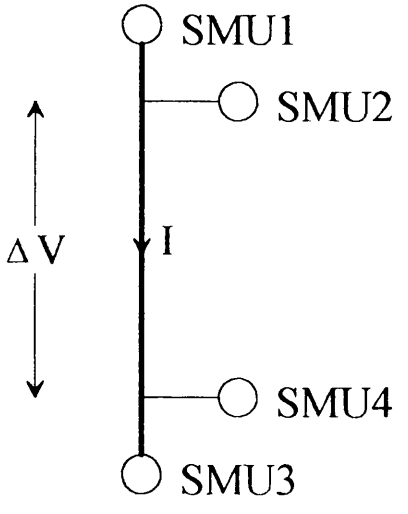

Figure 6.34
Schematic of wire measurement technique.

The conductance of the wire, G is related to the dimensions of the conducting core and the conductivity, σ of the material by

$$G = \sigma \frac{(w-2d_S)(t-d_0)}{l} \qquad \text{(eqn. 6.16)}$$

where w is the width of the wire, t the InGaAs epi-layer thickness and d_s and d_0 the width of the depletion layer at the sidewall and the top surface of the wire. The conductivity can be expressed as

$$\sigma = ne\mu \qquad \text{(eqn. 6.17)}$$

with n the free carrier concentration, e the electronic charge and μ the carrier mobility. Equation 6.15 can be written in terms of the sheet resistance, R_{SH}

$$G = \frac{w-2d_S}{R_{SH}.l} \qquad \text{(eqn. 6.18)}$$

$$R_{SH} = \frac{1}{ne\mu(t-d_0)} \qquad \text{(eqn. 6.19)}$$

A full description of the wire can now be calculated. Assuming a free carrier concentration of 5+/-0.3x10^{18} cm^{-3} the wires show an average sheet resistance of 58.58+/-0.89 Ω/□ and electron mobility of 5008+/-76 cm^2/Vs. As an independent check, n and μ may be found using Van der Pauw measurements.

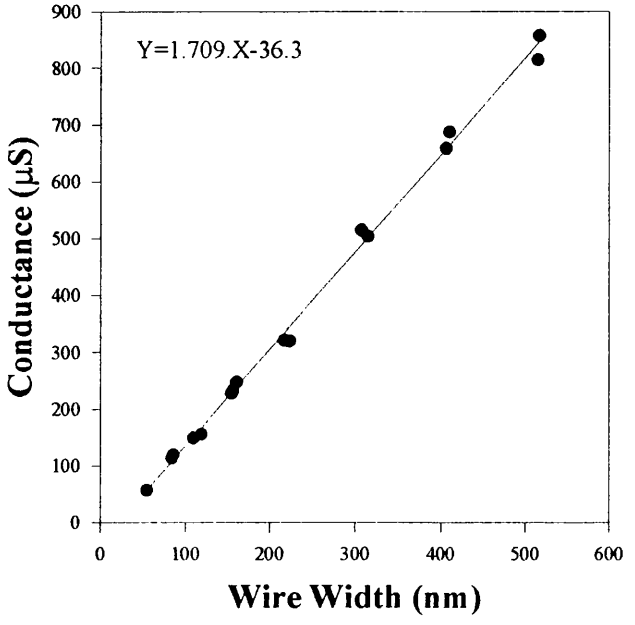

Figure 6.35
Conductance vs width for InGaAS wires.

Utilising a linear fit to the data of wire width verses conductance, then extrapolating to the point of zero conductance yields a width of 21.0+/-4.4 nm. This figure represents twice the sidewall depletion thickness thus a single depletion layer thickness is 10.5+/-2.2 nm.

The natural depletion thickness, d_0 can be obtained using eqn. 6.1. For InGaAs values for e_r=14+/-0.5, N_D-N_A=5+/-0.3x10^{18} cm^{-3} and V_b=0.2+/-0.02eV [6.44]. yield a depletion width of 7.4+/-0.9 nm. The effect of etching the wire and then annealing at 340 ^{0}C for 40 seconds is to introduce damage so as to increase the depletion width to 10.5+/-2.2 nm.

6.9 Chapter Summary

In this chapter the extent to which a semiconductor is damaged by the RIE process has been investigated. Under the same conditions used to establish etch rates of $Al_{0.3}Ga_{0.7}As$ Schottky contact studies were undertaken. After etching, ideality factors and reverse breakdown voltages were observed to rise but the barrier heights were lowered. The change to Schottky barrier characteristics were less at high powers where etching is more rapid and already damaged material is removed giving the impression that the potential for damage is less. Annealing the etched sample prior to contact metalisation allows hydrogen to diffuse out of the sample reactivating the donor species. Overall the etch is seen to lead to an increase in depletion layer thickness, introduction of additional surface states that lower the pinning of the Fermi-level reducing the barrier height and also an enhancement of recombination processes within the depletion layer.

$In_{0.53}Ga_{0.47}As$ was the second material in which damage was investigated but because of the low Schottky barrier height, other methods of surface damage determination were needed. Two approaches were taken: by analogy with the GaAs/AlGaAs materials and by the use of contactless, non-destructive methods on InGaAs itself.

Raman spectroscopy of hydrogen etched $4.4x10^{18}$ cm^{-3} GaAs indicates that by raising the dc self bias and hence hydrogen ion energy the ions penetrate further into the lattice, passivating donors to a greater depth and increasing depletion layer thickness. Using a bias voltage of -65 V the depletion layer was 25.2 nm thick. Adding methane results in etching of the surface, removal of depleted material and so a thinner depletion layer.

Using the Transmission Line Model, sheet resistance of a GaAs/AlGaAs layer structure saturated when exposed to a hydrogen plasma, with dc bias of -65 V, for 5 minutes. Modelling the band structure and calculating sheet resistance revealed that for the observed experimental change in sheet resistance, a depletion layer 23 nm thick must be evoked. Removing the GaAs capping layer and exposing the AlGaAs donor layer to the plasma resulted in a rapid rise in sheet resistance indicating that all the donors had been passivated. Van der Pauw measurements on another GaAs/AlGaAs layer structure showed that a d-doped donor layer under a 25 nm GaAs cap was only marginally effected by the -65 V bias plasma. The VDP measurements indicated that only a few hydrogen ions can penetrate 25 nm into GaAs. If InGaAs can be treaqted as a GaAs-like material we could estaimate that etch-induced damage should be of the same nature and extent.

Three non-destructive methods were used to investigate surface damage in InGaAs. Raman spectroscopy of $5x10^{18}$ cm^{-3} InGaAs was complicated due to scattering form the GaAs and InAs parts of the alloy. Upon etching one would expect the LO phonon peak to decrease in intensity relative to L_1 as donors were passivated and the depletion layer increased in thickness. However the most noticable change was the decrease in the GaAs-like LO phonon. Photoluminescence of InGaAs revealed that in the unetched material only the peak associated with the bound exciton was observable. After etching another luminescence peak was observed and likened to a surface InAs quantum well. PL indicates that a stiochiometry change at the etch surface may be responsible for the strange results form Raman spectroscopy.

To detect stiochiometrical changes at the surface X-ray Photoelectron Spectroscopy was employed. After etching the surface was enriched in both group III elements (In and Ga) at the expense of As. The surface was formed of a greater concentration of In than Ga and would seem to verify the InAs surface quantum well theory used to explain the PL data. The etch was also responsible for a increase in

the oxidation of all elements at the surface, either during the etch or by enhancing the surface reactivity to the atmosphere.

The damage to the sidewalls of etched features may also be an important for device fabrication. By etching a set of narrow wires into InGaAs this damage was estimated. Etching at 75 W and annealing the wires at 340 ^{o}C lead to the increase in depletion layer thickness from 7.4 to 10.5 nm.

References

[6.1] S.J. Pearton, W.C. Dautremont-Smith, J. Chevallier, C.W. Tu and K.D. Cummings, "Hydrogenation of shallow-donor levels in GaAs", *J. Appl. Phys.*, 1986, **59,** pp.2823-2827

[6.2] R. Cheung, S. Thoms, I. McIntyre, C.D.W. Wilkinson and S.P. Beaumont, "Passivation of donors in electron beam lithographically defined nanostructures after methane/hydrogen reactive ion etching", *J.Vac. Sci.Technol.*, 1988, **B6,** pp.1911-1915

[6.3] N.I. Cameron, S.P. Beaumont, C.D.W. Wilkinson, N.P. Johnson, A.H. Kean and C.R. Stanley, "An investigation of CH_4/H_2 reactive ion etching damage to thin heavily doped GaAs metal-semiconductor field effect transistor layers during gate recessing", *J. Vac. Sci. Technol.*, 1990, **B8,** pp.1966-1969

[6.4] P. Collot and C. Gaonach, "Electrical damage in n-GaAs due to methane-hydrogen RIE", *Semicond. Sci. Technol.*, 1990, **5,** pp.237-241

[6.5] J.C. Nabity, M. Stavola, J. Lopata, W.C. Dautremont-Smith, C.W. Tu and S.J. Pearton, "Passivation of Si domors and DX centres in AlGaAs by hydrogen plasma exposure", *Appl. Phys. Lett.*, 1987, **50,** pp.921-923

[6.6] S.J. Pearton, U.K. Chakrabarti and F.A. Baiocchi, "Electrical and structural changes in the near surface of reactively ion etched InP", *Appl. Phys. Lett.*, 1989, **50,** pp.1633-1635

[6.7] J. Singh, "Reactive ion etching of zinc doped InP using methane and hydrogen: Assessment of the degree and extent of changes in surface carrier concentration", *J. Appl. Phys.*, 1990, **68,** pp.5383-5384

[6.8] V.J. Law, S.G. Ingram, G.A.C. Jones, R.C. Grimwood and H. Royal, "CH_4:H_2:Ar rf/ECR plasma etching of GaAs and InP", *Mat. Res. Soc. Symp. Proc.*, 1991, **223,** pp. 191-196

[6.9] S.J. Pearton, U.K. Chabrabarti, A. Katz, A.P. Perley, W.S. Hobson and C. Constantine, "Comaprison of CH_4/H_2/Ar reactive ion etching and electron clyclotron resonance plasma etching of In-based III-V alloys", *J. Vac. Sci. Technol.*, 1991, **B9,** pp.1421-1432

[6.10] M. Rahman, M.A. Foad, S. Hicks, M.C. Holland and C.D.W. Wilkinson, "Defect penetration during the plasma etching of semiconductors", *Mat. Res. Soc. Symp. Proc.*, 1993, **279,** pp.775-780

[6.11] D.L. Green, E.L. Hu, P.M. Petroff, V. Liberman, M. Nooney and R. Martin, "Characterisation of low-energy ion-induced damage using the multiple-quantum-well probe technique with a intervening superlattice", *J. Vac. Sci. Technol.*, 1993, **B11,** pp.2249-2253

[6.12] W.J. Rao, S. Phulkar and P.B. Sinha, "Fermi level pinning and chemical interactions at metal/metal organc CVD grown GaAs interfaces: Schottky barrier height", *Thin Solid Films,* 1988, **164,** pp.21-25

[6.13] J.S. Best, "The Schottky-barrier height of Au on *n*-$Ga_{1-x}Al_xAs$ as a function of AlAs content", *Appl. Phys. Lett.*, 1979, **34,** pp.522-524

[6.14] A. Chandra, C.E.G. Wood, D.W. Woodard and L.F. Eastman, "Surface and Interface depletion corrections to free carrier-density determinations by Hall measurements", *Solid State Electronics,* 1979, **22,** pp.645-650

[6.15] E.H. Rhoderick and R.H. Williams "Metal-Semiconductor Contacts" Clarendon Press, Oxford (1988)

[6.16] W. Patrick, W.S. Mackie, S.P. Beaumont and C.D.W. Wilkinson, "Low-temperature annealed contacts to very thin GaAs epilayers", *Appl. Phys. Lett.* 1986, **48** (15) pp.986-988

[6.17] H. Shen, F.H. Pollak and R.N. Sacks, "Raman scattering determination of free-carrier concentration and surface space-charge layer in <100> *n*-GaAs", *Appl. Phys. Lett.*, 1985, **47,** pp.891-893

[6.18] D. Kirillov, C.B. Cooper and R.A. Powell, "Raman scattering study of plasma etching damage in GaAs", *J. Vac. Sci. Technol.*, 1986, **B4,** pp.1316-1318

[6.19] M. Watt, C.M. Sotomayor-Torres, R. Cheung, C.D.W. Wilkinson, H.E.G. Arnot and S.P. Beaumont, "Raman scattering of reactive-ion etched GaAs", *J. Mod. Opt.*, 1988, **35,** pp.365-370

[6.20] P.D. Wang, M.A. Foad, C.M. Sotomayor-Torres, S. Thoms, M. Watt, R. Cheung, C.D.W. Wilkinson and S.P. Beaumont, "Raman scattering of coupled longitudinal optical phonon-plasmon modes in dry etched n^+-GaAs", *J. Appl. Phys.*, 1992, **71,** pp.3754-3759

[6.21] A. Pinczik, A.A. Ballman, R.E. Nahory, M.A. Pollack and J.M. Worlock, "Raman scattering studies of surface space charge layers and Schottky barrier formation in InP", *J. Vac. Sci. Technol.*, 1979, **16,** pp.1168-1170

[6.22] J.E. Maslar, S.R. Kisting, P.W. Bohn, I. Adesida, D.G. Ballegeer, C. Caneau and R. Bhat, "Disorder-induced allowed-forbidden phonon splitting in ion-etched epitaxial InP", *Phys. Rev B,* 1992, **46,** pp.1820-1822

[6.23] G. Abstreiter, E. Bauser, A. Fischer and K. Ploog, "Raman spectroscopy-a versatile tool for the characterisation of thin films and hetrostructures of GaAs and $Al_xGa_{1-x}As$", *Appl. Phys.*, 1978, **16,** pp.345-352

[6.24] J.L. Shen, I.M. Chang, Y.M. Shu, Y.F. Chen, S.Z. Chang and S.C. Lee, "Raman-line-shape study of $In_xGa_{1-x}AS$ on InP and GaAs substrates", *Phys. Rev. B,* 1994, **50,** pp.1678-1683

[6.25] A. Mooradin and G.B. Wright, "First order Raman effect in III-V compounds", *Solid State Comm.*, 1966, **4,** pp.431-434

[6.26] R. Carles, N. Saint-Cricq, J.B. Renucci, M.A. Renucci and A. Zwick, "Second order Raman scattering in InAs", *Phys. Rev. B,* 1980, **22,** pp. 4804-4815 (1980)

[6.27] S. Emura, S. Gonda, Y. Matsui and H. Hayashi, "Internal-stress effects on Raman spectra of $In_xGa_{1-x}As$ on InP", *Phys. Rev. B,* 1988, **38,** pp.3280-3286

[6.28] H. Shen, F.H. Pollak and R.N. Sacks, "Raman scattering determination of free-carrier concentration and surface space-charge layer in <100> *n*-GaAs", *Appl. Phys. Lett.* **47** pp. 891-893 (1985)

[6.29] Bassignana, C.J. Miner and N. Puetz, "Photoluminescence and double-crystal x-ray study of InGaAs/InP: Effect of mismatch strain on band gap", *J. Appl. Phys.*, 1989, **65,** pp 4299-4305

[6.30] G. Wicks, C.E.C. Wood, H. Ohno and L.F. Eastman, "Optical quality GaInAs grown by molecular-beam epitaxy", *J. Elec. Mat.*, 1982, **11,** pp. 435-440

[6.31] M. McElhinney
PhD Thesis, University of Glasgow (1994)

[6.32] Z. Sobierieski, S.A. Clark, R.H. Williams, A. Tabata, T. Benyattou, G. Guillet, M. Gendry, G. Hollinger and P. Viktorovitch, "Inverstigation of photoluminescence from InAs surface quantum wells grown on InP(100) by molecular beam epitaxy", *Appl. Phys. Lett.*, 1991, **58**, pp.1863-1865

[6.33] R. McLeod
PhD Thesis, University of Glasgow (1993)

[6.34] T.R. Hayes, U.K. Chakrabarti, F.A. Baiocchi, A.B. Emerson, H.S. Luftman and W.C. Dautremont-Smith, "Damage to InP and InGaAsP surfaces resulting from CH_4/H_2 reactive ion etching", *J. Appl. Phys.*, 1990, **68,** pp.785-792

[6.35] G.K. Reeves and H.B. Harrison, "Obtaining the specific contact resistance from transmission line model measurements", *IEEE Electron Device Letts.*, 1982, **3,** pp.111-113

[6.36] D.C. Look
"Characterisation of GaAs devices" John Wiley (1989)

[6.37] S.K. Murad, C.D.W. Wilkinson and S.P. Beaumont, "Selective and nonselective RIE of GaAs and $Al_xGa_{1-x}As$ in $SiCl_4$ plasma", *Microelectronic Engineering*, 1994, **23,** pp.357-360

[6.38] The 1-dimensional Poisson/Schrodinger program was developed by G. Snider,
Department of Applied and Engineering Physics, Cornell University

[6.39] L.J. Van der Pauw, "A method of measuring the resistivity and Hall coefficient on lamellae of arbitary shape", *Philips Tech. Rev.*, 1958, **20,** pp.220-224

[6.40] S. Thoms, S.P. Beaumont, C.D.W. Wilkinson, J. Frost and C.R. Stanley, "Ultrasmall device fabrication using dry etching of GaAs", *Microelectronic Engineering 86* , 1986, Chp. 61, pp.249-256

[6.41] B.U.H. Klepser, C. Bergamaschi, W. Patrick and M. Beck, "Comparison and optimisation of different ohmic contact metalisations for InP-HEMT structures with doped and undoped cap-layers", *Proc. 6th Int. Conf. on InP and Related Materials*, 1994

[6.42] N.I. Cameron
Private Communication

[6.43] Y.P Song, P.D. Wang, C.M. Sotomayor-Torres and C.D.W. Wilkinson, "Magnetically confined plasma rective ion etching of GaAs/AlGaAs/AlAs quantum nano-structures", *J. Vac. Sci. Technol.*, 1994, **B12,** pp.3388-3392

[6.44] K. Kajima, Y. Mizushima and S. Sakata, "Schottky barrier height of n-$In_xGa_{1-x}As$ diodes", *Appl. Phys. Lett.*, 1973, **23,** pp.458-459

Chapter 7

Conclusions and Future Work

Chapter outline

The results presented within this thesis are summarised and conclusions drawn. Possible routes for continuation of this work are discussed and new techniques that are needed to further understanding of this subject introduced.

7.1 Instrumentation and process monitoring

The ability of the user to monitor the condition of the etch and its progress can greatly enhance device yield. The improvement is due to more accurate determination of the etch stop (compared to simply timing the etch) or tighter control of the environment that the etch takes place in i.e. control of air leaks into the chamber and deposits on the chamber walls.

A model based on the high frequency transmission line was developed to calculate the theoretical reflectance from the upper surface of a multiple layer structure as the etch front progresses through the layers. Experimental results have shown that the reflectance from multiple quantum well structures comprising 5.7 nm GaAs / 8.1 nm $In_{0.23}Ga_{0.67}As$ are clearly resolvable even though their refractive indices at the illuminating wavelength of 679 nm are similar at 3.81+j0.17 and 3.83+j0.21 respectively. The ability to "count" the layers during the etch has allowed the fabrication of S-SEEDs with high tolerance end-point detection.

The combination of attenuation coefficient and layer thickness may result in no penetration of the illuminating light to the underlying layers and hence no interference. Under such circumstances it becomes impossible to establish the exact position of the etch surface within that layer and only at an interface where an abrupt change to the reflectance signal can be observed is the position of the etch surface known exactly. The use of another illuminating wavelength with lower attenuation or longer wavelength would allow the underlying layers to be "seen" and a more accurate determination of the etch surface position would become possible. Further work using a range of illuminating wavelengths or preferably a dual beam reflectometer would allow both accurate position determination within thick layers

using the low attenuation wavelength and also within structures such as quantum wells where a high attenuation is beneficial.

Optical emission spectroscopy has been used to investigate the plasma state but little information could be gained about the precise conditions of the methane/hyrogen etch process. The spectra is dominated by molecular hydrogen (as would be expected considering the majority of the gas in the chamber is hydrogen) with atomic hydrogen and CH lines also present. Increasing the methane content of the gas mixture leads to an increase in the emission intensity of the CH species a cracking product of methane. The low emission intensities of species such as CH_2 and CH_3 prevent these species from being detected. Low etch rates for the materials investigated coupled with the small sample size does not allow for etch products to be observed. The use of larger samples (quarter 2" wafer and upwards) may produce a high enough concentration of etch products in the plasma to allow their observation.

The state of the reactor chamber can play an important role in the onset of polymer deposition onto the etch surface. When the chamber is clean and free from polymer deposition itself the chamber acts as a sink for excess polymer from within the plasma. On becoming heavily coated, the chamber can then become a source for polymer adding to the total flux to the etch surface. The polymer point may then be reached and etching halted. To prevent the uncertainty of how the chamber will effect the etch process a rigorous cleaning procedure has been implemented. Before an etch takes place the chamber is cleaned with an oxygen plasma. The oxygen reacts with the polymer forming the products CO and CO_2 which are volatile and can be pumped away. Monitoring of emission lines form these species by OES reveals that the direct ion bombardment of the cathode aids the cleaning process. The cathode is thus removed of its polymer coating first with the sidewalls of the chamber cleaned more slowly by the scattering of reactive oxygen out of the plasma. OES can detect

the point at which the relevant emission lines fall to a background level and the chamber declared fully cleaned of polymer.

Residual oxygen in the chamber may react with aluminium within the semiconductor forming the highly involatile aluminium oxides which can prevent etching. A hydrogen plasma is thus used to remove any remaining oxygen. Again OES may be used to monitor the state of species within the plasma. Reaction of hydrogen with oxygen can form the OH molecule. Again when emission from this species has fallen to a background level the chamber can be said to have been cleaned of oxygen.

The recent purchase of a quadrupole plasma probe capable of residual gas analysis (RGA) and ion detection will allow more detailed observations of species present within the plasma and their relative abundances. The ability of the instrument to detect product species that would normally be unobservable with OES may yield a complementary technique to laser reflectometry for end-point detection. Product species are collected from all sites on the etched sample making layer thickness variations crucial to the accuracy of this method.

7.2 RIE with methane and hydrogen

The methane/hydrogen etch chemistry is compatible with photoresist and electron beam resist at lower rf powers where sputtering of the organic material and substrate heating are minimal. At higher powers the resist may be degraded and lead to poor pattern transfer. Dielectric masks have been used but they too can be sputtered at higher powers. 100 nm thick titanium, nickel or nichrome metal masks

have proved to be very resilient at high power, providing excellent pattern transfer but are difficult to remove after the etch.

The etch rates of the ternary semiconductors $Al_{0.3}Ga_{0.7}As$, $In_{0.53}Ga_{0.47}As$ and $In_{0.52}Al_{0.48}As$ have been investigated over a range of rf power and with a variety of mixtures of the methane/ hydrogen etch gas. All three materials show broadly similar trends. As the methane content of the etch gas mixture is increased, the availability of methane related reactant species increases raising the etch rate. The competing process of polymer deposition onto the etch surface can dominate when the methane content of the gas mixture becomes too high. Polymer is then deposited onto the etch surface preventing etching taking place.

The precise set of circumstances for the onset of polymer deposition is related to the material being etched and the condition of the etch chamber. Aluminium containing materials suffer this deposition with lower amounts of methane in the gas mixture for all rf powers. These materials will also etch at a slower rate than non-aluminium containing semiconductors under the same conditions. The lower polymer point and slower etch rates of these aluminium containing materials is probably due to the lower volatility of aluminium etch products than gallium etch products. Increasing the applied rf power allows gas mixtures richer in methane to be used with enhanced etch rates but the greater DC bias created leads to greater penetration of damage. The increased rf power brings extra energy to the etch surface raising reaction rates. The higher power also increases the ion flux, generating more sputtering of polymers thus raising the polymer point. Use may be made of the lower polymer point of the aluminium semiconductors. Etching of GaAs or InGaAs using conditions below their own respective polymer points but beyond the polymer point of AlGaAs or InAlAs will allow for the upper GaAs or InGaAs layer to be etched but on exposing the underlying AlGaAs or InAlAs layer polymer deposition will occur halting the etch. A

selective etch process has thus been identified. The selectivity of InGaAs over InAlAs under identical conditions ranges from 3 to 5:1 below the polymer point with no strong relation to the rf power but with the higher selectivities with more methane rich gas mixtures.

Ideally when using an etch stop with a highly selective process one does not want deposition onto the etch surface as this deposit must be removed, so would not be suitable for self-aligned processes that use photoresist or PMMA. The addition of a gas to the methane/ hydrogen gas mixture should be investigated in the hope of improving selectivity without deposition. Fluorinated compounds such as SF_6 or CF_4 will form the highly involatile aluminium fluorides which may prevent etching and lead to high selectivity.

Induction times of around 30 seconds have been observed for methane/ hydrogen etching on GaAs or InGaAs capped layers. If there is no cap and the semiconducting layer contains aluminium then the aluminium will oxidise in the atmosphere. These oxides are highly involatile and can prevent etching. Etching of the unoxidised semiconductor can only start when the surface oxides have been removed by sputtering, thus making it difficult to know the start of the etch.

The cross-sectional profile formed under the mask as well as the absolute and relative etch rates of semiconducting materials are important quantities for fabrication of devices. It has been shown that both AlGaAs and InAlAs produce overcut etch profiles. The formation of a passivating layer upon the sidewall (most probably oxides of aluminium formed form residual oxygen within the chamber that can never be truly removed) will force out the base of the wall creating the overcut profile. Both materials show more vertical wall profiles as the etch rate is increased by either increasing the methane content of the etch gas mixture or by increasing the rf power.

The etch profiles obtained for InGaAs are vertical for all rf powers using a 4% mixture of methane in hydrogen. Increasing the methane content leads to the undercutting of the etch mask by reactive ions scattered from the etch surface. The increase in rf power which creates more methyl radicals leads to a greater flux to the etch surface hence greater scattering. The amount of undercut is seen to rise with rf power for all gas mixtures with greater than 4% methane.

The use of ethane and higher hydrocarbons in preference to methane should be expected. With a higher potential to supply reactant species for a given flow rate of etch gas improvements in etch rate may be experienced over methane. These gases however contain more carbon than methane so particular attention must be made to polymer points, chamber cleanliness and how additional gases may benefit the etch.

7.3 Fabrication of S-SEEDs

Fabrication of many types of optoelectronic device requires good verticality of the etch wall to minimise scattering losses. S-SEEDs have been fabricated using the 4% methane mixture producing vertical walls with etch surface smoothness <10 nm after etching to a depth of 1.5 μm. Because of the low methane content etch rates are low and etch times naturally long even using the highest rf power (200 W) available. The high ion energy (implying high sputter rates) and heating of the substrate rule out photoresist masks although photoresist can be used quite adequately for shorter etch times at lower DC self bias. Metal or metal-on-polymer masks have therefore been used. A thick >1 μm layer of polyimide is patterned with Ti/Ni/Au which forms a hard, low stress metal mask that readily adheres to polyimide and can be cleanly patterned by conventional lithography. The polyimide acts as both a planarisation layer and allows easy removal of the metal mask after etching. This

masking technology could be readily transferred to other problems where planarisation or removal of a hard mask is required.

The bi-level mask of NiCr on strontium fluoride was used. After etching the SrF_2 acts as a sacrificial layer which can be removed in very dilute HCl solutions allowing the NiCr to float free. Without the SrF_2 layer the NiCr mask could only be removed using concentrated HCl causing damage to the surface of the semiconductor, reducing the quality of the subsequently deposited mirrors.

7.4 Addition of O_2 or Cl_2 to the CH_4/H_2 plasma

Etching InGaAs with high methane content mixtures gives higher etch rates but with undercutting of the mask. By adding other gases to the methane/hydrogen mixture etch rates can be maintained or improved upon but with a reduction in the undercutting of the etch mask. For these experiments metal masks were used to overcome photoresist etching.

The addition of oxygen (the exact amount depends upon the methane to hydrogen ratio of the gas mixture used) improves wall verticality in InGaAs and enhances etch rates. The role of oxygen is two-fold. The oxygen can react with polymer or polymer precursors on the etch surface or in the plasma reducing the amount of polymer deposited on the mask or transported to the etch surface. Reduction of polymer on the mask prevents the sideways growth of polymer that can in effect act as a growing mask shadowing the etch surface directly underneath forcing out the foot of the sidewall. Lowering the transport of polymer to the etch surface removes the inhibiting influence of these species allowing the etch to proceed at a greater rate (up to 60% higher when 1.5 sccm O_2 are added to 5 sccm CH_4, 20

sccm H_2 at 75 W, 20 millitorr), moving the polymer point to higher methane contents allowing more methane to be incorporated into the gas mixture to further enhance etch rates. The second role of oxygen is to form a possible sidewall passivation layer that protects the sidewall from etching by scattered reactant species.

Adding chlorine to the methane/hydrogen gas mixture can also aid in the improvement of wall verticality and etch rate. The most probable role that chlorine plays is as a sputtering agent removing polymer growth from the mask and etch surface. Profiles are immediately more vertical and etching occurs at a higher rate. No undercutting of the original mask was observed indicating again that a passivating layer may be formed on the sidewalls in a similar way to oxygen. Chlorine ions are massive and when at a shallow angle of incidence with the sidewall can be reflected and cause trenching at the bottom of the wall.

To fully understand how the addition of oxygen or chlorine to the gas mixture brings about the improvements in wall verticality surface analytical techniques such as XPS should be employed. Problems may arise due to the difficulty of fabricating suitable structures and arranging for measurements to be taken on sidewalls.

7.5 RIE induced damage

Ideally the electrical and optical properties of the etched semiconductor should not change from those of the unetched material. Ion bombardment, chemical reactions at the surface and penetration of hydrogen into the lattice lead to damage altering the characteristics of the semiconductor at and near to the surface. Several techniques have been used to investigate damage to GaAs, AlGaAs and InGaAs.

Schottky contacts were formed on $3x10^{17}$ cm^{-3} $Al_{0.3}Ga_{0.7}As$ that had been etched with 6 sccm CH_4, 19 sccm H_2 at 20 millitorr pressure for 5 minutes. The contacts were formed upon as-etched or annealed samples etched over a range of rf powers. Measurements of the Schottky contact characteristics yielded qualitative information on the modification to the near surface.

Barrier heights were lower than the control for the as-etched samples but recovered to very near the control value upon annealing. The reverse breakdown occurred at greater biases for both as-etched and annealed samples but the bias at breakdown was greater with the etched samples. Measurements of the ideality factor could only be achieved once the sample had been annealed. Pooling these results reveals that etching creates more surface states lowering the surface pinning. The introduction of hydrogen into the lattice is greater with the higher DC bias and hence ion energy at higher rf power resulting in a greater surface depletion depth and enhanced reverse breakdown voltages. At higher rf powers etching is faster so more damaged material is being removed by the etch than at low rf power. The ideality factor a measure of the number density of surface recombination centres thus falls to near the control value as the power is increased for the annealed samples. Annealing the etched samples results in changes to all three measured parameters with their values moving towards those of the control sample. The anneal removes hydrogen from within the lattice reactivating donors and may help in the reconstruction of the etched surface.

Raman spectroscopy of $4.4x10^{18}$ cm^{-3} GaAs reveals that the surface depletion depth increases from 13.7 nm in the as-grown material to 25.2 nm when exposed to a hydrogen plasma with a DC bias of -65 V and further to 54.6 nm with a DC bias of -1000 V. The increased ion energy will allow deeper penetration of hydrogen ions into the lattice and hence passivation of donor atoms will occur at these greater depths forming a larger depletion layer. If methane is added to the plasma etching in

initiated and with a DC bias of -1000 V the depletion layer formed is 41.6 nm thick. Etching will remove already passivated material from the GaAs surface not allowing the hydrogen to build up to the same extent and so a narrower depletion layer is formed.

TLM and Van der Pauw studies on GaAs/$Al_{0.3}Ga_{0.7}$/$In_{0.3}Ga_{0.7}As$ pseudomorphic HEMT structures set an upper limit for hydrogen ion penetration to 25 nm at a DC bias of -65 V. If it can be arranged for the donor layer the lie at least 25 nm under the etch stop layer then methane/hydrogen based selective RIE processes (e.g. $CH_4/H_2/SF_6$) could be used for gate recessing at a DC bias of -65 V without significant carrier loss. The need for such a selective etch has already been discussed and once demonstrated should be used to fabricate HEMT structures and establish the feasibility of the process for HEMT structures based on InGaAs/InAlAs/InP.

Raman spectroscopy has also been performed on $5x10^{18}$ cm^{-3} $In_{0.53}Ga_{0.47}As$. Because the material is an alloy of InAs and GaAs an LO phonon and a phonon-plasmon scattering mode are observed for each of the constituents of the alloy. Upon etching the ratio of the InAs-like peaks remains constant but the GaAs-like LO phonon decreases in intensity relative to the phonon-plasmon mode. In the light of the results for hydrogenation of GaAs this would suggest a narrowing of the depletion layer, not the increase that would be expected. Photoluminescence form the etched $In_{0.53}Ga_{0.47}As$ surface show an additional peak at 0.776 eV, to the single bound-exciton peak (0.807 eV) of the unetched material. This second peak has been identified with luminescence form InAs surface quantum wells on thick $In_{0.53}Ga_{0.47}As$ epi-layers. The lowering of the GaAs-like LO phonon peak may therefore be due to a decrease in the amount of gallium at the etch surface.

The elemental surface compositions of as-grown and methane/hydrogen etched $In_{0.53}Ga_{0.47}As$ have been established by x-ray photoelectron spectroscopy. In the as-grown material there is nearly equal amounts of indium, gallium and arsenic. Upon etching, of these three elements using a take-off angle of 0^0 the amount of arsenic remains at approximately 34% but the indium content can rise to 54% and gallium fall to 12%. The outer most layers of the surface show less arsenic and more gallium. This surface is also heavily oxidised. XPS has thus confirmed that the surface becomes rich in indium during the etch with the surface behaving in a similar manner to an InAs surface quantum well.

The enrichment of the surface with indium is due to the low volatility of the indium etch products relative to the products of gallium. During the etch trimethylgallium will readily desorb form the surface leaving behind an increasingly indium rich surface. If the etch conditions are far from ideal indium droplets may form. The vapour pressures of trimethylaluminium and trimethylgallium also differ and XPS should be used to establish the state of the etch surface of AlGaAs after methane/hydrogen RIE. Compositional changes of the surface may be responsible for the change in Schottky barrier heights observed with $Al_{0.3}Ga_{0.7}As$.

Fabrication of a set of narrow wires in $5x10^{18}$ cm^{-3} $In_{0.53}Ga_{0.47}As$ have established the presence of residual sidewall damage even after annealing. The natural surface depletion layer thickness should be 7.4+/-0.9 nm but the etched wires show a sidewall depletion thickness of 10.5+/-2.2 nm. To fully understand the effect of the continual bombardment on the sidewall wires should be fabricated without an anneal stage after etching and the sidewall depletion thickness established. $CH_4/H_2/O_2$ RIE should also be investigated by this method in order to understand further the effect of oxygen passivation at the sidewall.

7.6 RIE with Halogens at Elevated Temperatures

The low volatility of indium chlorides at room temperature prevent the use (for InP, InGaAs and InAlAs) of wide number of already established low damage processes using $SiCl_4$ that etch GaAs/AlGaAs. By increasing the temperature of the cathode, energy is supplied to the surface reaction site increasing the volatility of the chlorides. Etch rates are seen to rise and with a temperature of 180 ^{0}C and 100 W rf power vertical etch profiles are produced in $In_{0.53}Ga_{0.47}As$ using NiCr masks at an etch rate of 250 nm/min. Photoresist or PMMA cannot be used at such high temperatures. The etch surface is very rough but because of the 250:1 selectivity with $In_{0.52}Al_{0.48}As$ the etch surface becomes smoother as the etch slows down in the $In_{0.52}Al_{0.48}As$. If the roughness of the etch surface can be reduced by optimising the plasma conditions or by the addition of another gas then the high etch rate and vertical wall profiles could be put to good use for optical device fabrication where the etch rates in CH_4/H_2 are prohibitively slow for deep etches. Substituting BBr_3 for $SiCl_4$ resulted in undercutting of the mask and rough surfaces, so proved not viable for RIE of InP related materials.

7.7 Chapter Summary

Using a hard metal mask $Al_{0.3}Ga0_{.7}As$, $In_{0.53}Ga_{0.47}As$ or $In_{0.52}Al_{0.48}As$ can be etched to form near vertical sidewalls by choosing the correct methane:hydrogen ratio and rf power. Undercutting of the etch mask on InGaAs can be overcome by the addition of a small amount of oxygen or chlorine to the gas mixture. The lessening of the undercut is believed to be due to the formation of a passivating layer upon the sidewall.

The use of halogenated gases such as $SiCl_4$ and BBr_3 has shown that the use of elevated etch temperatures can overcome the low product vapour pressure under normal etch conditions. Only $SiCl_4$ was able to produce vetical etches in InGaAs with high selectivity over InAlAs. The etch surface is however very rough.

Optical emission spectroscopy has been used for leak testing and monitoring removal of deposited polymer within the chamber using an oxygen plasma. Excess polymer is responsible for poor etch quality. The etch stop within multilayer structures can be pinpointed using laser interferometry giving 10 nm accuracy.

Etching with higher rf powers leads to greater penetation of damage into the semiconductor but lower rf powers create greater stoichiometric changes at the surface. Annealing the semiconductor releases hydrogen from within the semiconductor reactivating donors but does not effect the composition of the etched surface.